Electronic Supplementary Information

Selective recognition and extraction of arsenate by a urea-functionalized tripodal receptor from competitive aqueous media

Sandeep Kumar Dey,*[a,b] Beatriz Gil-Hernández,[c] Vivekanand V. Gobre,[d] Dennis Woschko,[e] Sarvesh S. Harmalkar,[d] Firdaus Rahaman Gayen,[a,b] Biswajit Saha,[a,b] Rajib Lochan Goswamee,[a,b] and Christoph Janiak[d]

[a]Materials Science and Technology Division, CSIR-North East Institute of Science and Technology, Jorhat, Assam 785006, India. Email: sandeep@neist.res.in.

[b]Academy of Scientific and Innovative Research (AcSIR), Ghaziabad-201002, Uttar Pradesh, India.

[c]Departmento de Química, Facultad de Ciencias, Sección Química, Universidad de La Laguna, 38206 La Laguna, Tenerife, Spain. Email: beagher@ull.es

[d]School of Chemical Sciences, Goa University, Taleigao Plateau, Goa 403206, India. Email: vvgobre@gu.ac.in.

[e]Institute of Inorganic and Structural Chemistry, Heinrich-Heine University, Düsseldorf 40225, Germany. Email: janiak@uni.duesseldorf.de.

Electronic Supplementary Information

1. Materials and experimental methods

All reagents and solvents were obtained from commercial sources and used as received without further purification. Tris(2-aminoethyl) amine (Tren), 3-nitrophenyl isocyanate, 4-nitrobenzoyl chloride, Pd 10% on carbon, hydrazine monohydrate and all quaternary ammonium (tetraalkylammonium) salts were purchased from Sigma-Aldrich (Merck) or TCI Chemicals. Solvents (analytical grade) for synthesis and crystallization experiments were purchased from Merck, and used without further purification.

^{1}H, and ^{31}P NMR spectra were recorded on a Bruker FT-400 MHz instrument and chemical shifts were recorded in parts per million (ppm) on the scale using tetramethylsilane or residual solvent peak as a reference and ^{13}C spectra were obtained at 100 MHz at 298 K. Powder X-ray diffraction patterns of dried crystalline powder were recorded using a Bruker-D8 X-ray diffractometer with Cu-*K*α radiation at λ = 0.15418 Å. HR-MS analyses were carried out using Xevo XS QTof mass spectrometer, Waters ACQUITY UHPLC. UV-vis spectral analyses were carried out using a Perkin-Elmer spectrophotometer at 298 K.

2. Synthesis and characterization of urea-functionalized tripodal receptor L

Tris(4-amino-N-ethylbenzamide)amine (**AL**) was synthesized following the recently published literature procedure.[1] Receptor **L** was synthesized by the reaction of **AL** with 3-nitrophenylisocyante in a 1:3.2 molar ratio at room temperature (Scheme S1). In a 50 mL flat bottom flask, 500 mg of **AL** (1 mmol) was dissolved in 10 mL of dimethylformamide (DMF) and 0.520 g of 3-nitrophenylisocyante (3.2 mmol) was added into the above solution mixture and was allowed to stir at room temperature (25−30 ºC) for about 12 hours. The solution was then filtered in a 25 ml beaker and allowed to remain at room temperature for crystallization. Pale yellow solid of the receptor precipitated out from the DMF solution in quantitative yield within 2-3 days. The precipitated compound was collected by filtration and washed with 30 mL methanol (3 x 10 mL). The compound was then dissolved in 5 mL DMF for recrystallization to ensure its purity for spectroscopy analysis. The precipitated compound was again collected by filtration and washed with 30 mL methanol (3 x 10 mL) and dried at room temperature. The compound was characterized by NMR spectroscopy in DMSO-d_6 and HR-MS in acetonitrile.

Isolated yield of **L** after recrystallization: 625 mg (% yield 62%, based on three experimental runs). The compound is soluble in dimethylformamide, dimethyl sulfoxide, and acetone, insoluble in acetonitrile, chloroform/dichloromethane and methanol/ethanol.

Characterization of **L**: ^{1}H-NMR (400 MHz, DMSO-d_6) chemical shift in δ ppm: 2.50 (Residual DMSO), 2.72 (t, J = 8 Hz, 3xNCH_2), 3.38 (3xCH_2 + H_2O), 7.52 (t, J = 8 Hz, 9xCH), 7.66 (d, J = 8 Hz, 3xCH), 7.79 (d, J = 8 Hz, 9xCH), 8.51 (d, J = 4 Hz, 3xCH), 8.26 (t, J = 4 Hz, 3x Amide-**NH**), 9.03 (s, 3x Urea-$\mathbf{NH_\alpha}$), 9.24 (s, 3x Urea-$\mathbf{NH_\beta}$).

^{13}C-NMR (100 MHz, DMSO-d_6) chemical shift in δ ppm: 42.9 (3xCH_2), 58.7 (3xCH_2), 117.4 (3xCH), 121.7 (3xCH), 122.7 (3xCH), 129.62 (3xCH), 133.2 (3xCH), 135.3 (3xCH), 146.0 (3xCH), 147.1 (3xCH), 153.3 (3xCH), 157.4 (3xC=O), 171.1 (3xC=O).

HR-MS of **L** (negative ion): m/z 994.380 [$\mathbf{L}-H^+]^-$ and 995.388 [**L**]

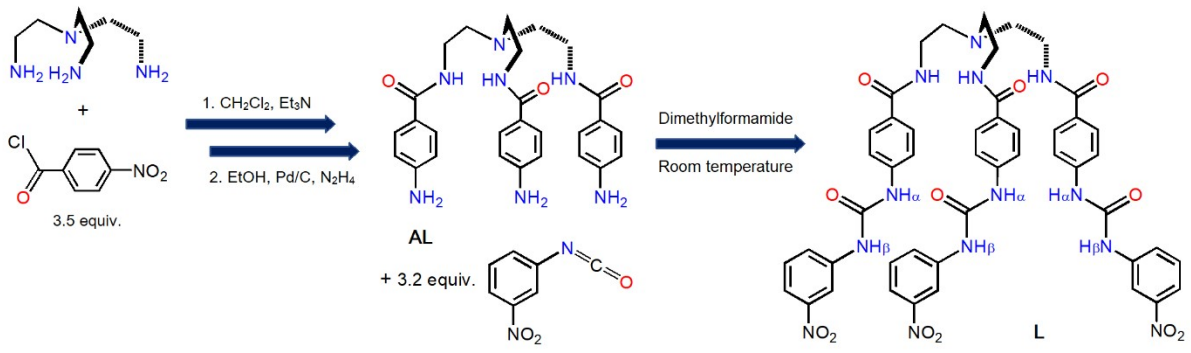

Scheme S1. Synthesis of hydrogen bond donor tripodal receptor **L**.

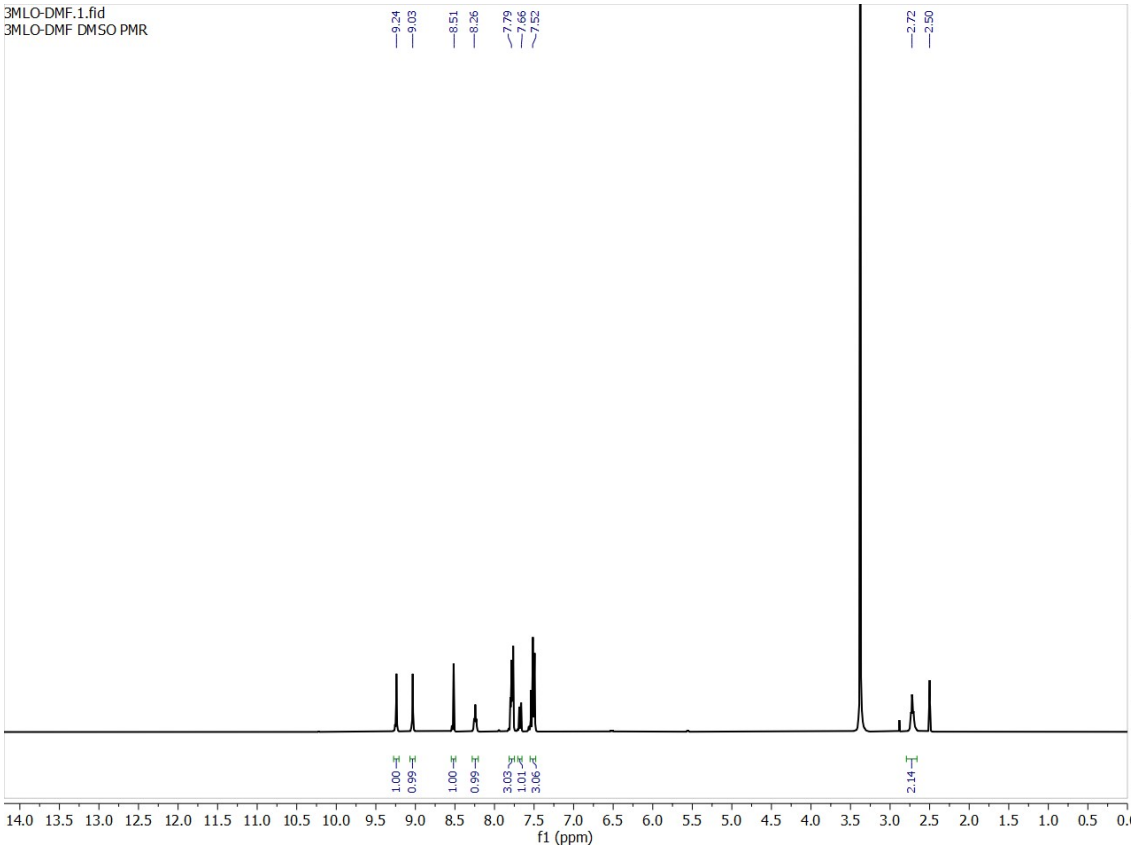

Fig. S1. ^{1}H-NMR spectrum of receptor **L** in DMSO-d_6 (400 MHz).

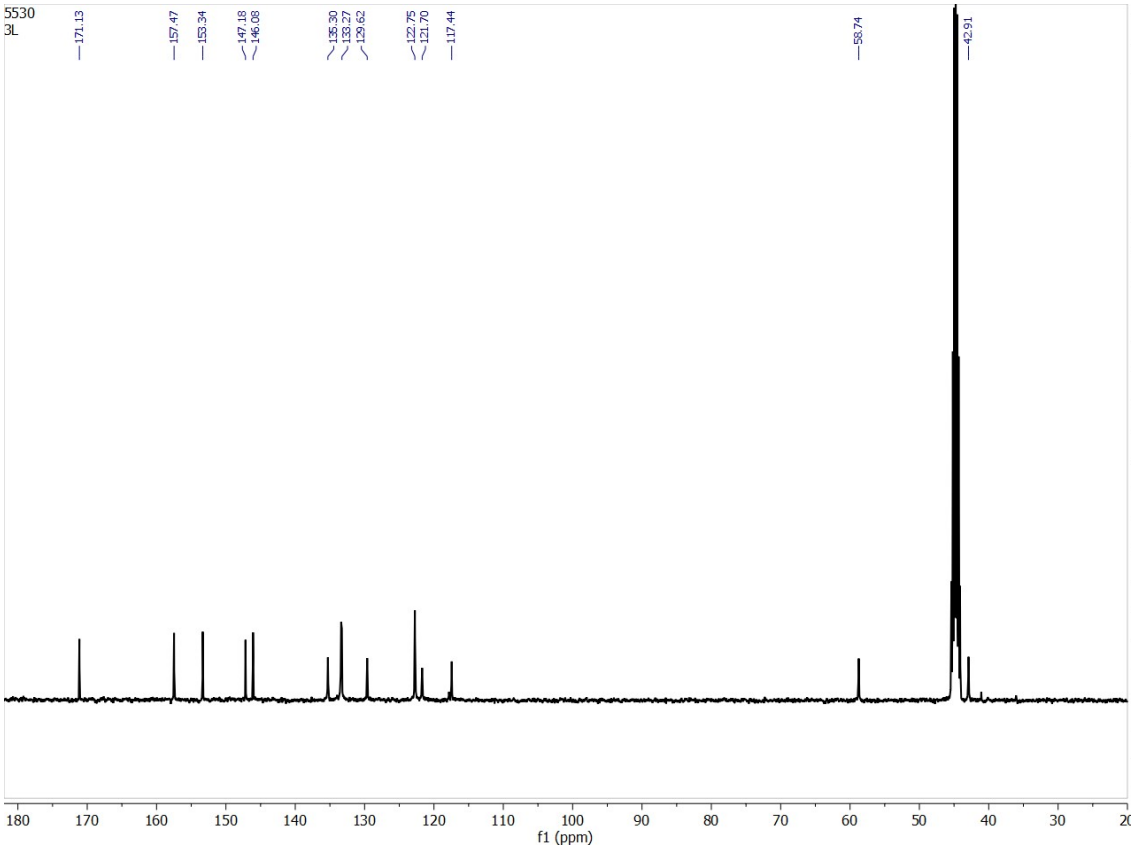

Fig. S2. ^{13}C-NMR spectrum of receptor **L** in DMSO-d_6 (100 MHz).

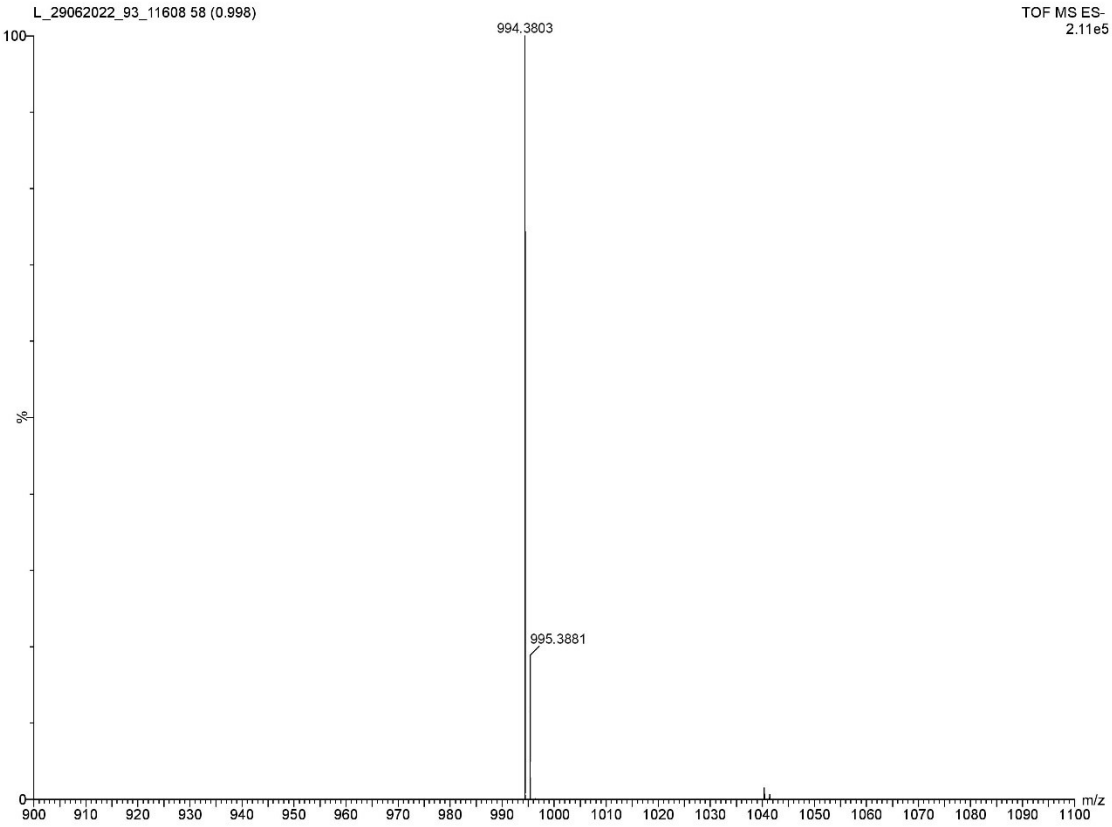

Fig. S3. HR-MS of **L** in acetonitrile.

3. Synthesis and characterization of receptor-oxoanion complexes

The receptor-oxoanion complexes were obtained by liquid-liquid extraction experiments. In a typical liquid-liquid extraction experiment, **L** (200 mg) was dissolved in dichloromethane (DCM, 20 mL) in the presence of three equivalents (n-Bu_4N^+)OH^- and an aqueous solution of an oxoanion (one equivalent of Na_2HPO_4, Na_2HAsO_4 or Na_2SO_4, dissolved in 20 mL of double distilled water) was added into the DCM solution. The solution mixture was then stirred at room temperature for about half an hour and the separated organic layer was washed with 10 mL of double distilled water in each case. The DCM layer was then isolated again using a separating funnel and treated with anhydrous sodium sulfate in each case. The solution was then filtered and evaporated to dryness at room temperature to obtain yellow crystalline powder of the host-guest complex which was characterized by NMR spectroscopy in DMSO-d_6 and HR-MS in acetonitrile.

Characterization of the arsenate complex [(n-Bu_4N)$_3$·(2**L**·AsO_4)]: ^{1}H-NMR (400 MHz, DMSO-d_6) chemical shift in δ ppm: 0.88 (t, J = 8 Hz, 36H, 12 x **C**$\mathbf{H_3}$, (n-Bu_4N^+)$_3$), 1.25 (m, 24H, 12 x **C**$\mathbf{H_2}$, (n-Bu_4N^+)$_3$), 1.50 (m, 24H, 12 x **C**$\mathbf{H_2}$, (n-Bu_4N^+)$_3$), 2.50 (Residual DMSO), 2.59 (s, 12H, 6xN**C**$\mathbf{H_2}$, 2**L**), 3.09 (t, J = 8 Hz, 24H, 12 x N^+**C**$\mathbf{H_2}$, (n-Bu_4N^+)$_3$), 3.45 (12H, 6x**C**$\mathbf{H_2}$, 2**L**), 6.73−7.76 (48H, Aromatic-**C**H, 2**L**), 8.20 (s, 6H, Amide-**NH**, 2**L**), 11.84 (s, 6H, Urea-**NH**$_{\alpha}$, 2**L**), 12.90 (s, 6H, Urea-**NH**$_{\beta}$, 2**L**) (See Fig. S4 below).

^{13}C-NMR (100 MHz, DMSO-d_6) chemical shift in δ ppm: 13.8 (12C, 12 x **C**$\mathbf{H_3}$, (n-Bu_4N^+)$_3$), 19.6 (12C, 12 x **C**$\mathbf{H_2}$, (n-Bu_4N^+)$_3$), 23.4 (12C, 12 x **C**$\mathbf{H_2}$, (n-Bu_4N^+)$_3$), 36.6 (6C, 6 x NCH_2, 2**L**), 52.8 (6C, 6 x CH_2, 2**L**), 57.9 (12C, 12 x **C**$\mathbf{H_2}$, (n-Bu_4N^+)$_3$), 111.1 (6C, 6xCH, 2**L**), 115.3 (6C, 6xCH, 2**L**), 118.0 (6C, 6xCH, 2**L**), 124.0 (6C, 6xCH, 2**L**), 128.0 (6C, 6xCH, 2**L**), 128.4 (6C, 6xCH, 2**L**), 142.1 (6C, 6xCH, 2**L**), 143.4 (6C, 6xCH, 2**L**), 147.8 (6C, 6xCH, 2**L**), 153.3 (6C, 6x Amide-CO, 2**L**), 167.3 (6C, 6x Urea-CO, 2**L**) (See Fig. S5 below).

HR-MS of the arsenate complex (negative ion): m/z 1136.152 [**L**·H_2AsO_4]$^-$, 1065.689 [2**L**·$HAsO_4$]$^{2-}$, 994.238 [**L**−H^+]$^-$, 567.594 [**L**·$HAsO_4$]$^{2-}$, 140.934 [H_2AsO_4]$^-$ (See Fig. S6 below).

Characterization of the phosphate complex [(n-Bu_4N)$_3$·(2**L**·PO_4)]: ^{1}H-NMR (400 MHz, DMSO-d_6) chemical shift in δ ppm: 0.87 (t, J = 8 Hz, 36H, 12 x **CH$_3$**, (n-Bu_4N^+)$_3$), 1.23 (m, 24H, 12 x **CH$_2$**, (n-Bu_4N^+)$_3$), 1.49 (m, 24H, 12 x **CH$_2$**, (n-Bu_4N^+)$_3$), 2.50 (Residual DMSO), 2.58 (s, 12H, 6xN**CH$_2$**), 3.06 (t, J = 8 Hz, 24H, 12 x N$^+$**CH$_2$**, (n-Bu_4N^+)$_3$), 6.71−7.75 (48H, Aromatic-**CH**, 2**L**), 8.15 (s, 6H, Amide-**NH**, 2**L**), 11.87 (s, 6H, Urea-**NH$_\alpha$**, 2**L**), 12.98 (s, 6H, Urea-**NH$_\beta$**, 2**L**) (See Fig. S7 below).

^{31}P-NMR (400 MHz, DMSO-d_6): 8.12 ppm (See Fig. S8 below).

^{13}C-NMR (100 MHz, DMSO-d_6) chemical shift in δ ppm: 13.9 (12C, 12 x **CH$_3$**, (n-Bu_4N^+)$_3$), 19.6 (12C, 12 x **CH$_2$**, (n-Bu_4N^+)$_3$), 23.5 (12C, 12 x **CH$_2$**, (n-Bu_4N^+)$_3$), 36.5 (6C, 6 x NCH_2, 2**L**), 52.8 (6C, 6 x CH_2, 2**L**), 57.9 (12C, 12 x **CH$_2$**, (n-Bu_4N^+)$_3$), 111.2 (6C, 6xCH, 2**L**), 115.5 (6C, 6xCH, 2**L**), 118.2 (6C, 6xCH, 2**L**), 124.3 (6C, 6xCH, 2**L**), 128.1 (6C, 6xCH, 2**L**), 128.4 (6C, 6xCH, 2**L**), 142.1 (6C, 6xCH, 2**L**), 143.4 (6C, 6xCH, 2**L**), 147.9 (6C, 6xCH, 2**L**), 153.5 (6C, 6x Amide-CO, 2**L**), 167.5 (6C, 6x Urea-CO, 2**L**) (See Fig. S9 below).

HR-MS of the phosphate complex (negative ion): m/z 1092.426 [**L**·H_2PO_4]$^-$, 1043.925 [2**L**·HPO_4]$^{2-}$, 994.444 [**L**−H^+]$^-$, 545.762 (**L**·HPO_4)$^{2-}$ (See Fig. S10 below).

Characterization of the sulfate complex [(n-Bu_4N)$_2$·(2**L**·SO_4)]: ^{1}H-NMR (400 MHz, DMSO-d_6) chemical shift in δ ppm: 0.90 (t, J = 8 Hz, 24H, 8 x **CH$_3$**, (n-Bu_4N^+)$_2$), 1.27 (m, 16H, 8 x **CH$_2$**, 2(n-Bu_4N^+)), 1.53 (m, 16H, 8 x **CH$_2$**, 2(n-Bu_4N^+)), 2.51 (Residual DMSO), 2.65 (t, J = 4 Hz, 12H, 6xN**CH$_2$**), 3.13 (t, J = 12 Hz, 16H, 8 x N$^+$**CH$_2$**, 2(n-Bu_4N^+)), 3.43 (12H, 6xNCH_2**CH$_2$**), 7.38−7.77 (48H, Aromatic-**CH**, 2**L**), 8.49 (s, 6H, Amide-**NH**, 2**L**), 10.04 (s, 6H, Urea-**NH$_\alpha$**, 2**L**), 10.53 (s, 6H, Urea-**NH$_\beta$**, 2**L**) (See Fig. S11 below).

^{13}C-NMR (100 MHz, DMSO-d_6) chemical shift in δ ppm: 13.9 (8C, 8 x **CH$_3$**, (n-Bu_4N^+)$_3$), 19.7 (8C, 8 x **CH$_2$**, (n-Bu_4N^+)$_3$), 23.5 (8C, 8 x **CH$_2$**, (n-Bu_4N^+)$_3$), 36.9 (6C, 6 x NCH_2, 2**L**), 52.2 (6C, 6 x CH_2, 2**L**), 58.0 (8C, 8 x **CH$_2$**, (n-Bu_4N^+)$_3$), 112.3 (6C, 6xCH, 2**L**), 116.2 (6C, 6xCH, 2**L**), 118.1 (6C, 6xCH, 2**L**), 124.6 (6C, 6xCH, 2**L**), 127.3 (6C, 6xCH, 2**L**), 128.0 (6C, 6xCH, 2**L**), 130.0 (6C, 6xCH, 2**L**), 142.0 (6C, 6xCH, 2**L**), 143.0 (6C, 6xCH, 2**L**), 148.40 (6C, 6xCH, 2**L**), 152.9 (6C, 6x amide-CO, 2**L**), 166.4 (6C, 6x urea-CO, 2**L**) (See Fig. S12 below).

HR-MS of the sulfate complex (negative ion): m/z 1333.692 [n-Bu_4(**L**·SO_4)]$^-$, 994.444 [**L**−H^+]$^-$, 545.762 [**L**·SO_4]$^{2-}$, 97.023 [HSO_4]$^-$ (See Fig. S13 below).

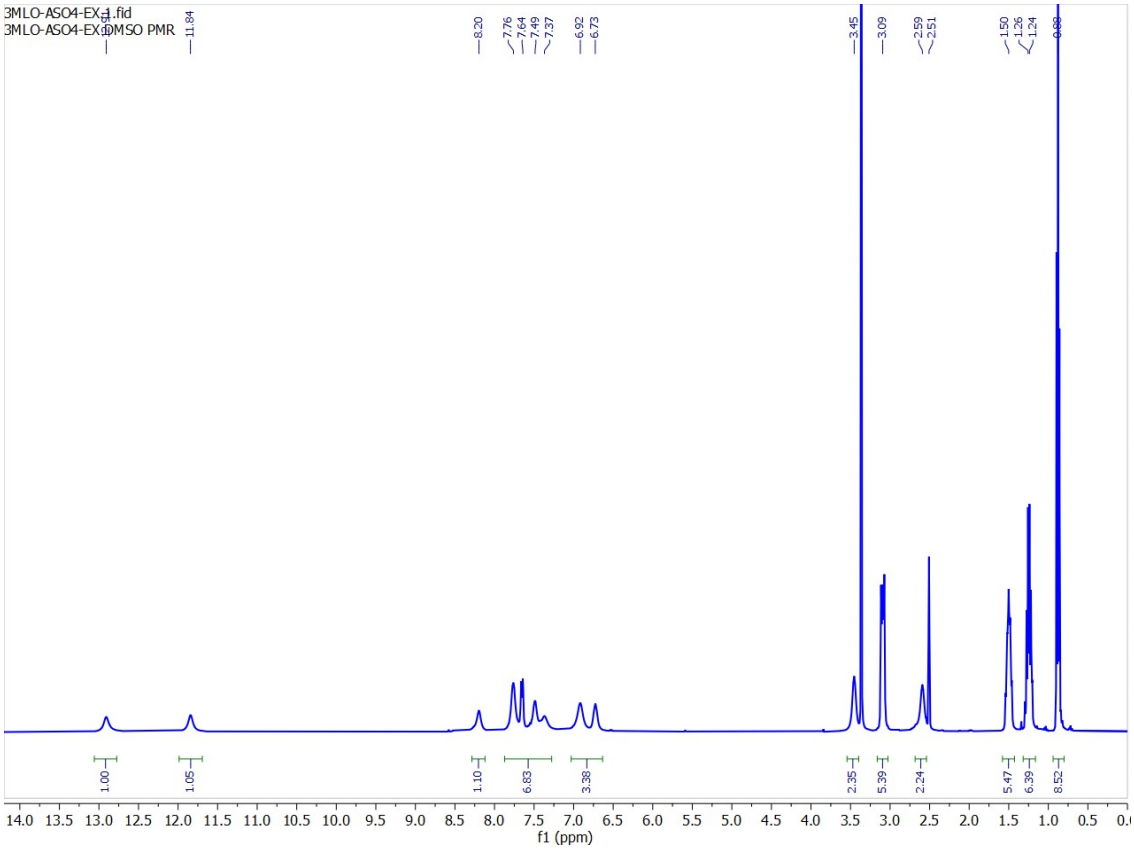

Fig. S4. ^{1}H-NMR spectrum of the arsenate complex $[(n\text{-}Bu_4N)_3\cdot(2\mathbf{L}\cdot AsO_4)]$ crystals in DMSO-d_6.

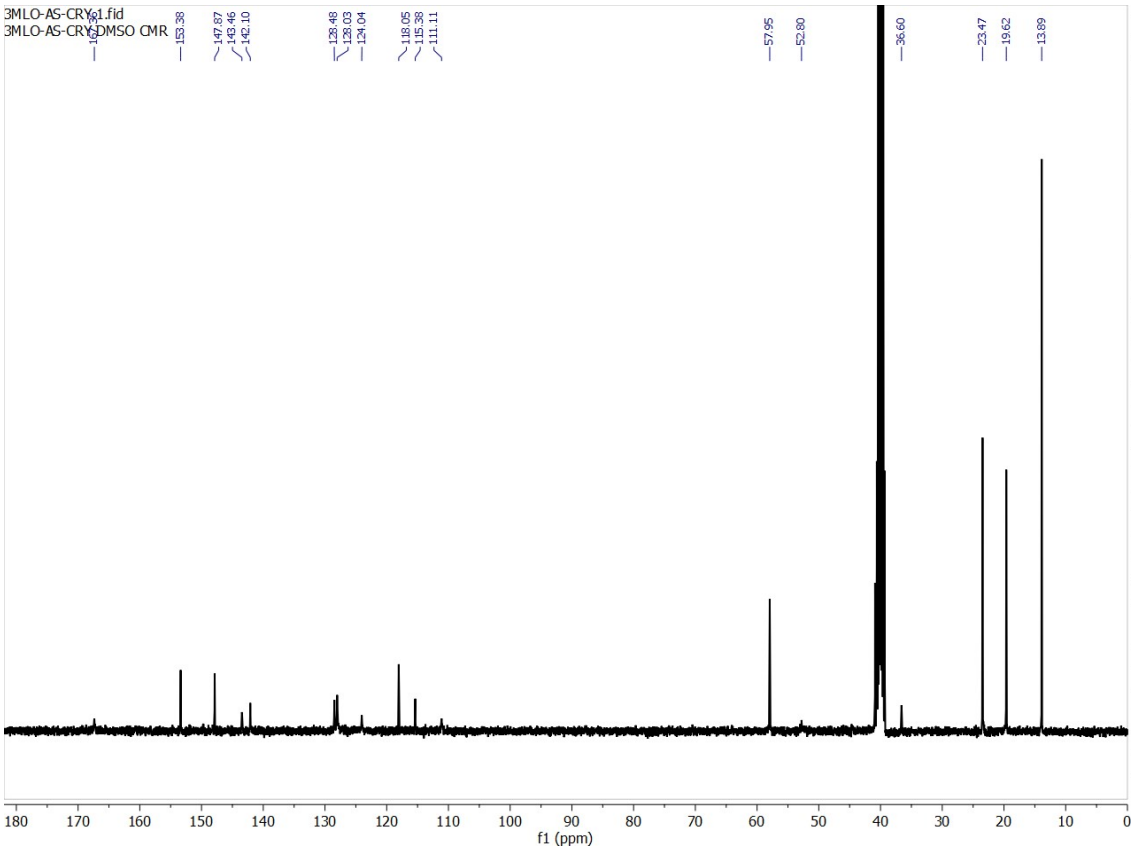

Fig. S5. ^{13}C-NMR spectrum of the arsenate complex $[(n\text{-}Bu_4N)_3\cdot(2\mathbf{L}\cdot AsO_4)]$ crystals in DMSO-d_6.

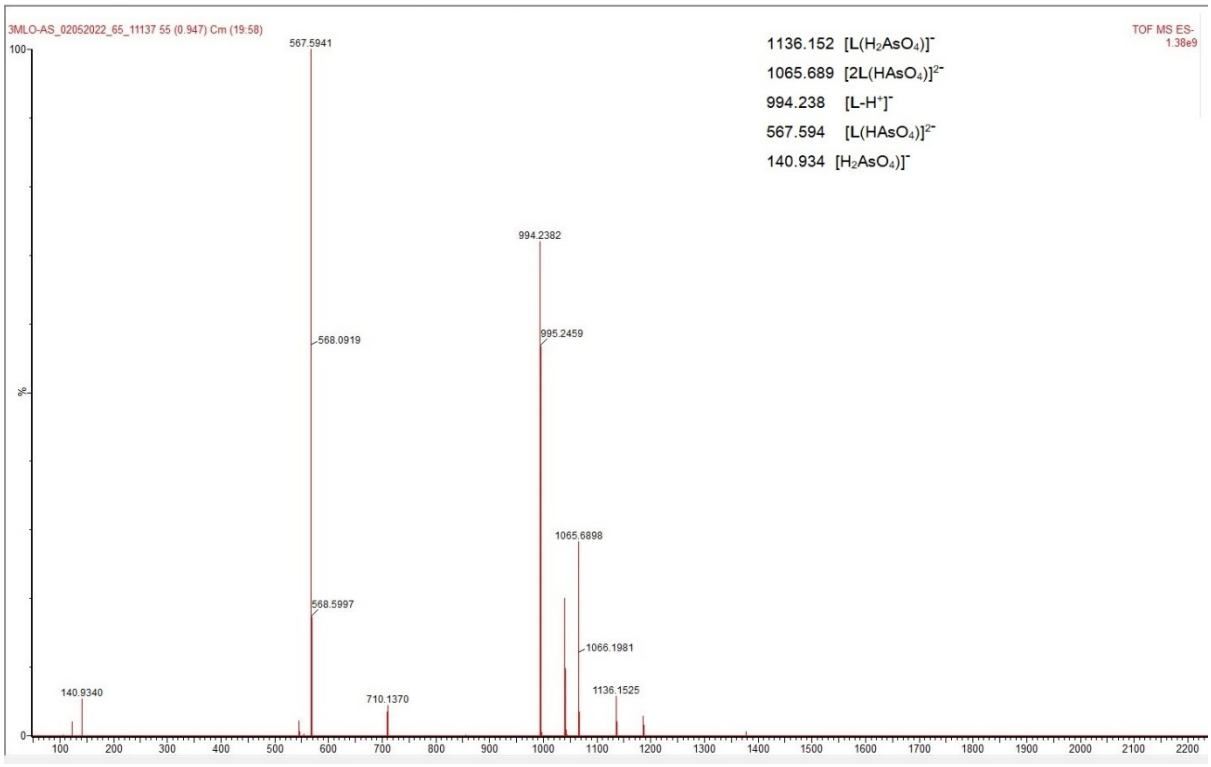

Fig. S6. HR-MS of the arsenate complex $[(n\text{-}Bu_4N)_3{\cdot}(2\mathbf{L}{\cdot}AsO_4)]$ crystals in acetonitrile in negative mode. Peak patterns with a 0.5 mass difference indicate doubly-charged species.

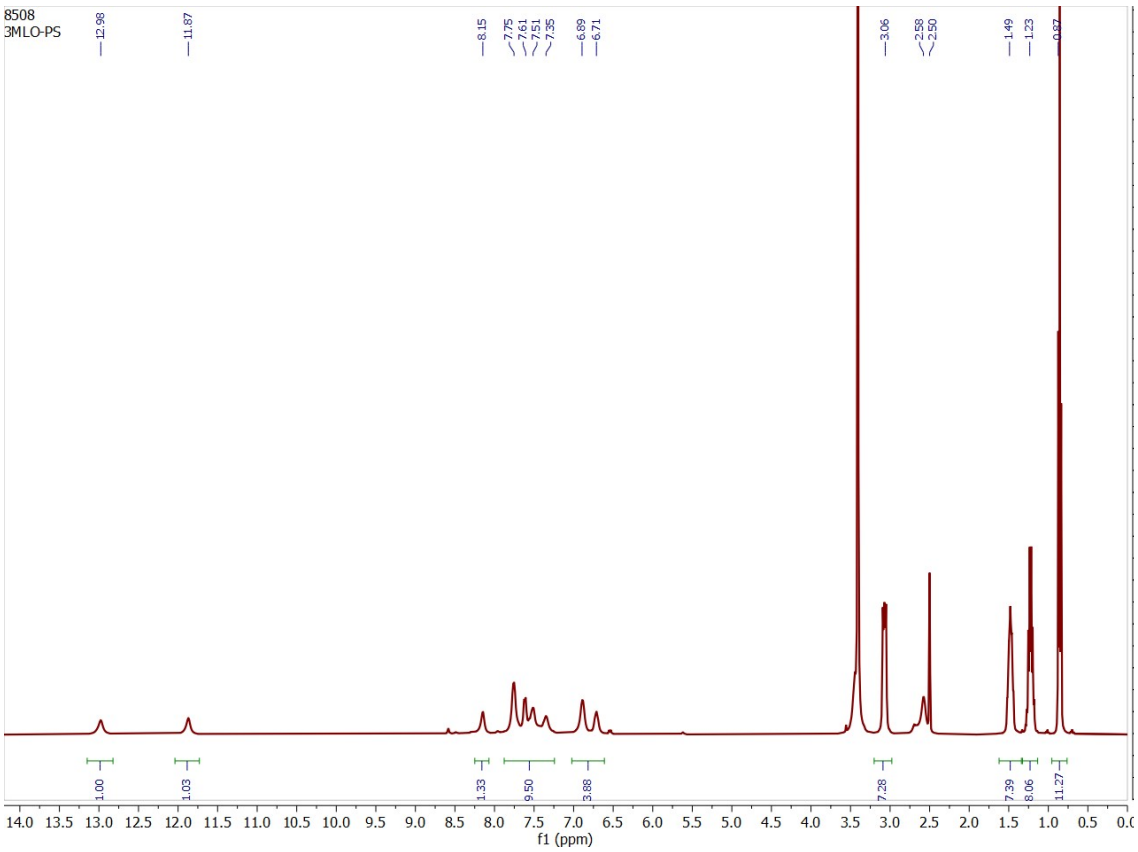

Fig. S7. ^{1}H-NMR spectrum of the phosphate complex $[(n\text{-}Bu_4N)_3{\cdot}(2\mathbf{L}{\cdot}PO_4)]$ crystals in DMSO-d_6.

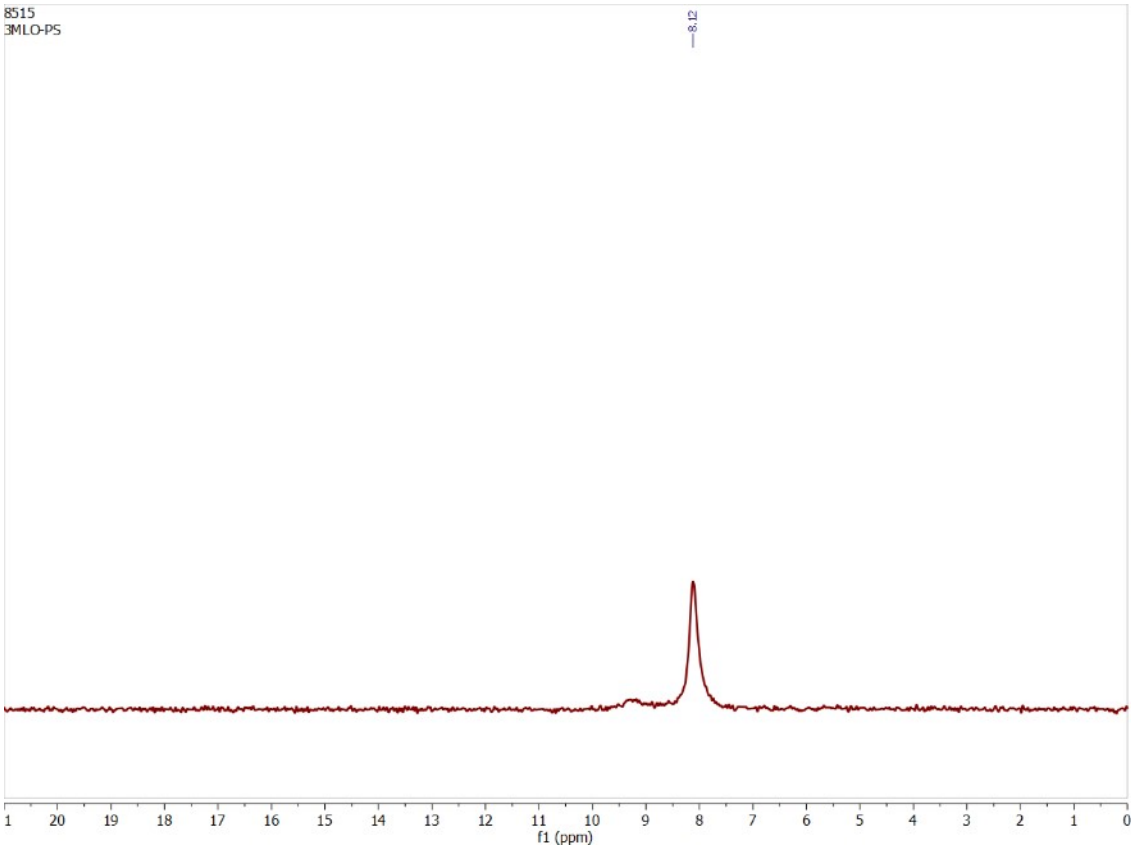

Fig. S8. ^{31}P-NMR spectrum of the phosphate complex [(n-$Bu_4N)_3$·(2**L**·PO_4)] crystals in DMSO-d_6.

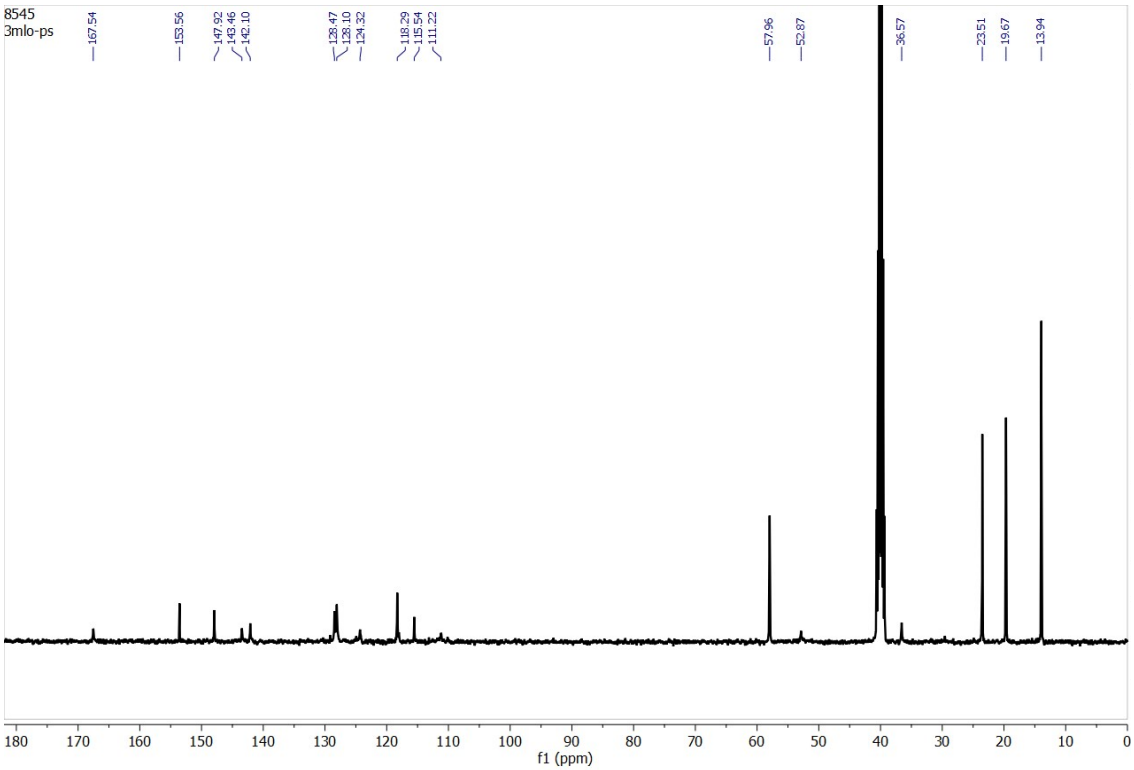

Fig. S9. ^{13}C-NMR spectrum of the phosphate complex [(n-$Bu_4N)_3$·(2**L**·PO_4)] crystals in DMSO-d_6.

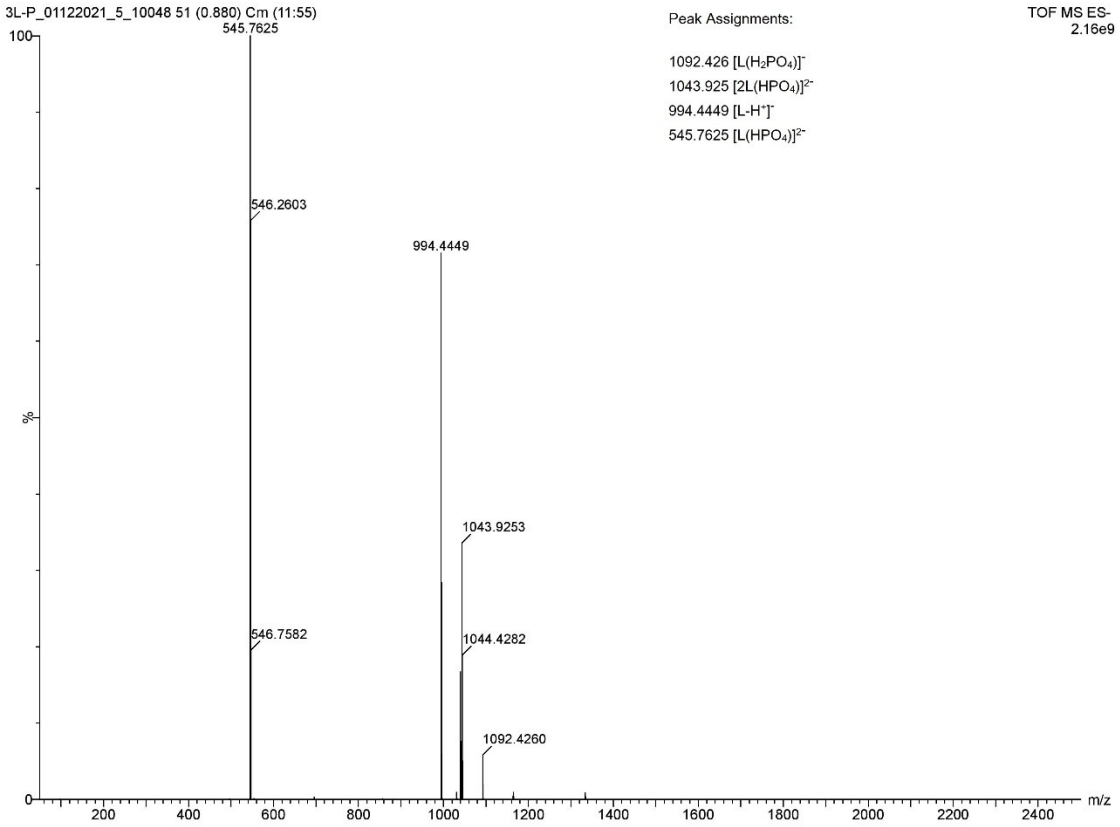

Fig. S10. HR-MS of the phosphate complex $[(n\text{-}Bu_4N)_3\cdot(2\mathbf{L}\cdot PO_4)]$ crystals in acetonitrile in negative mode. Peak patterns with a 0.5 mass difference indicate doubly-charged species.

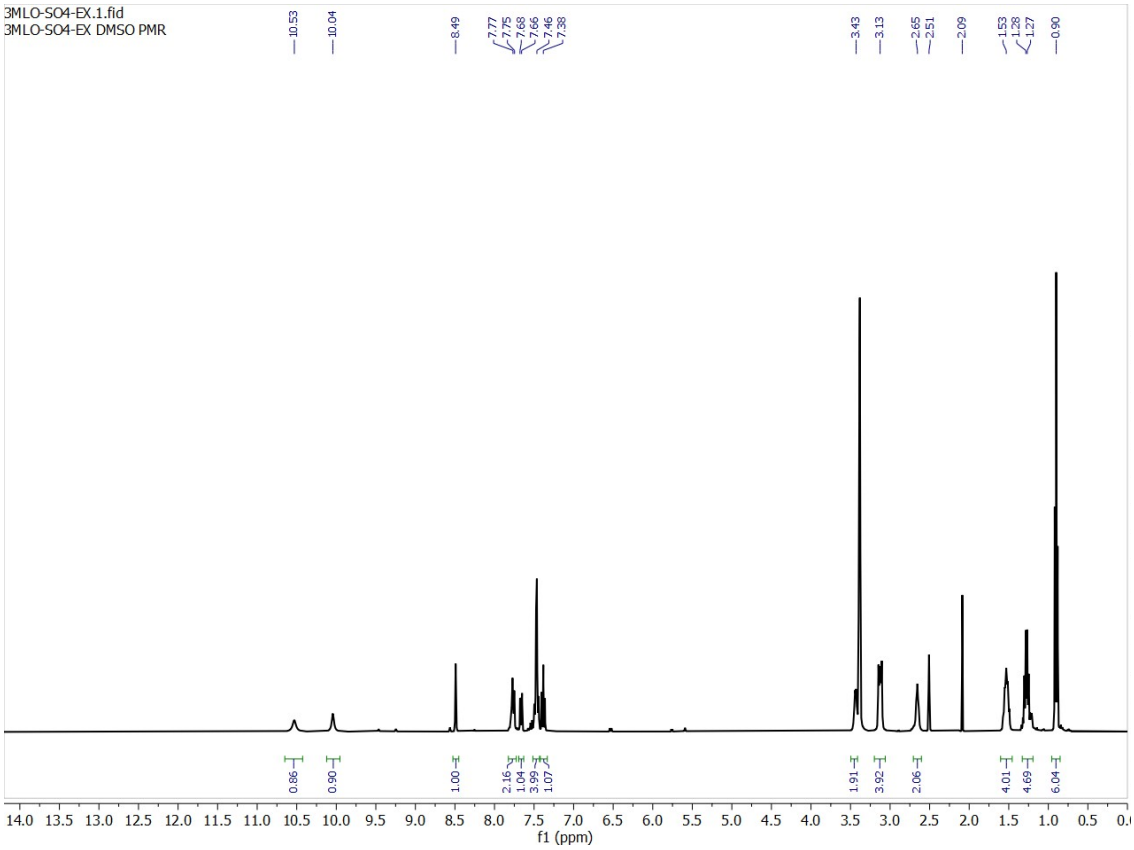

Fig. S11. ^{1}H-NMR spectrum of the sulfate complex [(n-$Bu_4N)_2$·(2**L**·SO_4)] crystals in DMSO-d_6.

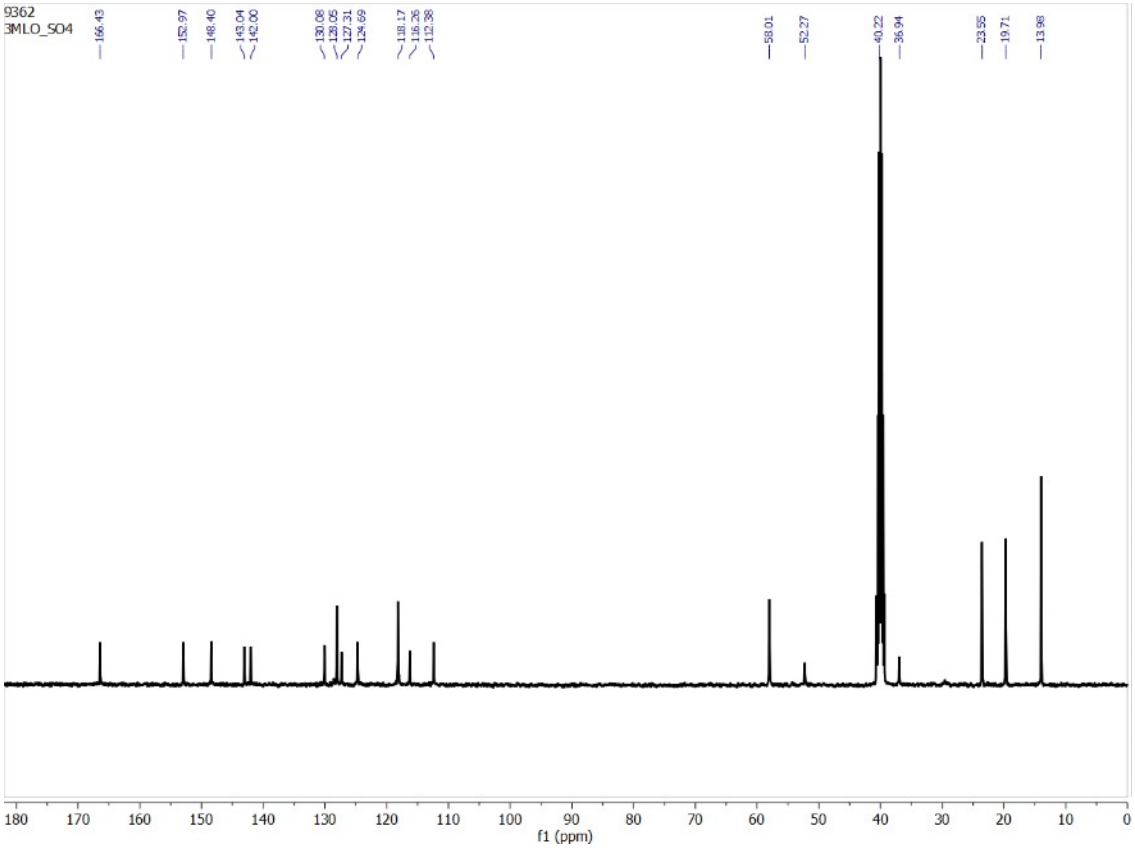

Fig. S12. ^{13}C-NMR spectrum of the sulfate complex [(n-$Bu_4N)_2$·(2**L**·SO_4)] crystals in DMSO-d_6.

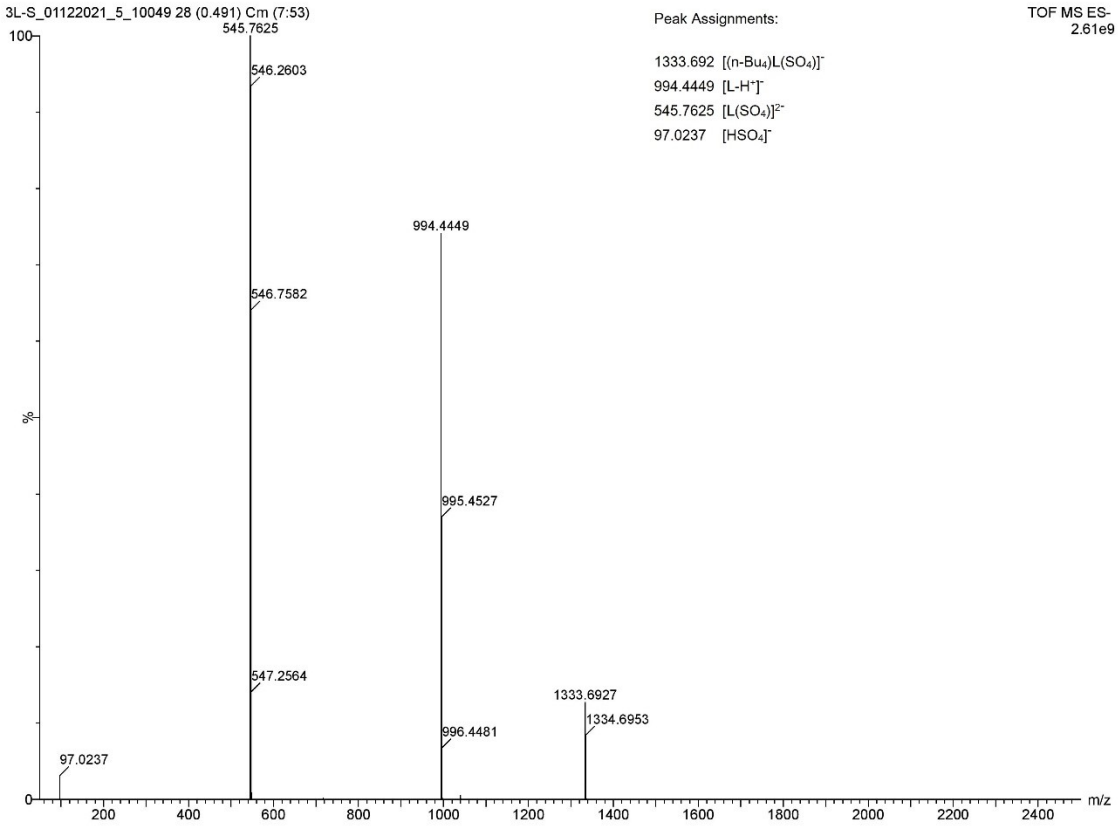

Fig. S13. HR-MS of the sulfate complex $[(n\text{-}Bu_4N)_2\cdot(2\mathbf{L}\cdot SO_4)]$ crystals in acetonitrile in negative mode. Peak patterns with a 0.5 mass difference indicate doubly-charged species.

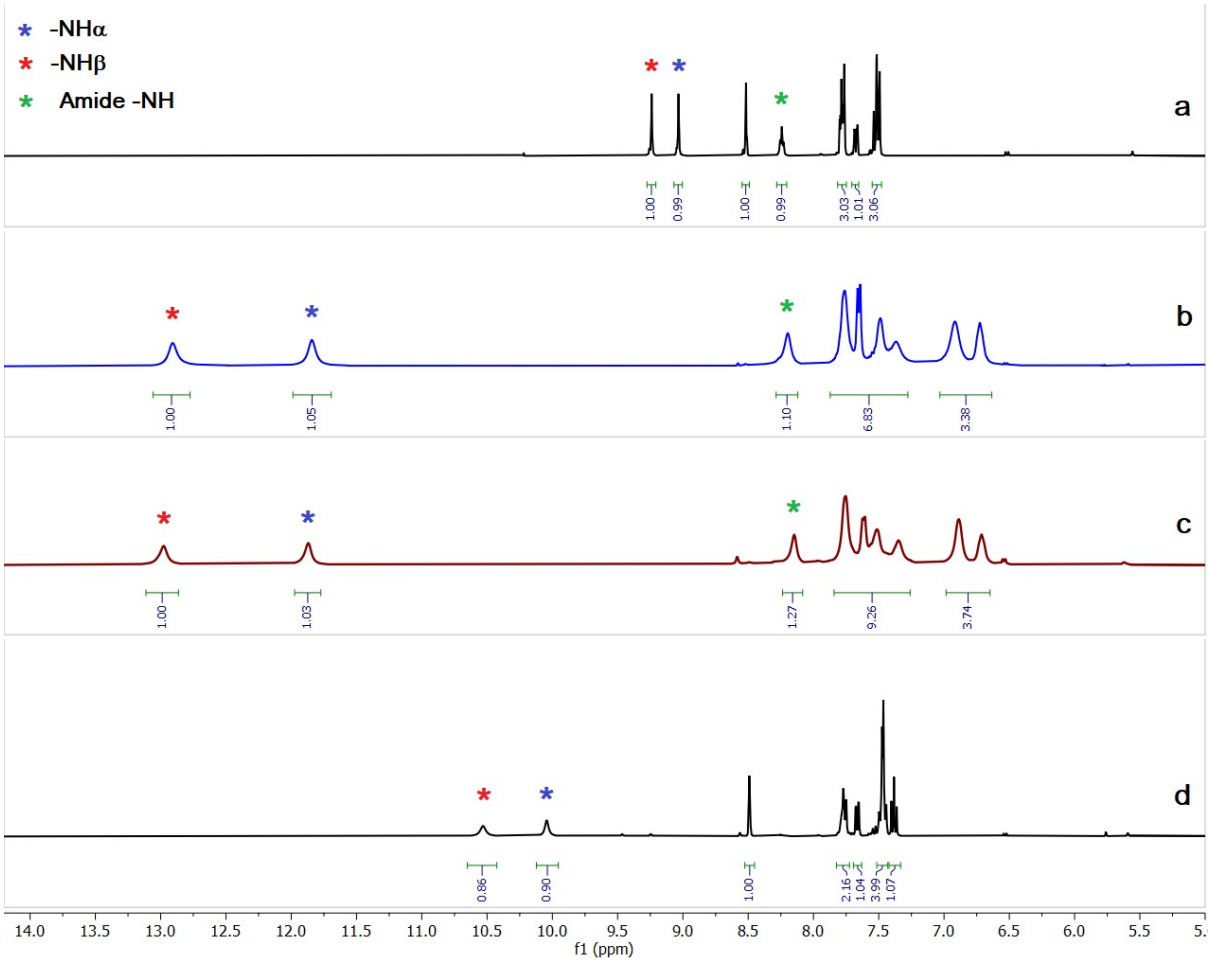

Fig. S14. Aromatic region of the ^{1}H-NMR spectra of (a) receptor **L**, (b) crystals of the arsenate complex [(n-$Bu_4N)_3$(2**L**·AsO_4)], (c) crystals of the phosphate complex [(n-$Bu_4N)_3$(2**L**·PO_4)] and (d) crystals of the sulfate complex [(n-$Bu_4N)_2$(2**L**·SO_4)].

4. ^{1}H-NMR spectra of L in the presence of quaternary ammonium (n-$Bu_4N)^+$/($Et_4N)^+$ salts.

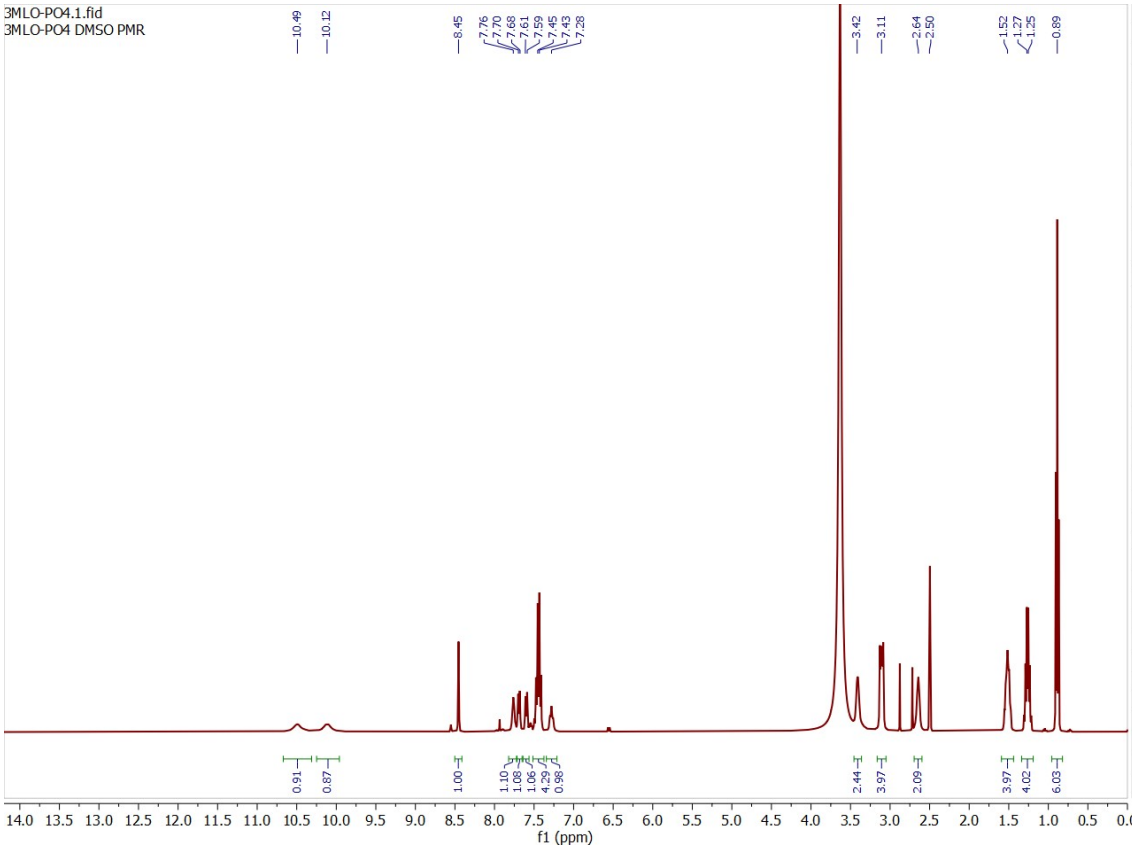

Fig. S15. ^{1}H-NMR spectrum of **L** in the presence of 1.5 equiv. $(n\text{-}Bu_4N)^+H_2PO_4^-$ in DMSO-d_6.

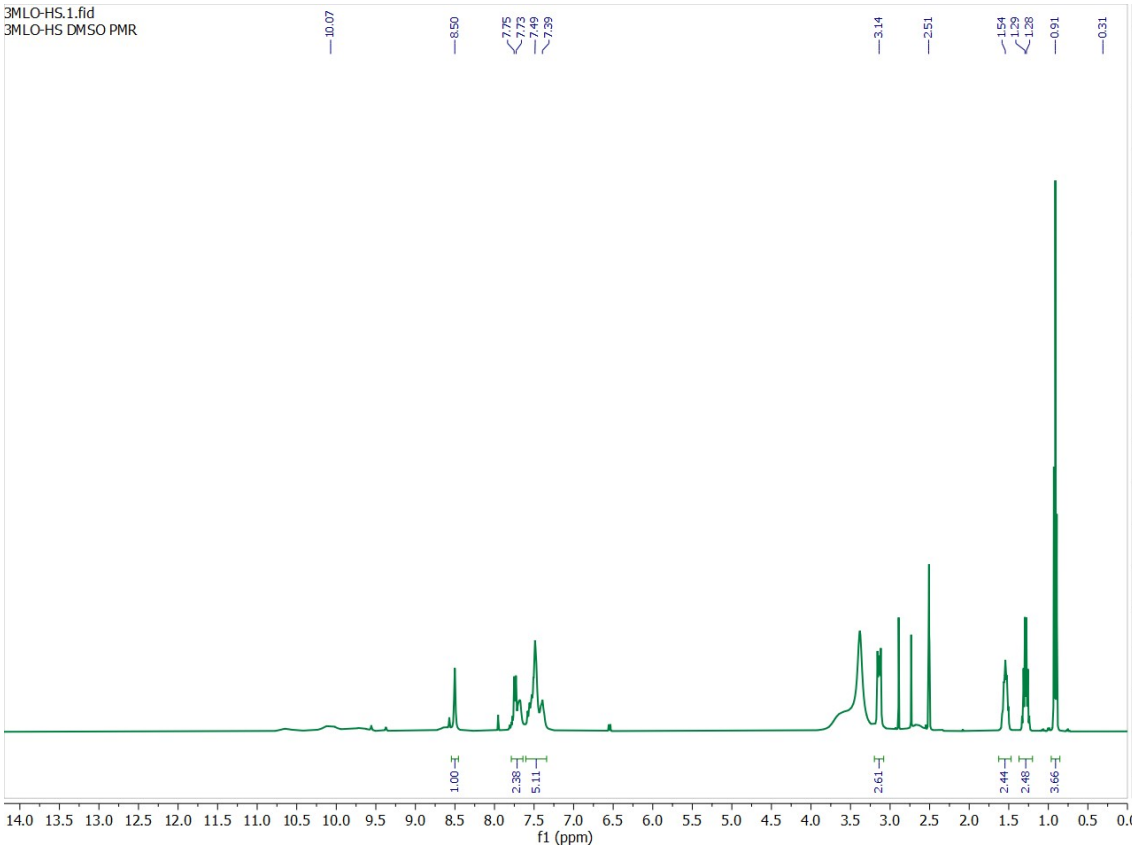

Fig. S16. ^{1}H-NMR spectrum of **L** in the presence of 1.0 equiv. $(n\text{-}Bu_4N)^+HSO_4^-$ in DMSO-d_6.

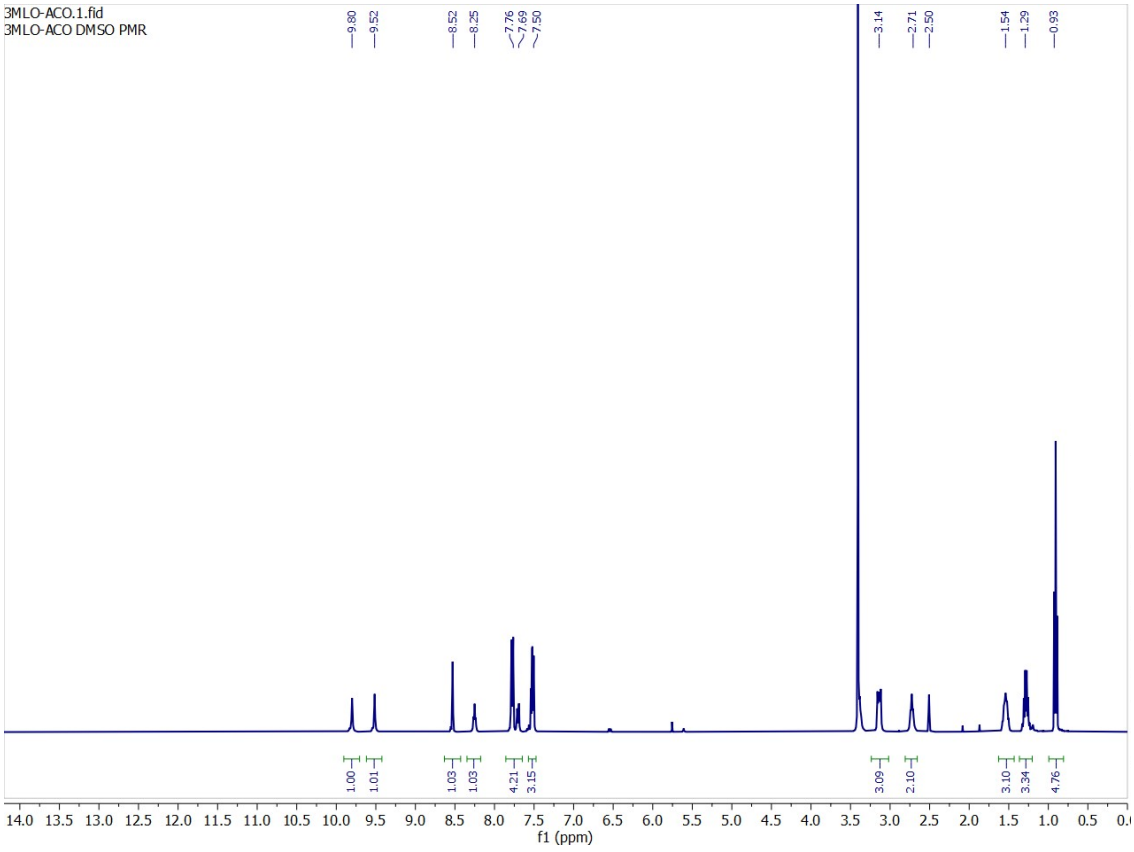

Fig. S17. ^{1}H-NMR spectrum of **L** in the presence of 1.0 equiv. $(n\text{-}Bu_4N)^{+}CH_3CO_2^{-}$ in DMSO-d_6.

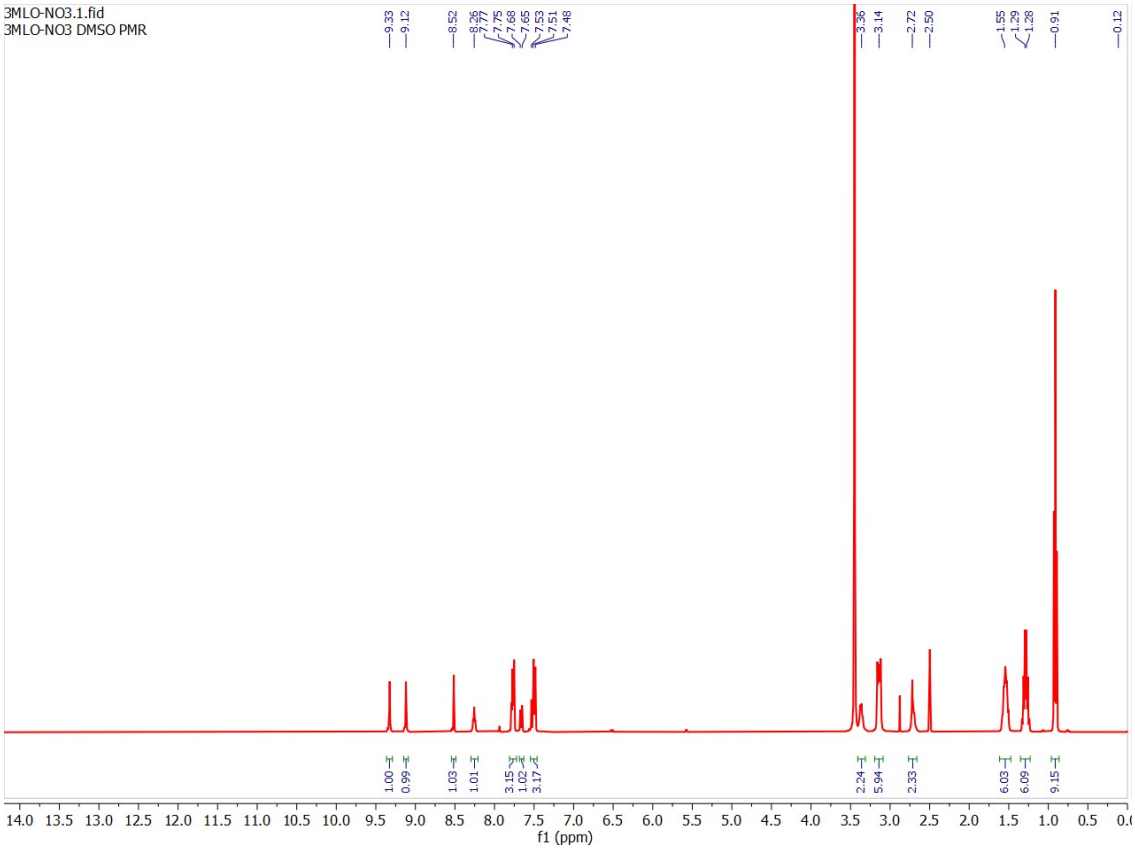

Fig. S18. ^{1}H-NMR spectrum of **L** in the presence of 2.0 equiv. $(n\text{-}Bu_4N)^{+}NO_3^{-}$ in DMSO-d_6.

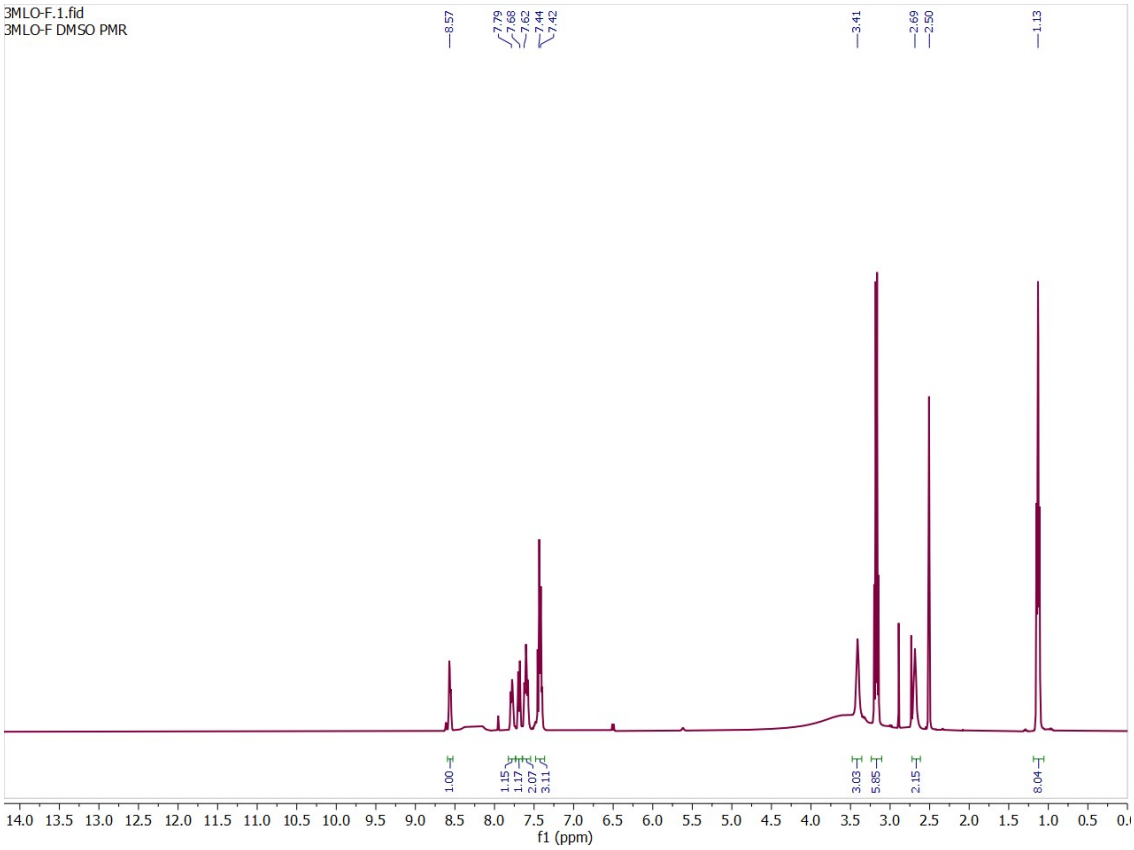

Fig. S19. ^{1}H-NMR spectrum of **L** in the presence of 2.0 equiv. $(Et_4N)^+F^-$ in DMSO-d_6.

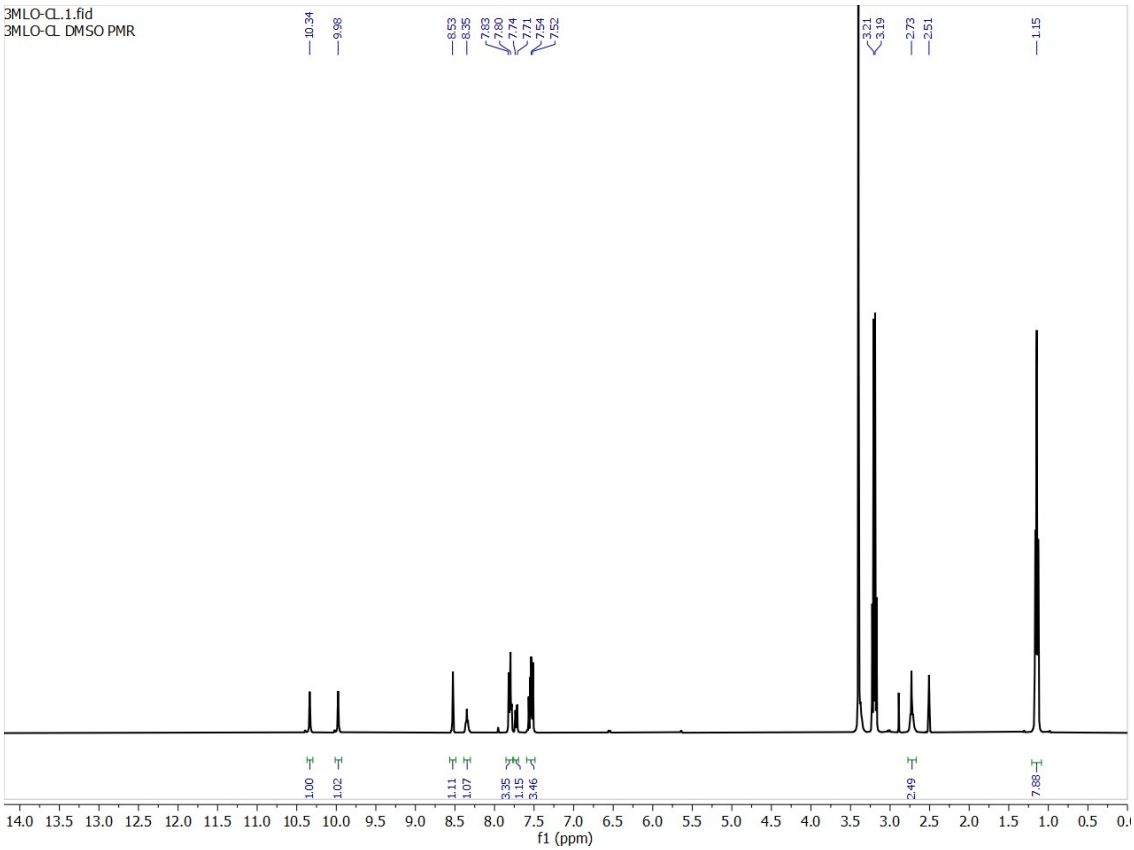

Fig. S20. ^{1}H-NMR spectrum of **L** in the presence of 2.0 equiv. $(Et_4N)^+Cl^-$ in DMSO-d_6.

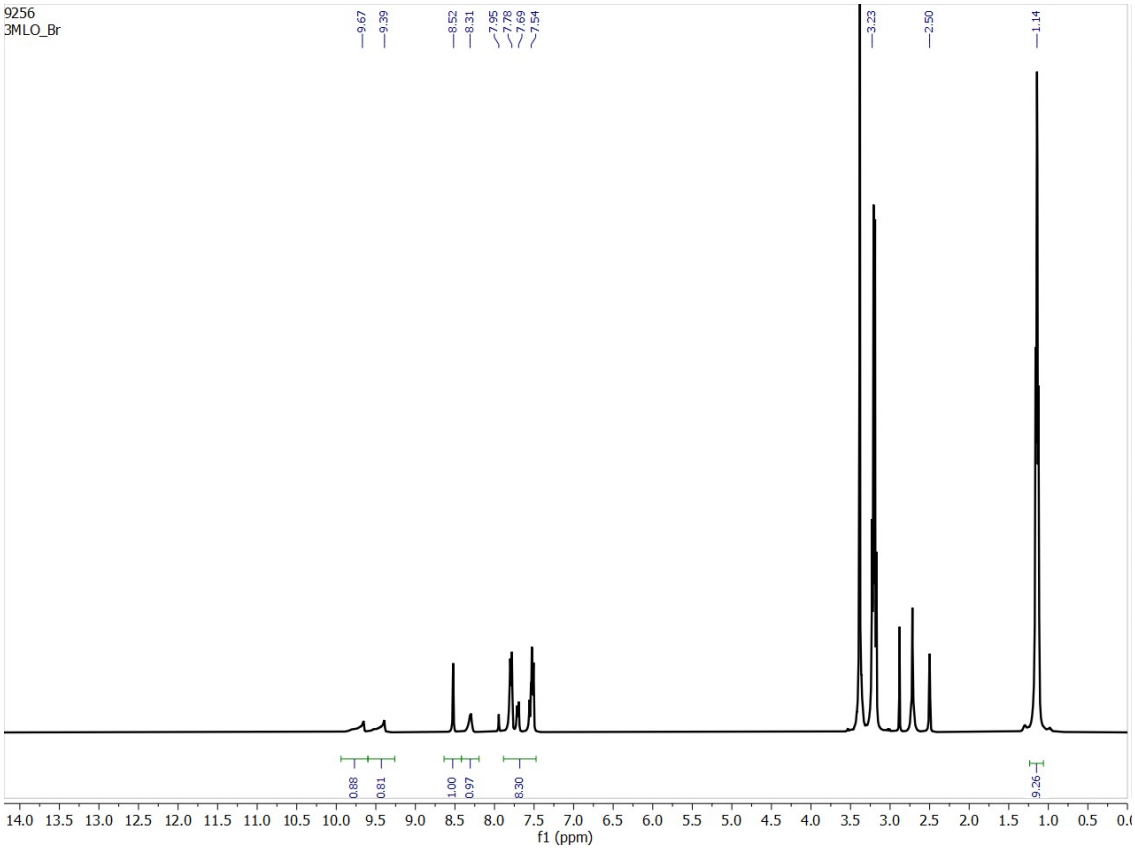

Fig. S21. ^{1}H-NMR spectrum of **L** in the presence of 2.0 equiv. $(Et_4N)^+Br^-$ in DMSO-d_6.

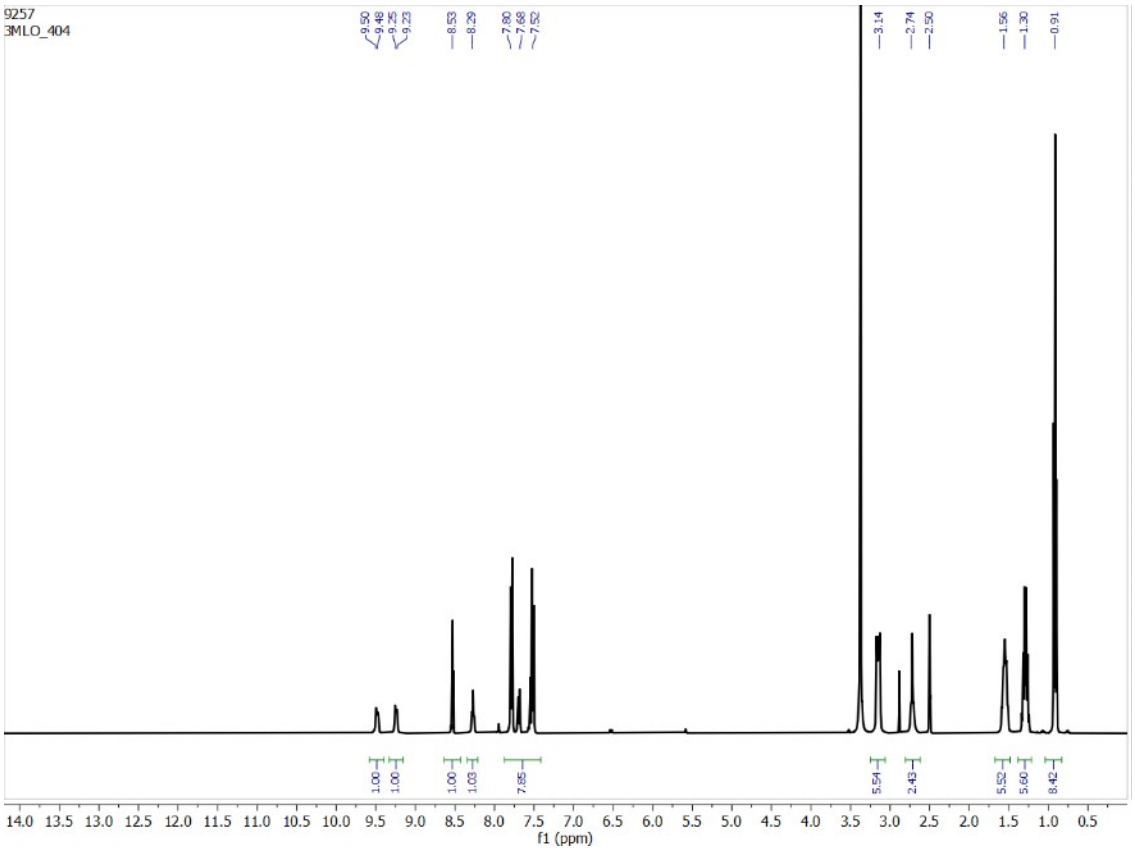

Fig. S22. ^{1}H-NMR spectrum of **L** in the presence of 2.0 equiv. $(n\text{-}Bu_4N)^+ClO_4^-$ in DMSO-d_6.

5. ^{1}H-NMR spectra of oxoanion complexes obtained from liquid-liquid extraction experiments

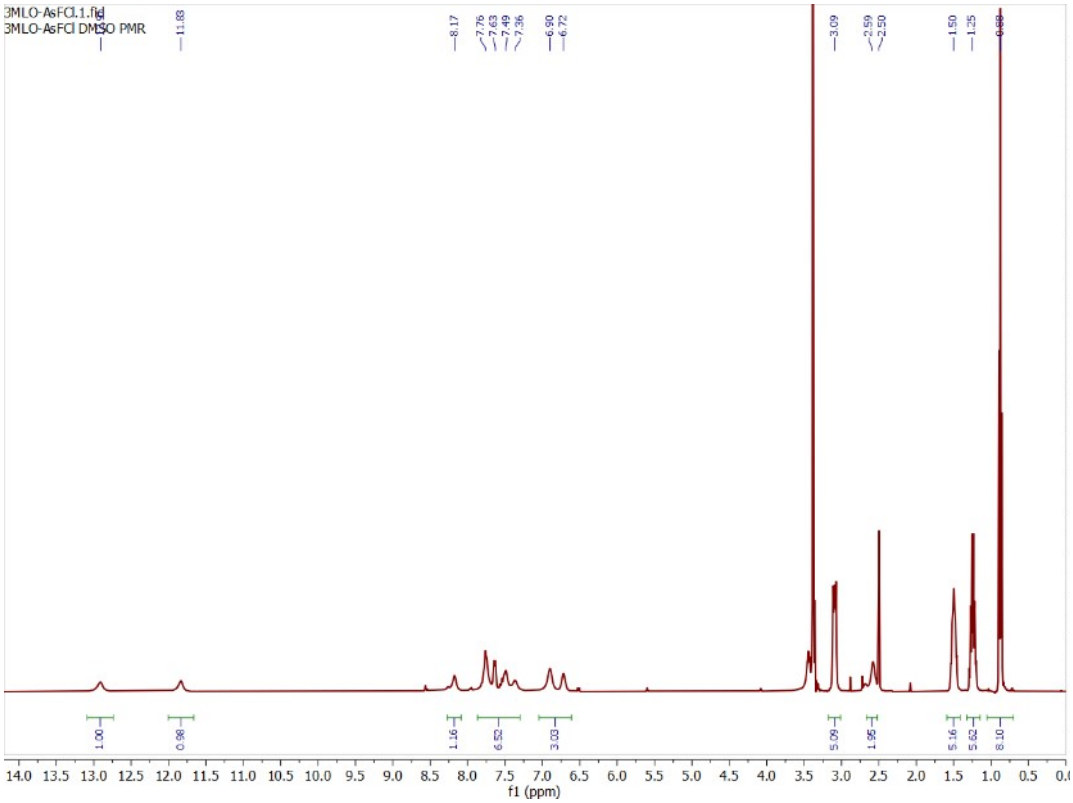

Fig. S23. ^{1}H-NMR spectrum of the arsenate complex (DMSO-d_6) extracted in the presence of NaF and NaCl.

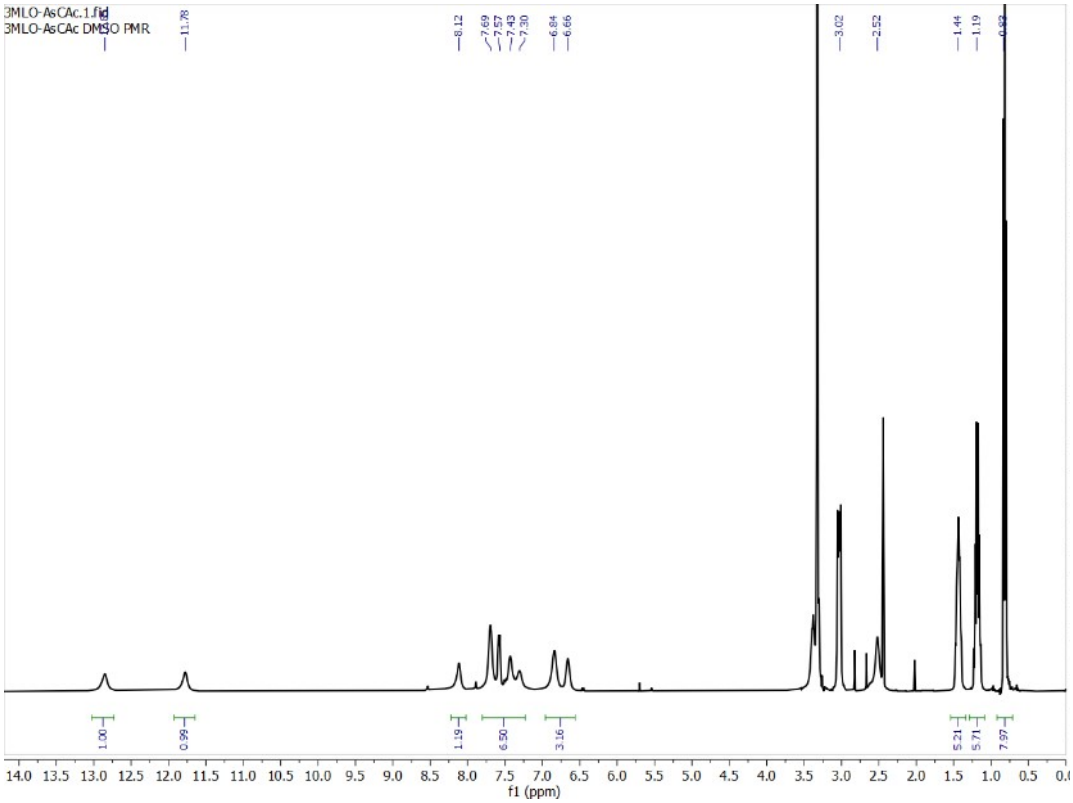

Fig. S24. ^{1}H-NMR spectrum of the arsenate complex extracted in the presence of Na_2CO_3 and $NaCH_3CO_2$.

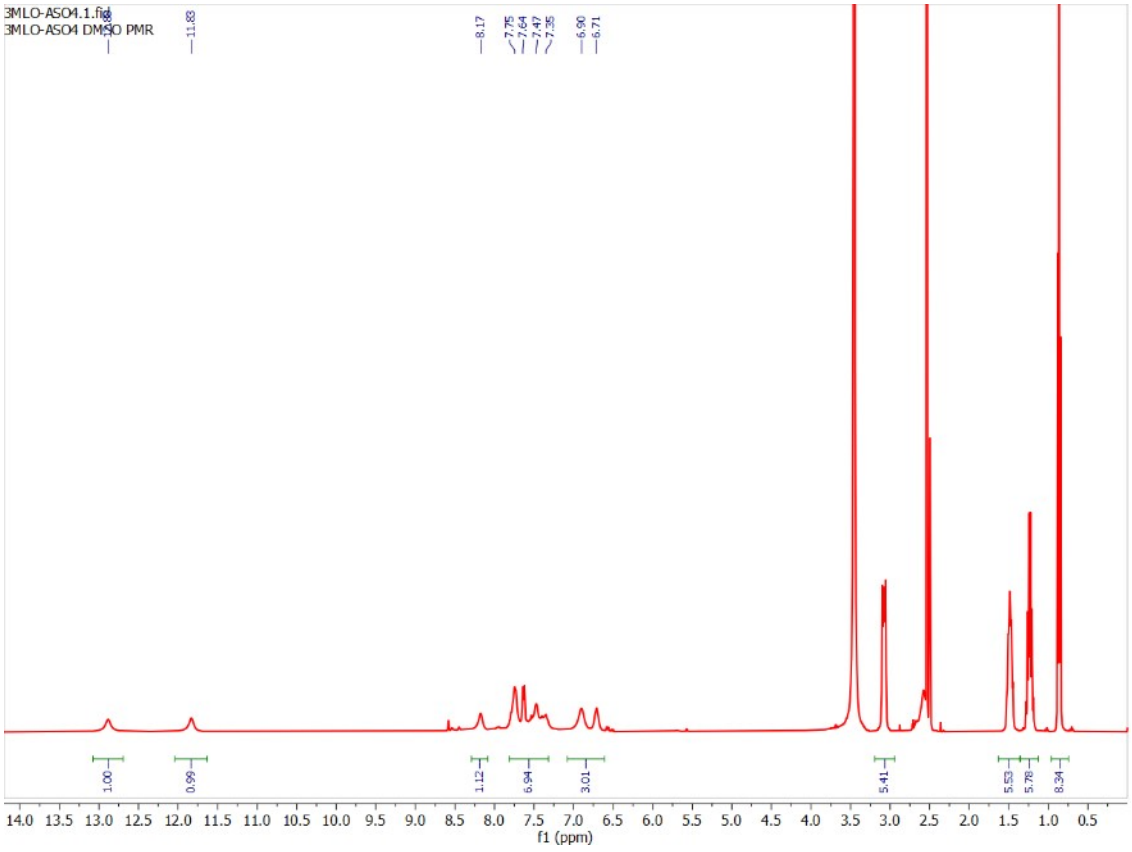

Fig. S25. ^{1}H-NMR spectrum of the arsenate complex (DMSO-d_6) extracted in the presence of Na_2SO_4 and $NaNO_3$.

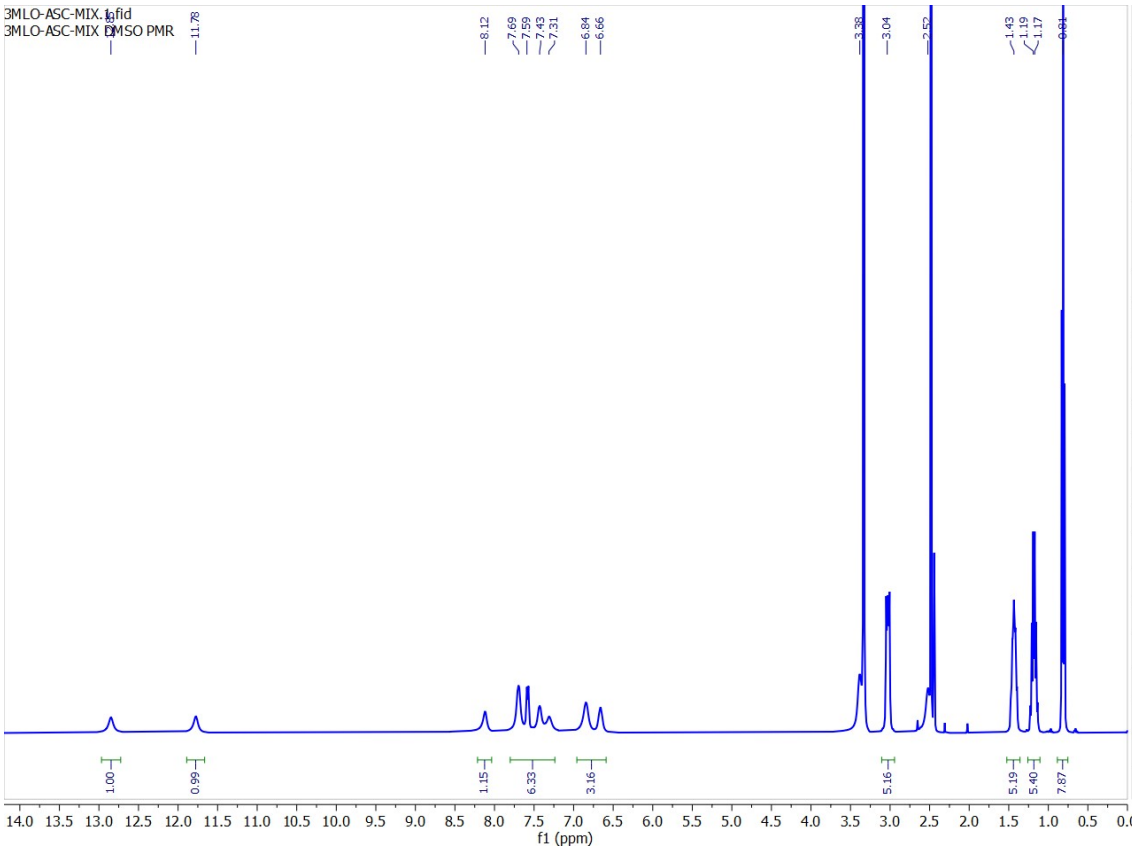

Fig. S26. ^{1}H-NMR spectrum of recrystallized arsenate complex (DMSO-d_6) extracted in the presence of Na_2HPO_4.

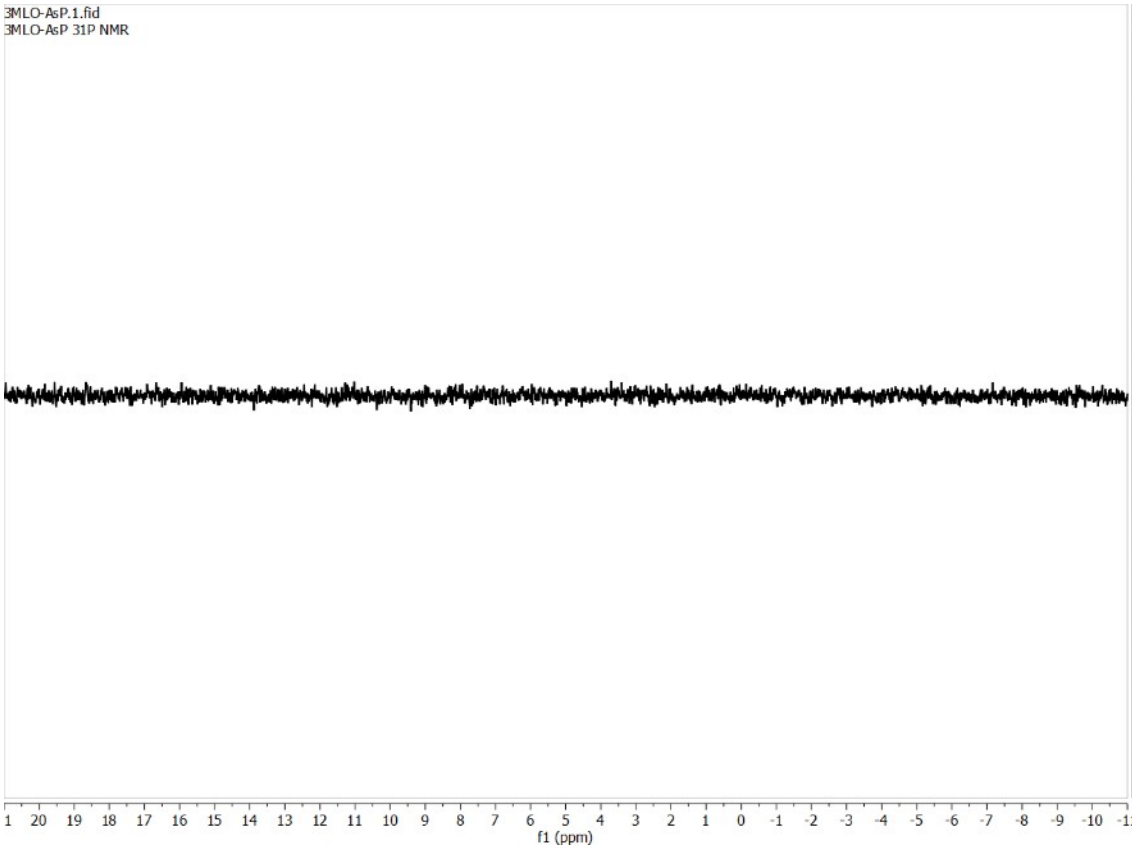

Fig. S27. ^{31}P-NMR spectrum of the arsenate complex (DMSO-d_6) extracted in the presence of Na_2HPO_4 showing the absence of phosphate signal at 8.1 ppm observed in the phosphate complex (see Fig. S8).

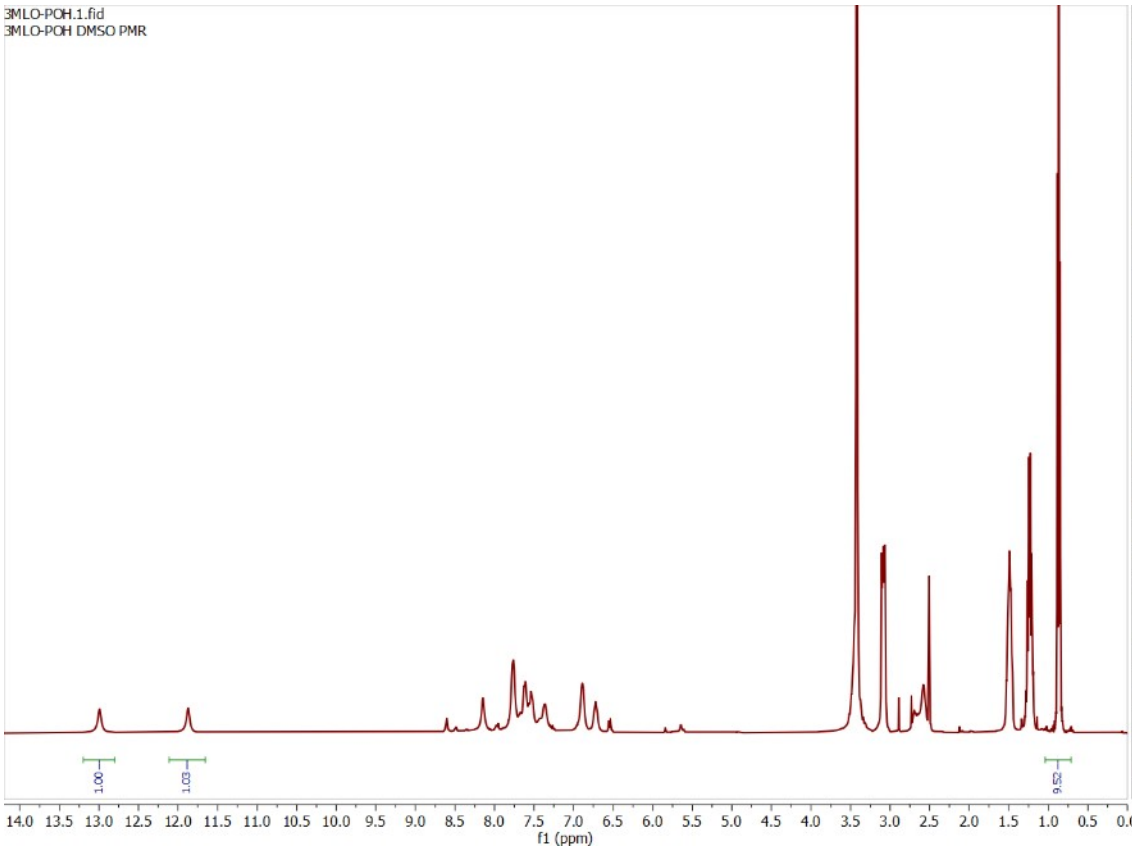

Fig. S28. ^{1}H-NMR spectrum of the phosphate complex (DMSO-d_6) extracted in the absence of competitive anions.

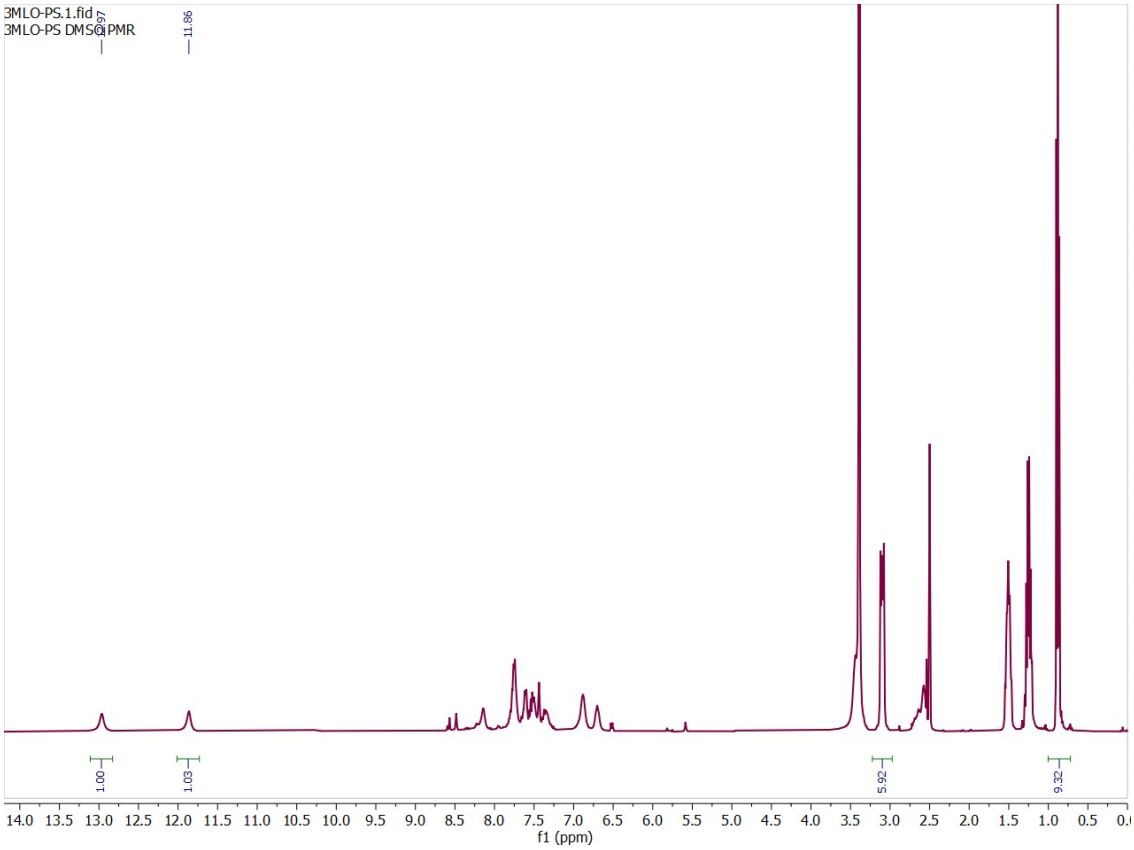

Fig. S29. ^{1}H-NMR spectrum of phosphate complex (DMSO-d_6) extracted in the presence of Na_2SO_4 and $NaNO_3$.

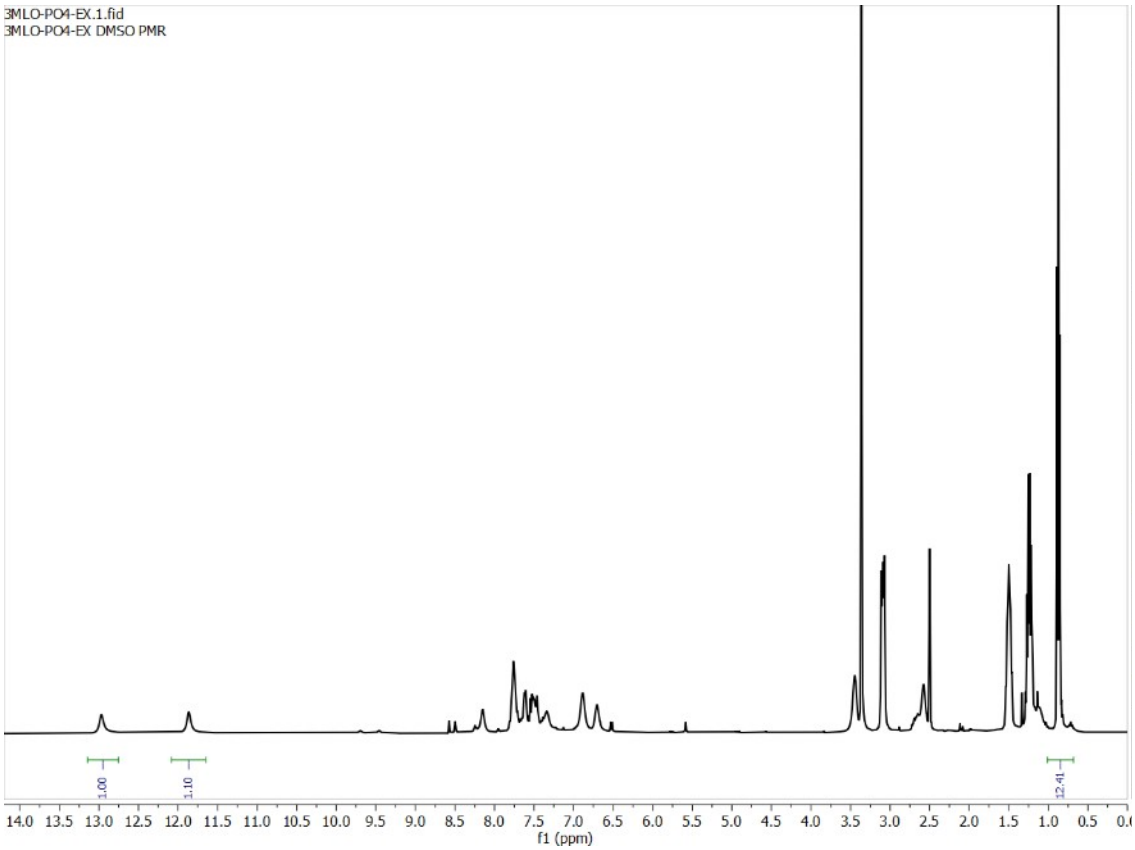

Fig. S30. ^{1}H-NMR spectrum of the phosphate complex (DMSO-d_6) extracted in the presence of NaF and NaCl.

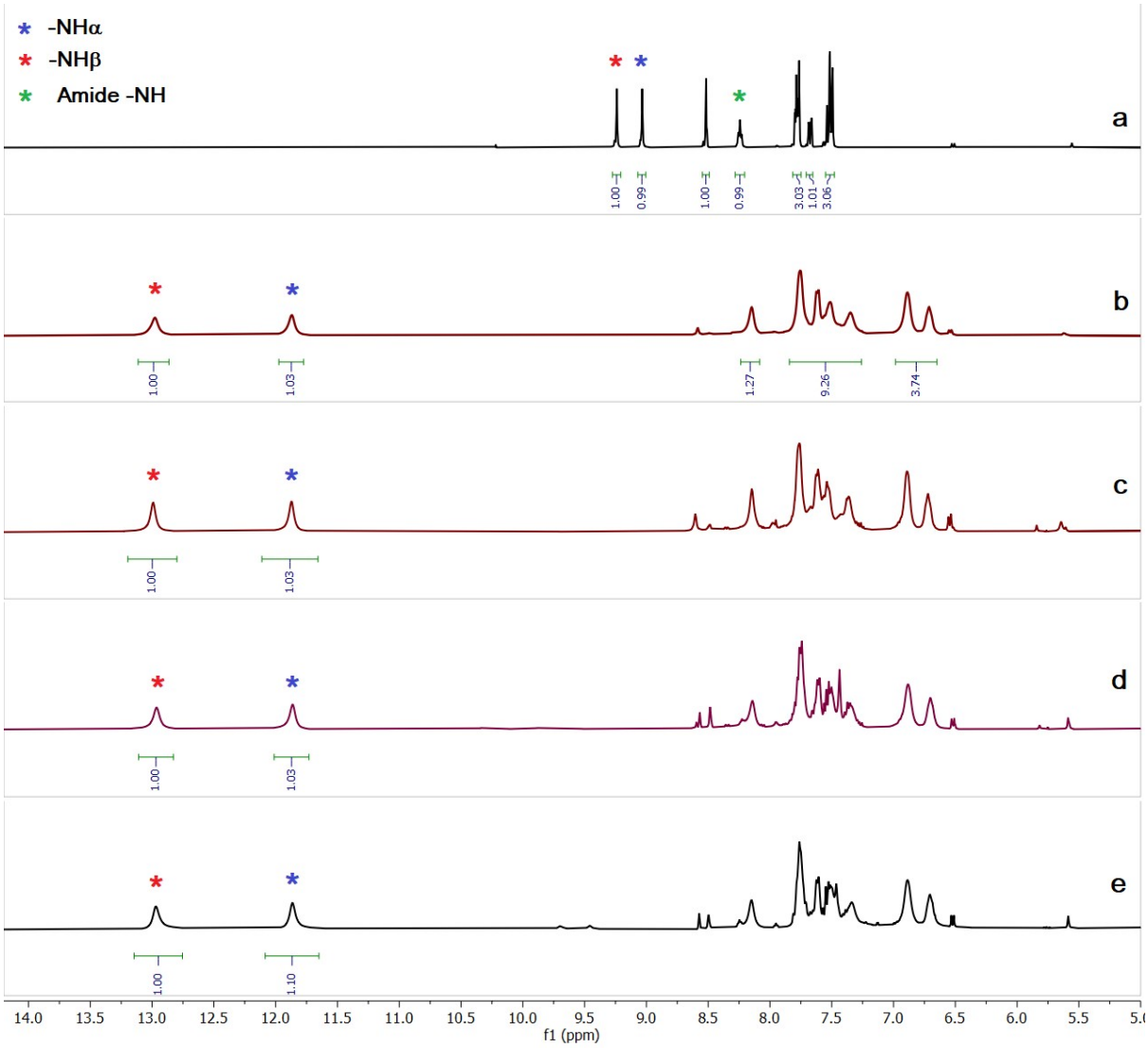

Fig. S31. Aromatic region of the ^{1}H-NMR spectra of (a) receptor **L**, (b) crystals of the phosphate complex [(n-$Bu_4N)_3$(2**L**·PO_4)], (c) phosphate complex extracted in the absence of competitive anions, (d) phosphate complex extracted in the presence of sulfate and nitrate, (e) phosphate complex extracted in the presence of fluoride and chloride.

6. 2D-NOESY NMR, powder XRD and UV-vis spectra of Arsenate and Phosphate complexes.

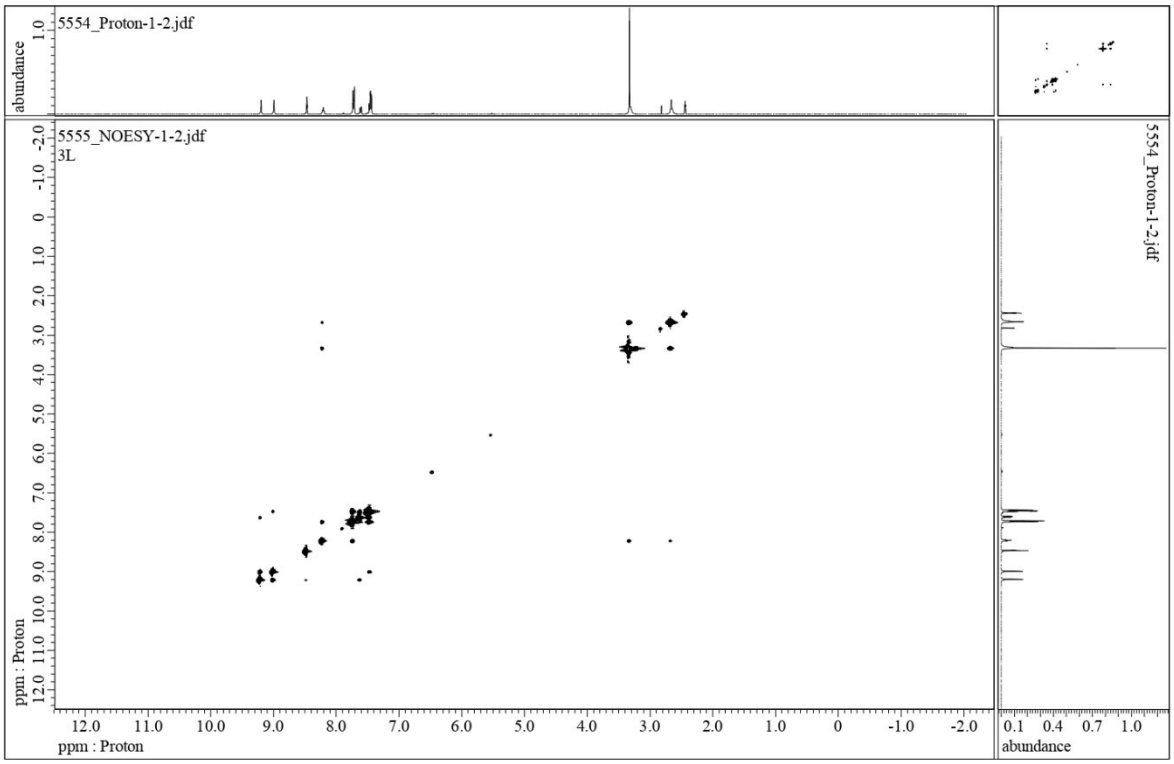

Fig. S32. 2D-NOESY NMR spectrum of receptor **L** in DMSO-d_6.

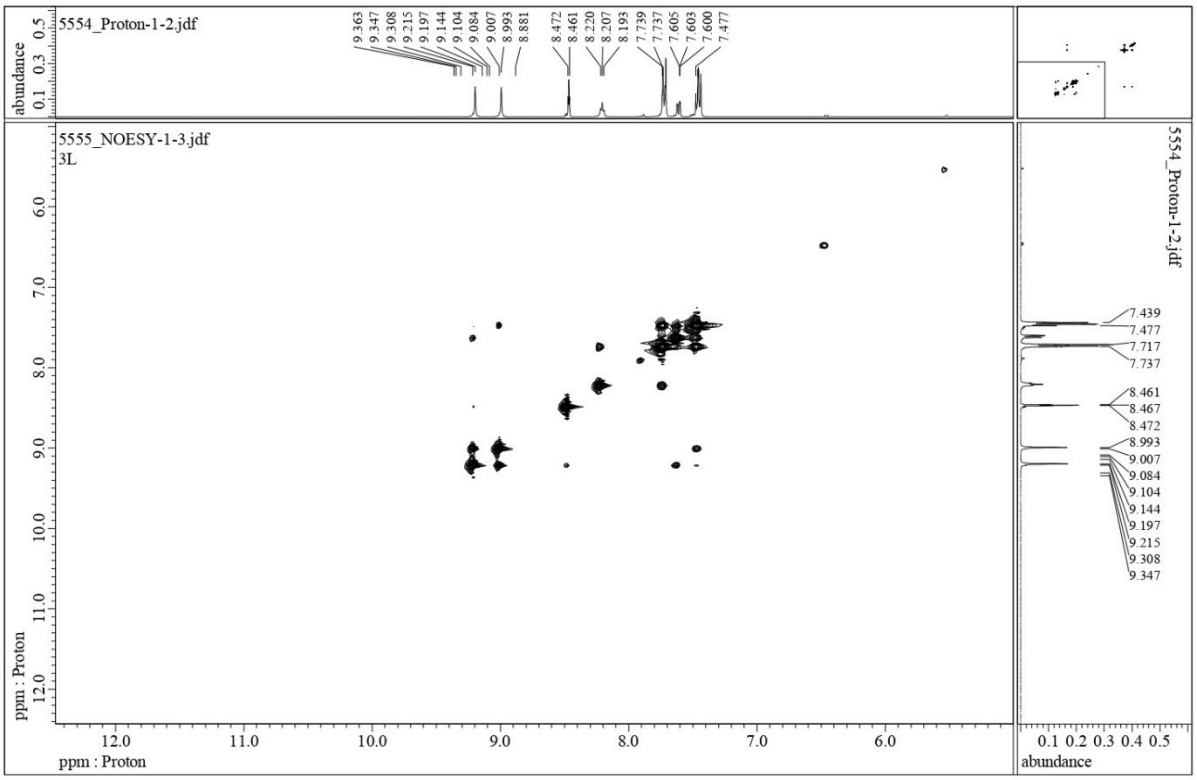

Fig. S33. Aromatic region of the 2D-NOESY NMR spectrum of receptor **L** in DMSO-d_6.

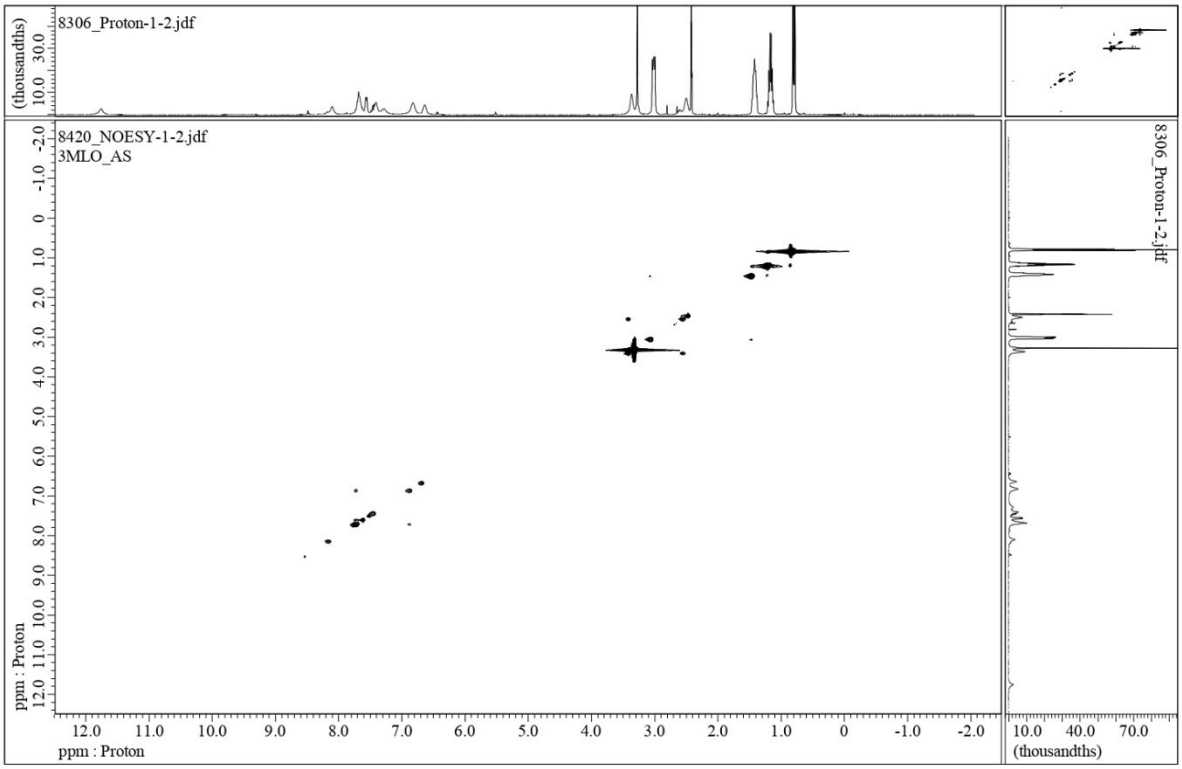

Fig. S34. 2D-NOESY NMR spectrum of the arsenate complex $[(n\text{-}Bu_4N)_3{\cdot}(2\mathbf{L}{\cdot}AsO_4)]$ in DMSO-d_6.

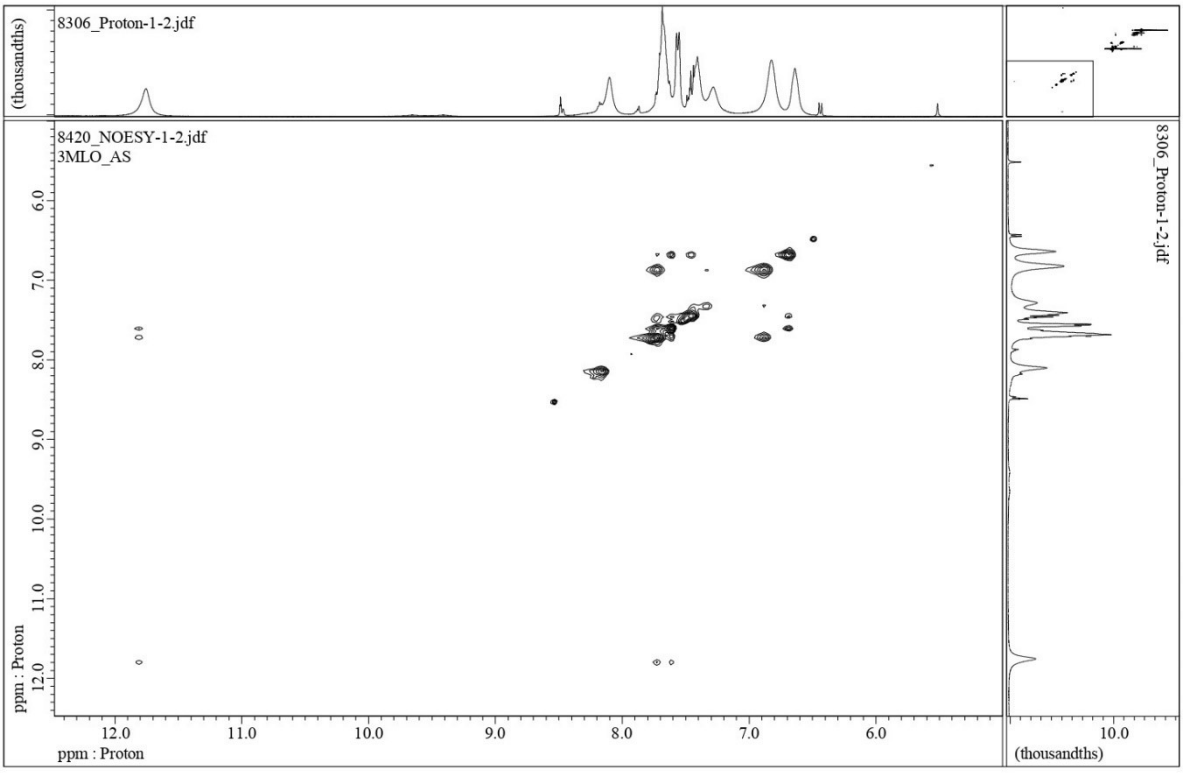

Fig. S35. Aromatic region of the 2D-NOESY NMR spectrum of the arsenate complex $[(n\text{-}Bu_4N)_3{\cdot}(2\mathbf{L}{\cdot}AsO_4)]$ in DMSO-d_6.

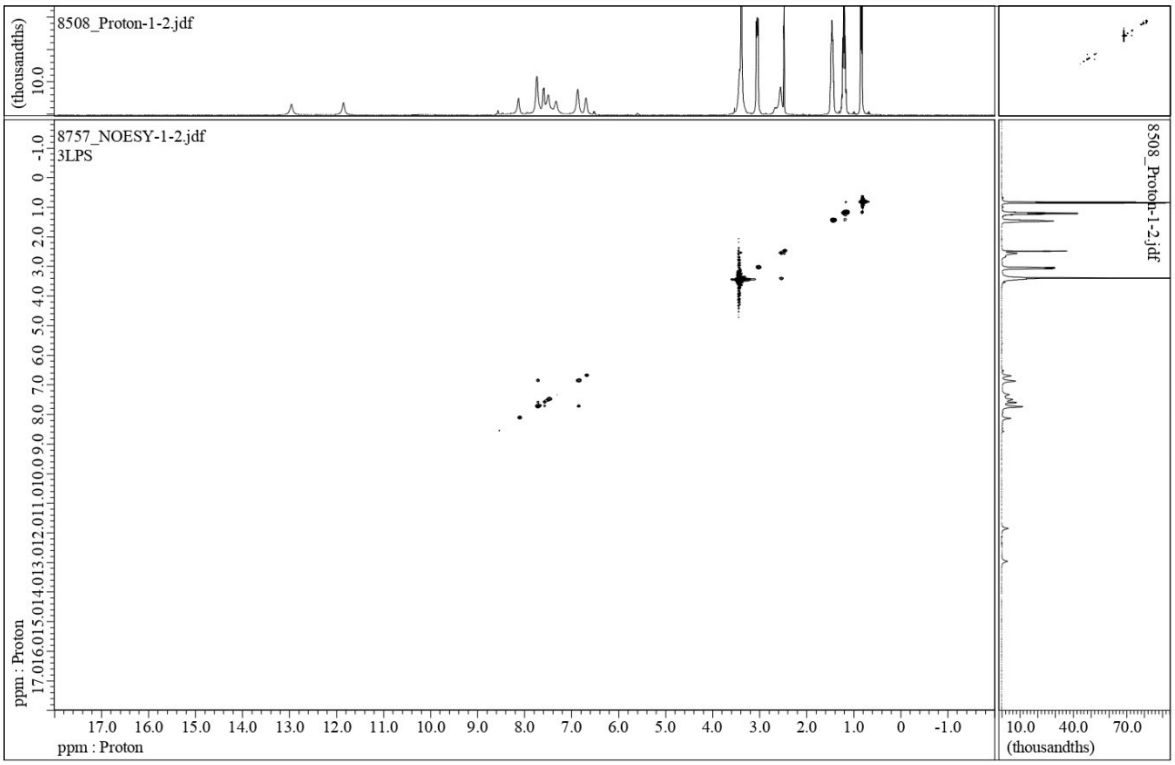

Fig. S36. 2D-NOESY NMR spectrum of the phosphate complex $[(n\text{-}Bu_4N)_3{\cdot}(2\mathbf{L}{\cdot}PO_4)]$ in DMSO-d_6.

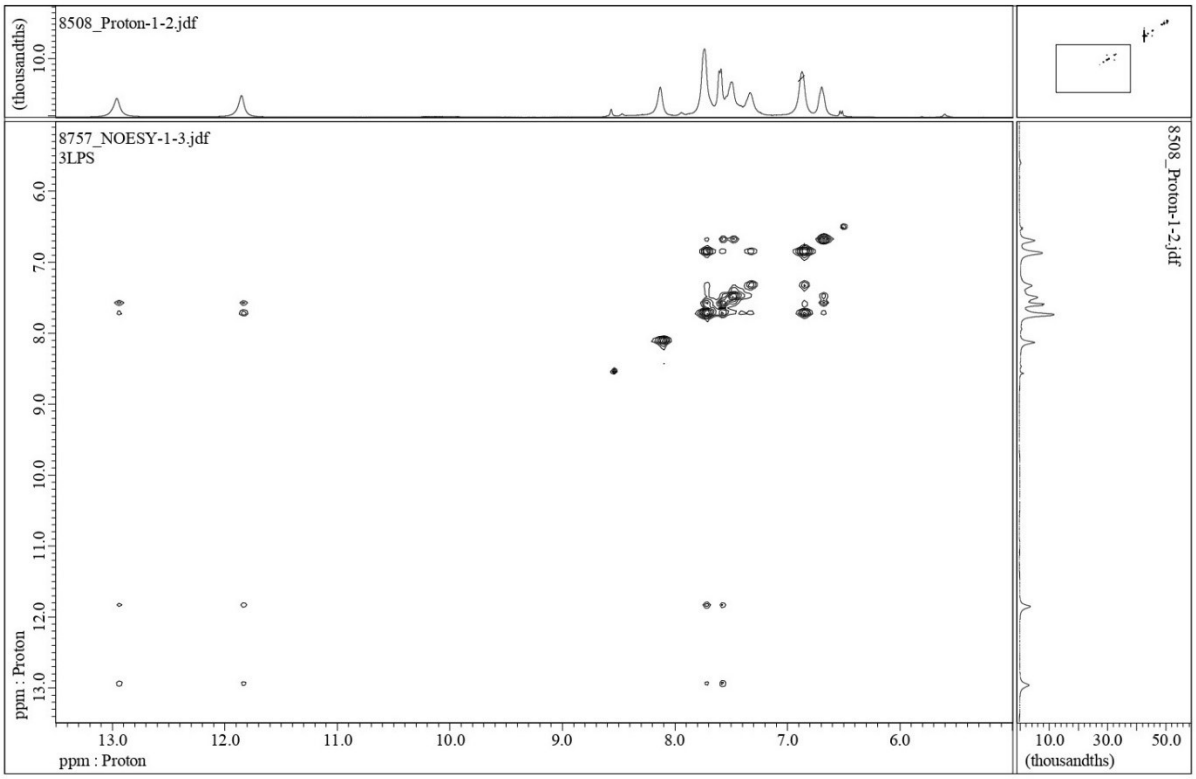

Fig. S37. Aromatic region of the 2D-NOESY NMR spectrum of the phosphate complex $[(n\text{-}Bu_4N)_3{\cdot}(2\mathbf{L}{\cdot}PO_4)]$ in DMSO-d_6.

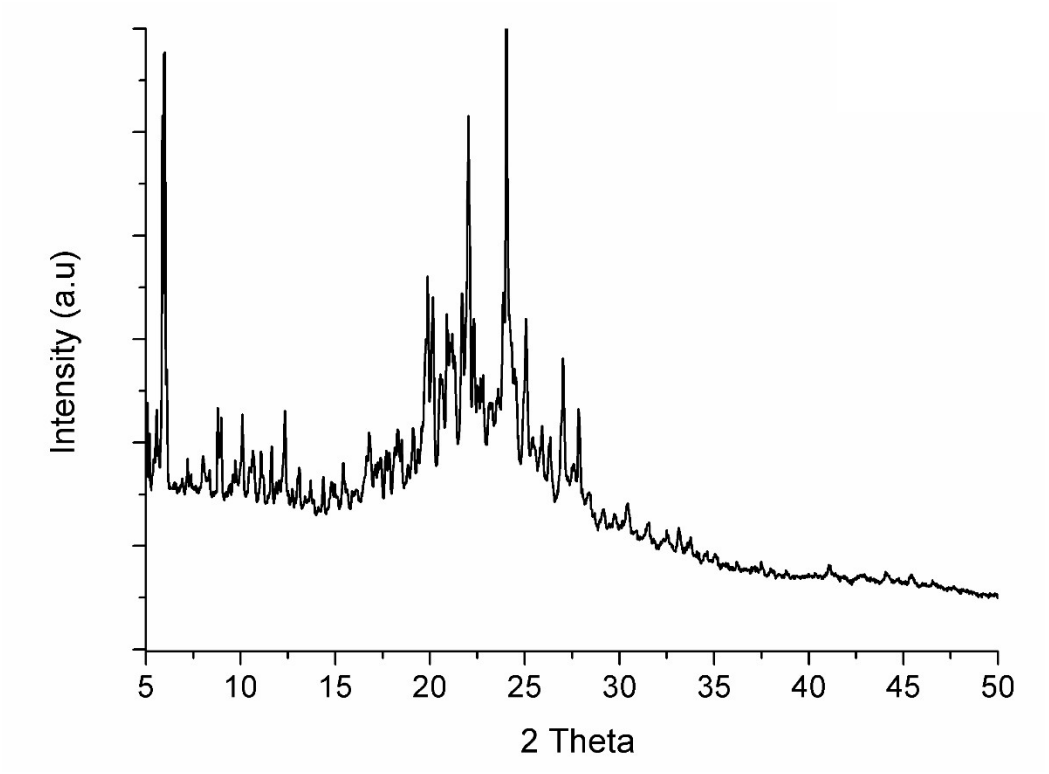

Fig. S38. Powder X-ray diffraction patterns of the bulk crystals of arsenate complex $[(n\text{-}Bu_4N)_3\cdot(2\mathbf{L}\cdot AsO_4)]$ (dried) obtained from a DMSO solution under ambient conditions.

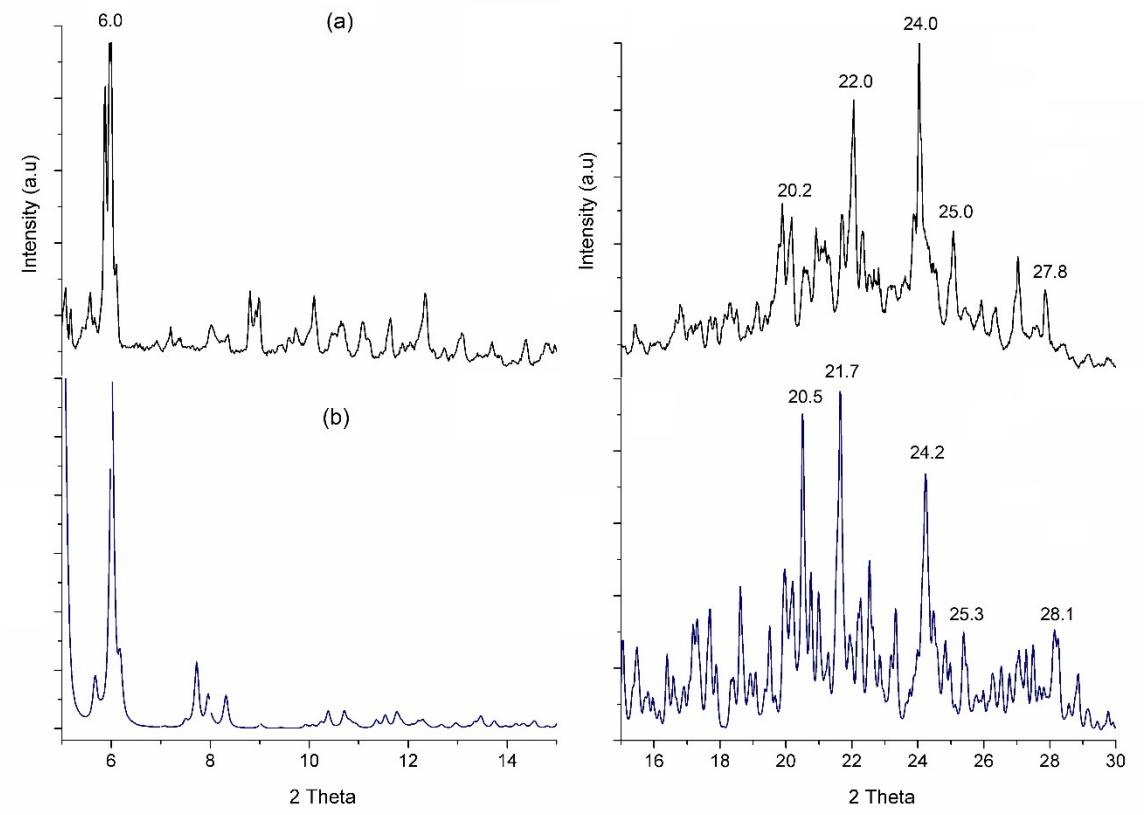

Fig. S39. Powder X-ray diffraction patterns of the bulk crystals of arsenate complex $[(n\text{-}Bu_4N)_3\cdot(2\mathbf{L}\cdot AsO_4)]$ (a, black) and simulated powder X-ray diffraction patterns of the crystal structure $[(n\text{-}Bu_4N)_3(2\mathbf{L}\cdot AsO_4)]$ (b, blue) separately shown in the 2θ region of 5−15 and 15−30.

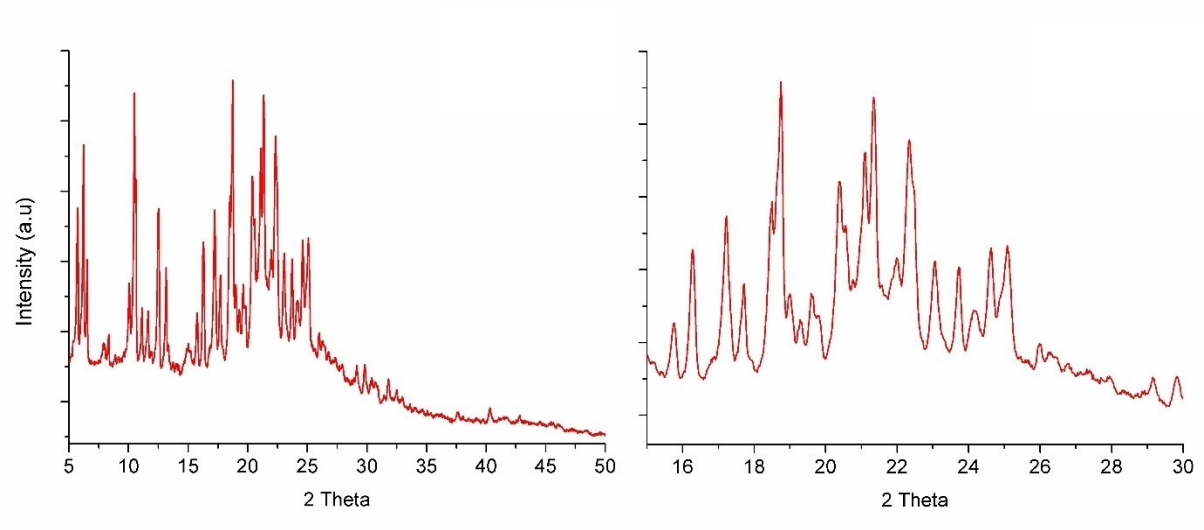

Fig. S40. Powder X-ray diffraction patterns of the bulk crystals of phosphate complex (dried) obtained from a DMSO solution under ambient conditions.

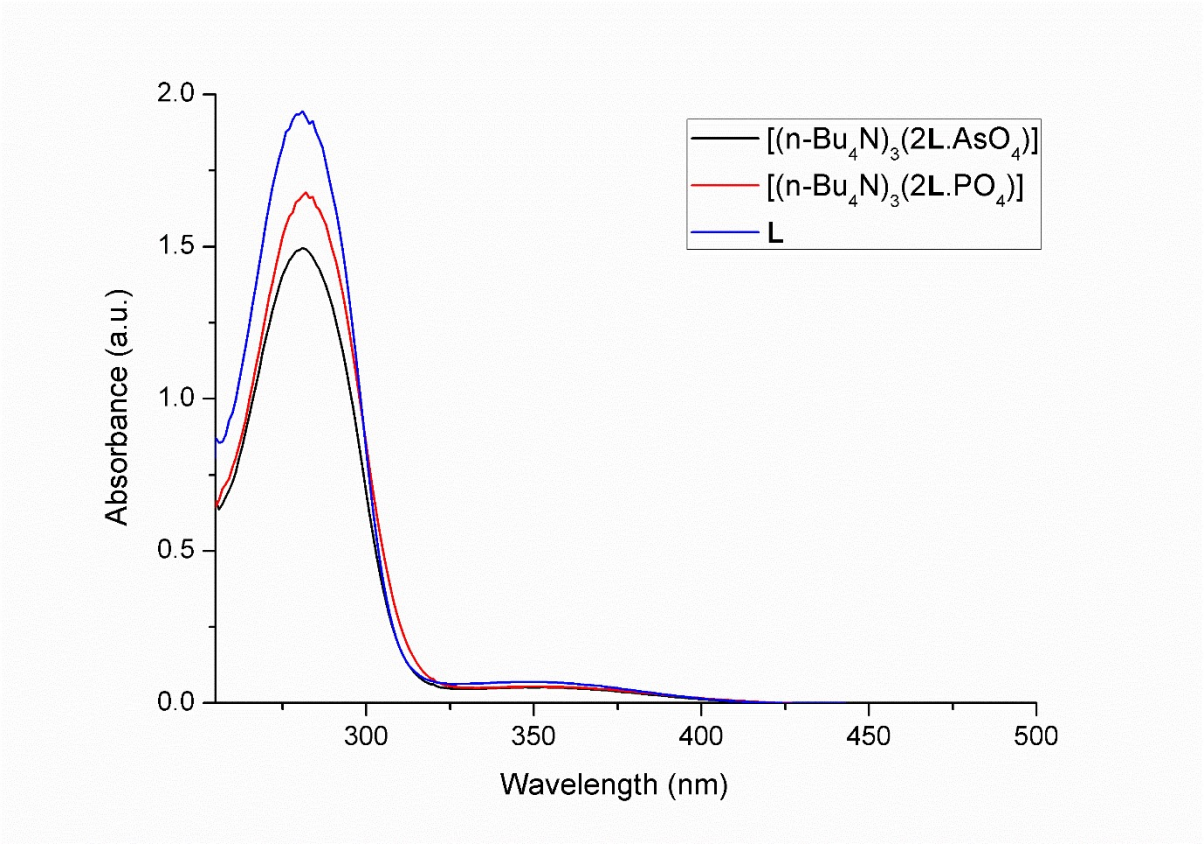

Fig. S41. UV-vis spectra of **L** and oxoanion (arsenate and phosphate) complexes in DMSO.

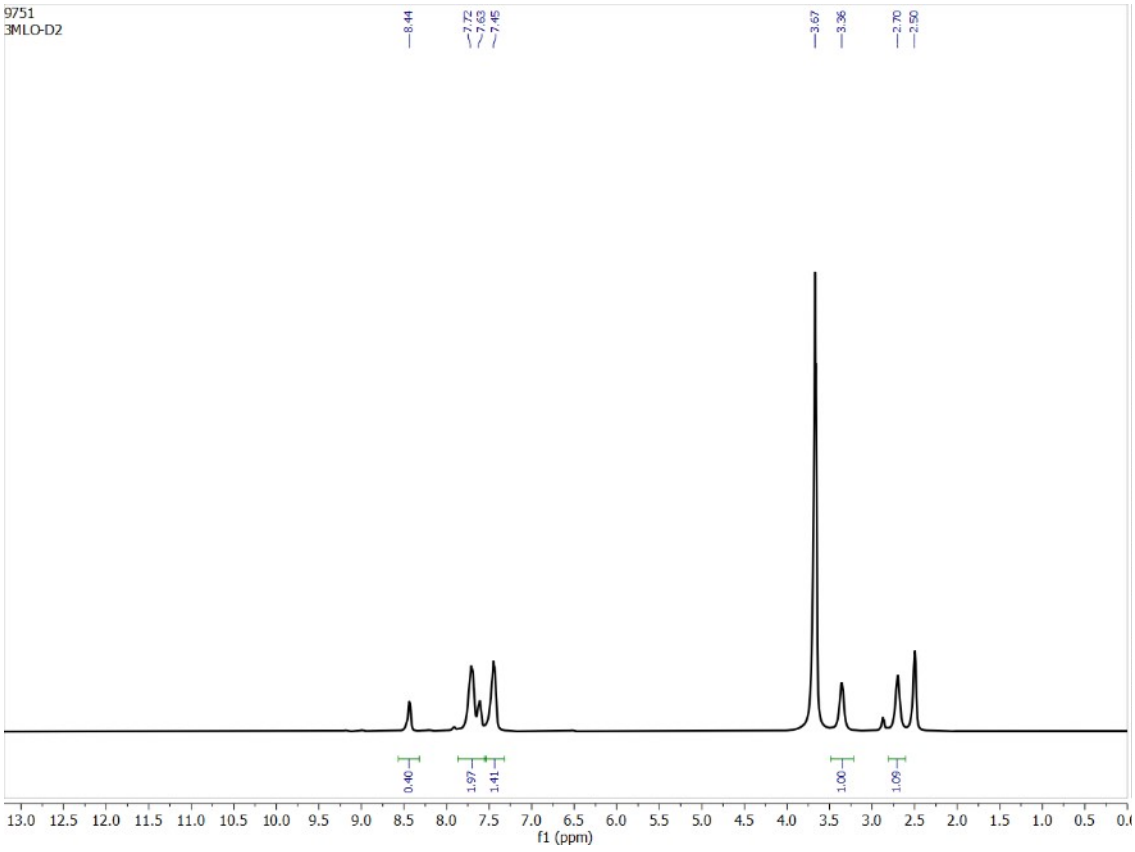

Fig. S42. ^{1}H-NMR spectrum of the receptor **L** in DMSO-d_6/D_2O (9:1, v/v) solution.

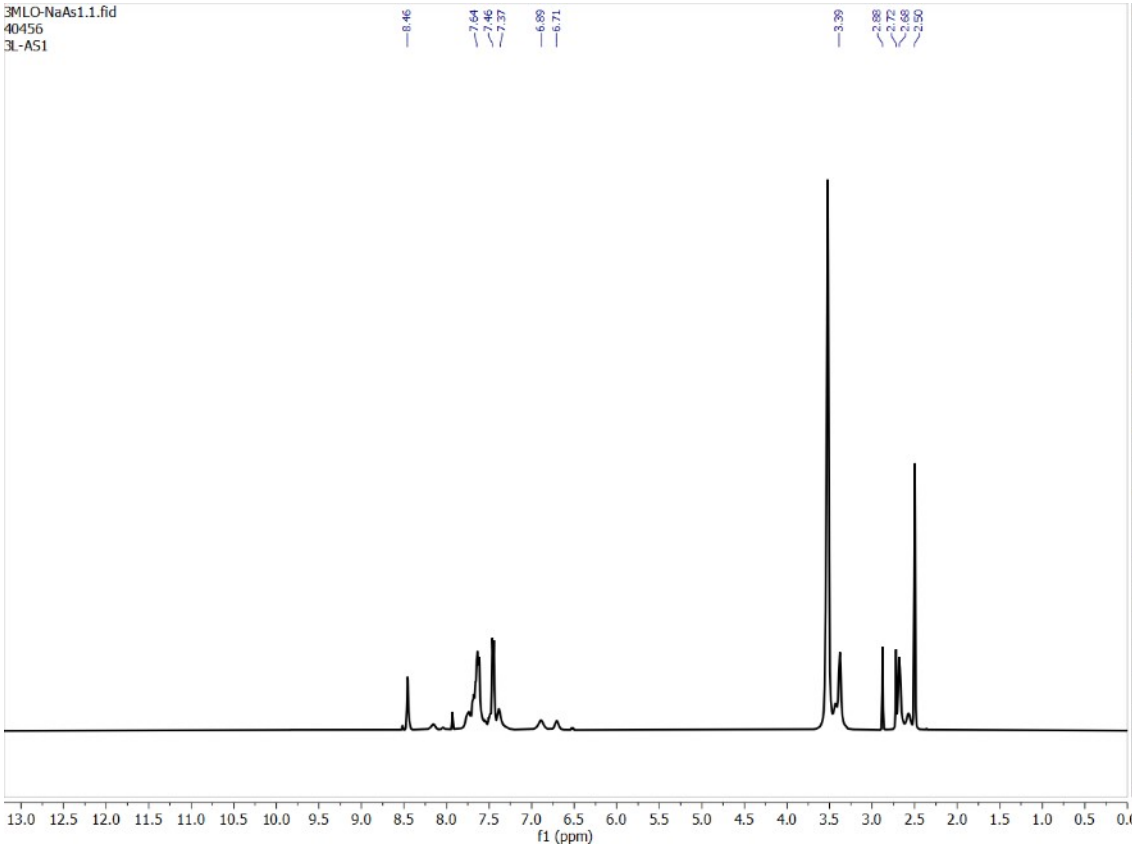

Fig. S43. ^{1}H-NMR spectrum of **L** upon addition of 0.5 equiv. of Na_2HAsO_4 solution in DMSO-d_6/D_2O (9:1, v/v).

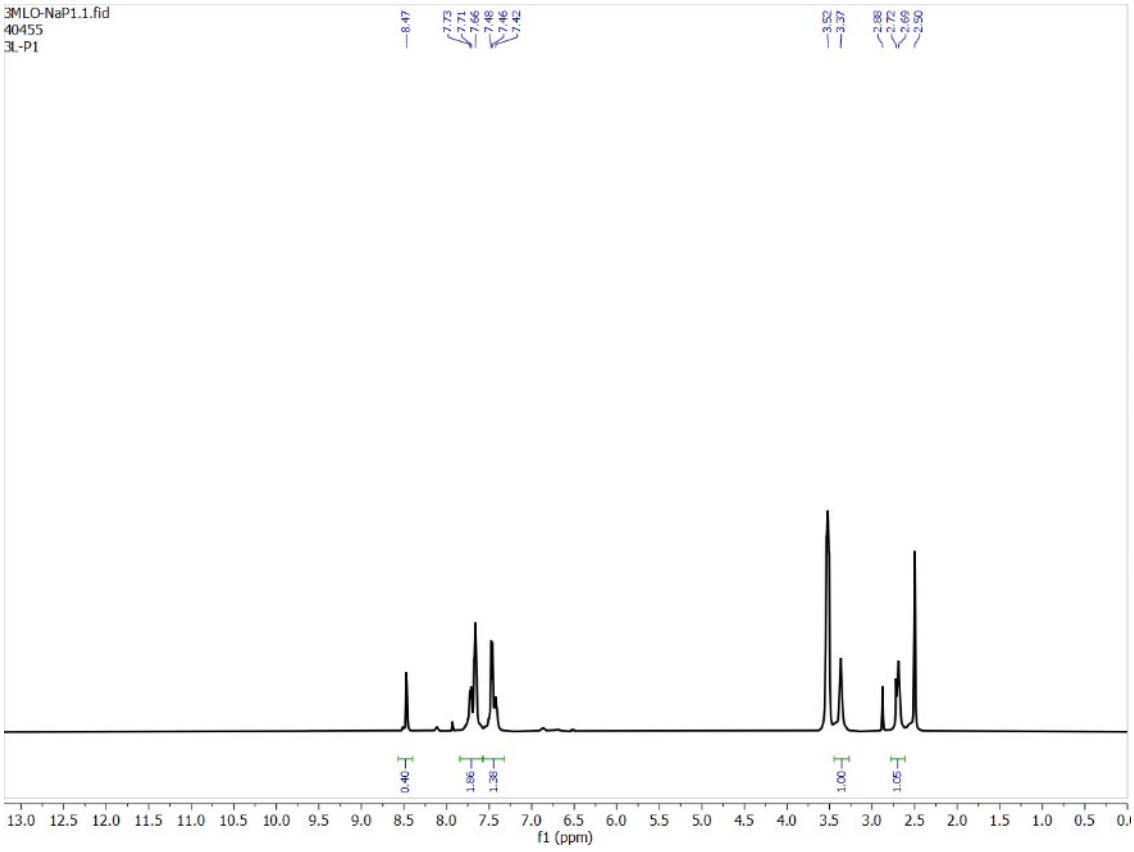

Fig. S44. ^{1}H-NMR spectrum of **L** upon addition of 0.5 equiv. of Na_2HPO_4 solution in DMSO-d_6/D_2O (9:1, v/v).

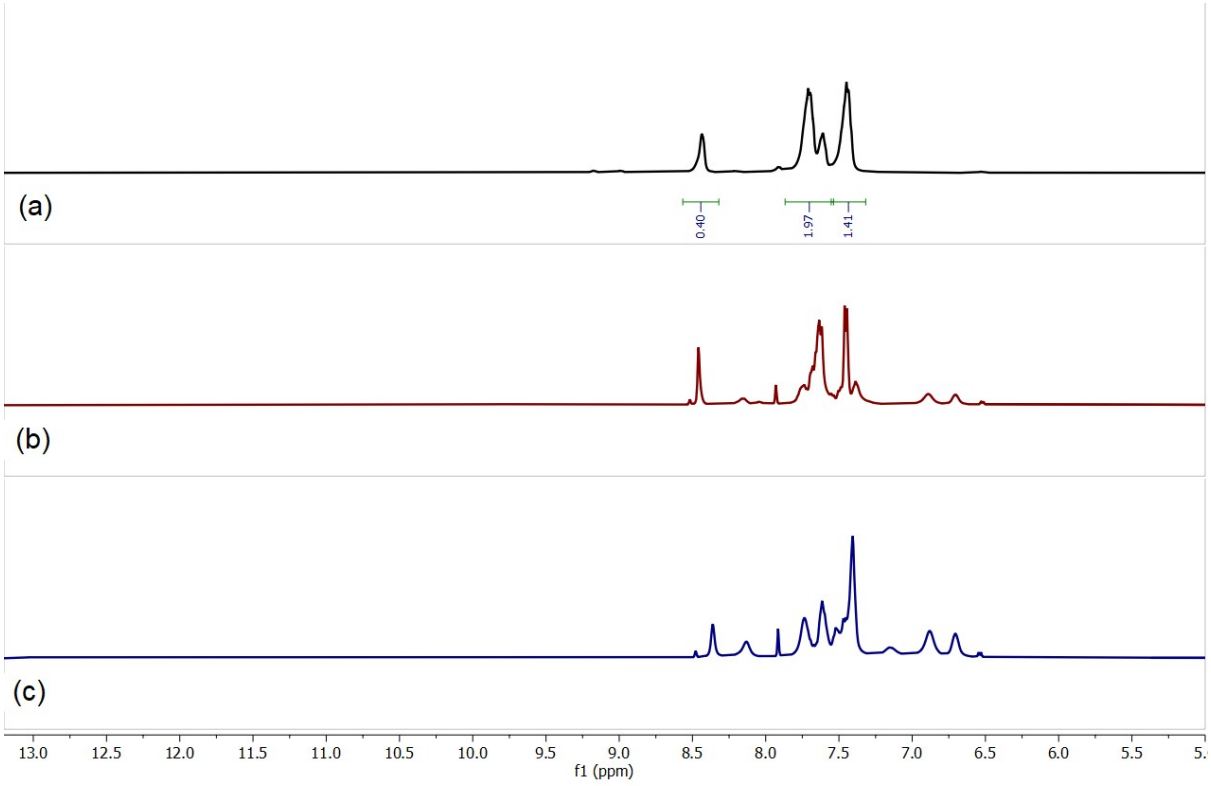

Fig. S45. ^{1}H-NMR spectrum of (a) receptor **L** (b) **L** upon addition of 0.5 equivalent of Na_2HAsO_4 and (c) **L** upon addition of 1.0 equivalent of Na_2HAsO_4 in DMSO-d_6/D_2O (9:1, v/v).

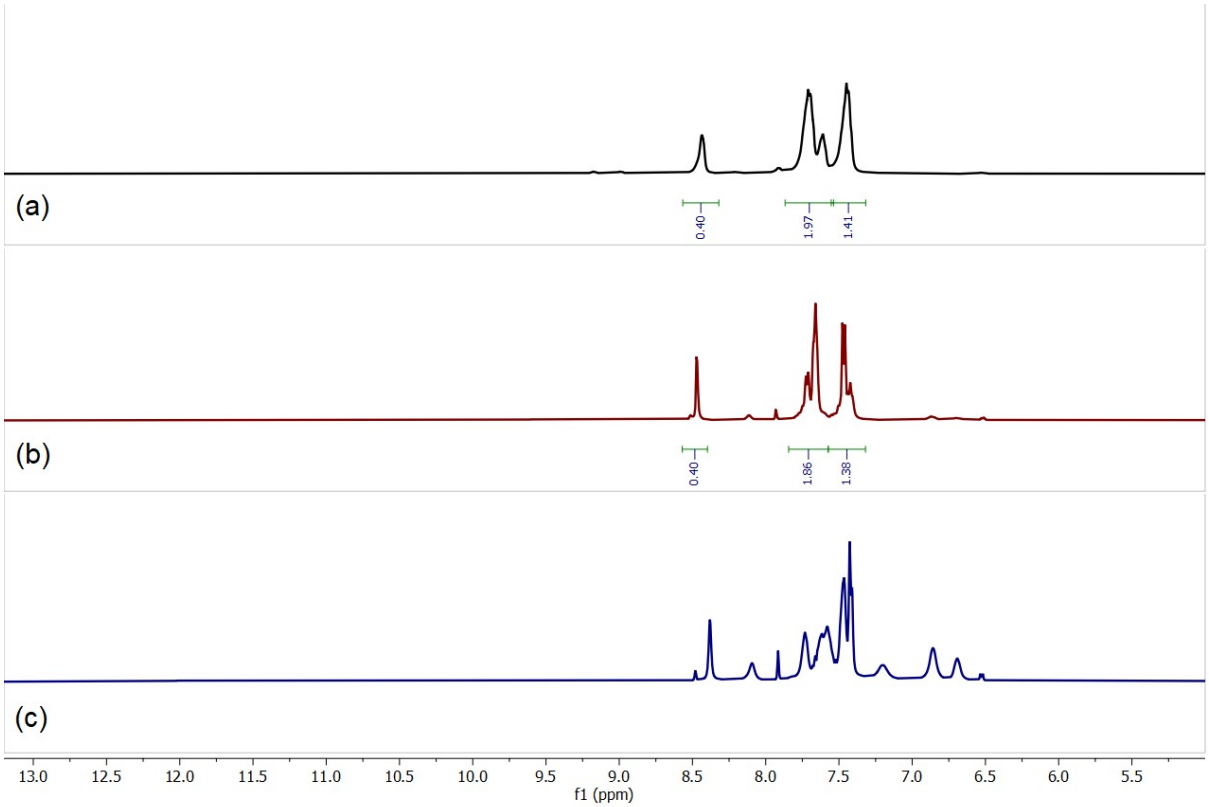

Fig. S46. ^{1}H-NMR spectrum of (a) receptor **L** (b) **L** upon addition of 0.5 equivalent of Na_2HPO_4 (c) **L** upon addition of 1.0 equivalent of Na_2HPO_4 in DMSO-D_6/D_2O (9:1, v/v).

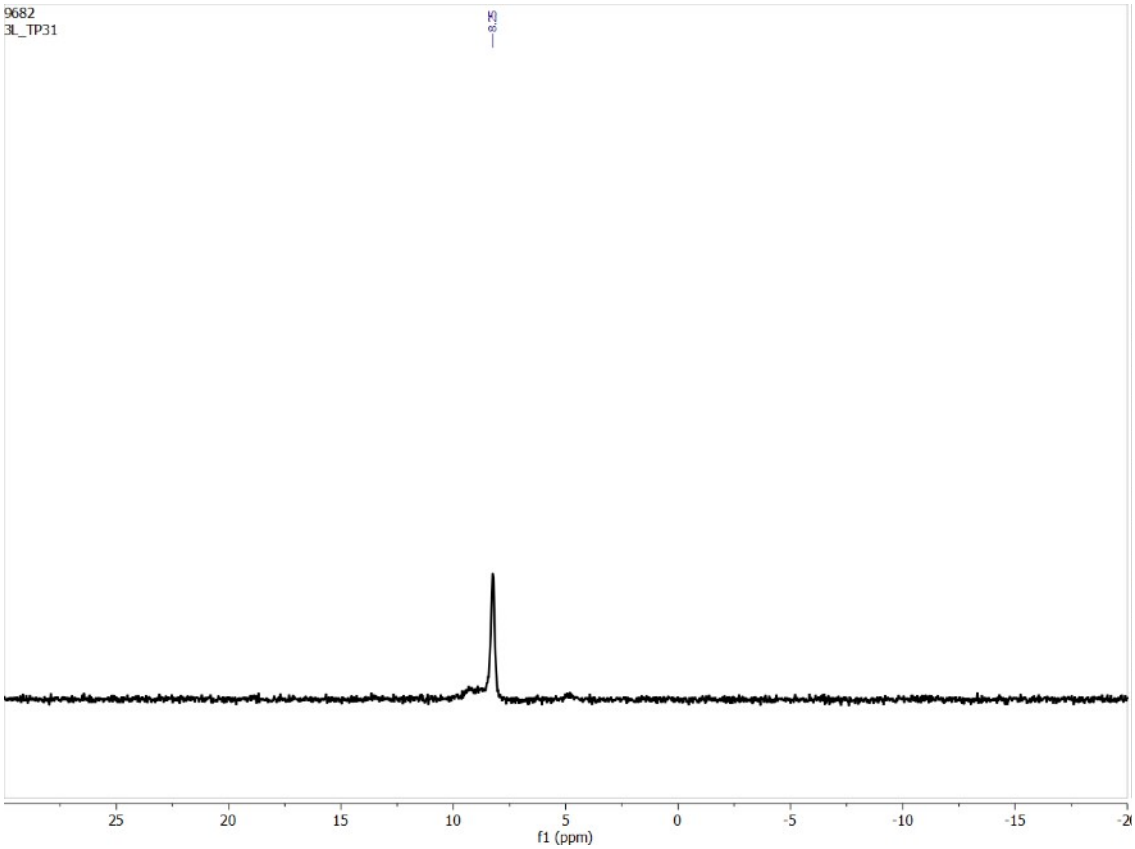

Fig. S47. ^{31}P NMR spectrum of the crystals of phosphate complex [(n-$Bu_4N)_3$·(2**L**·PO_4)] in DMSO-d_6/D_2O (9:1).

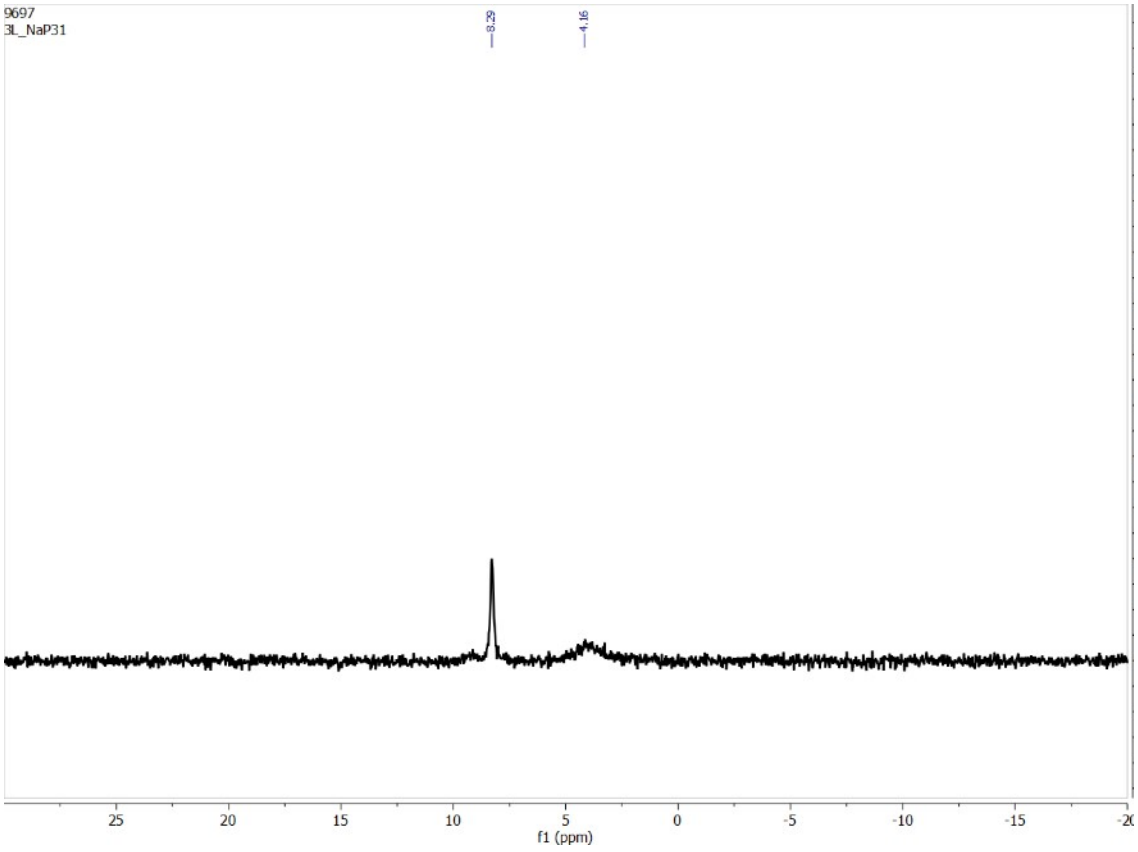

Fig. S48. ^{31}P NMR spectrum of **L** upon addition of 1.0 equivalent of Na_2HPO_4 in DMSO-d_6/D_2O (9:1, v/v).

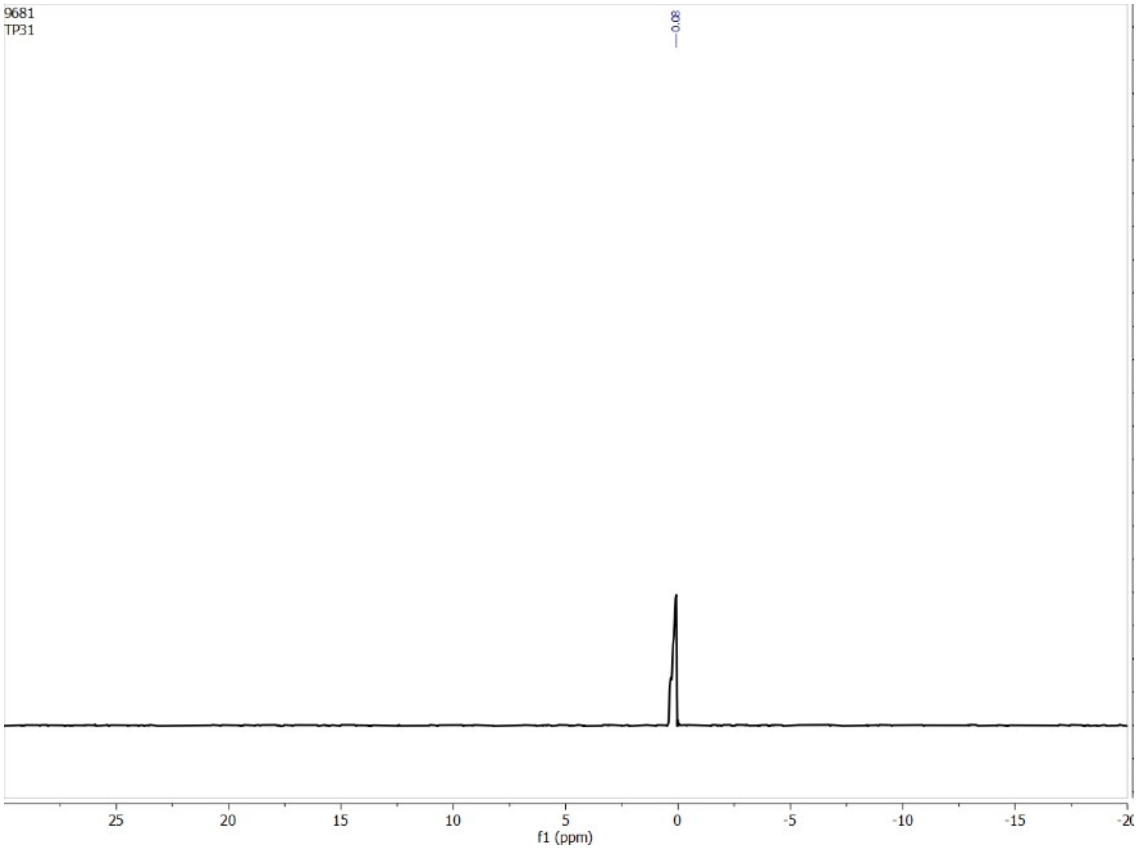

Fig. S49. ^{31}P NMR spectrum of (n-Bu_4N^+)$H_2PO_4^-$ in DMSO-d_6/D_2O (9:1, v/v).

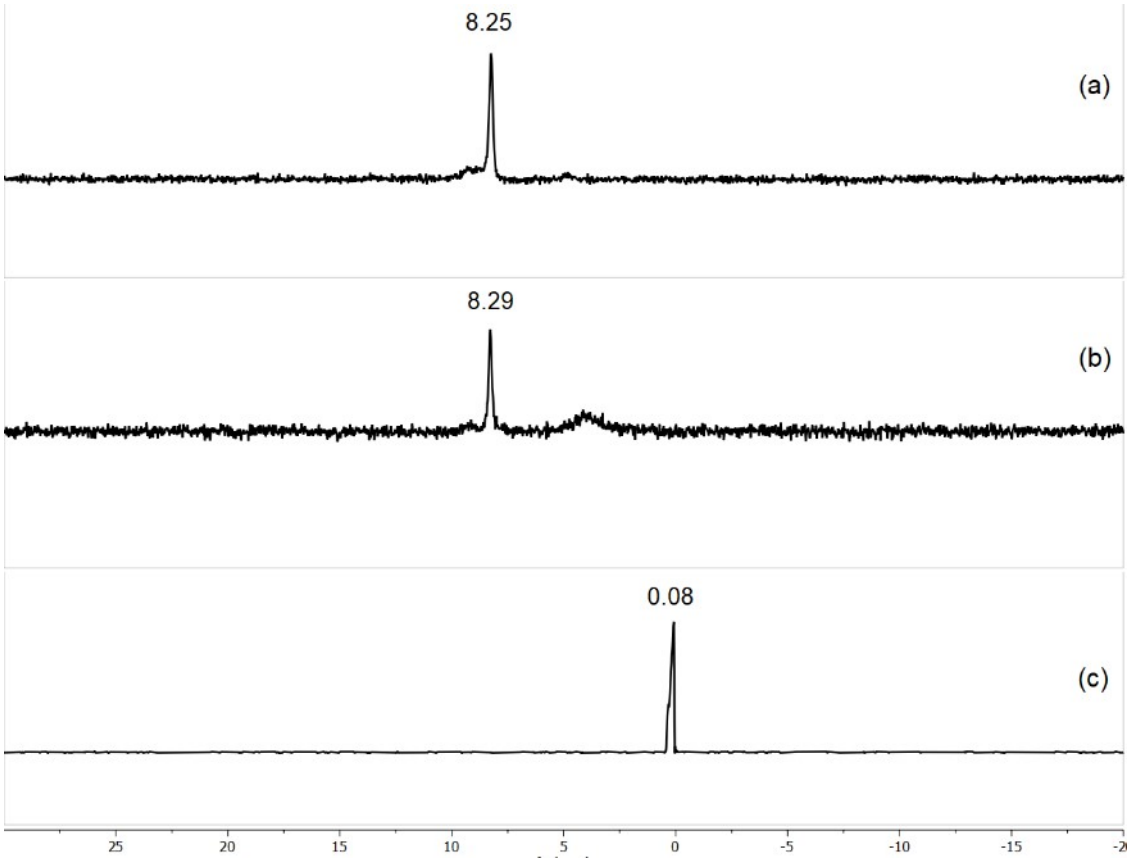

Fig. S50. ^{31}P NMR spectrum of (a) crystals of phosphate complex, (b) **L** in the presence of 1.0 equivalent of (n-Bu_4N^+)$H_2PO_4^-$ and (c) (n-Bu_4N^+)$H_2PO_4^-$ in DMSO-d_6/D_2O (9:1, v/v).

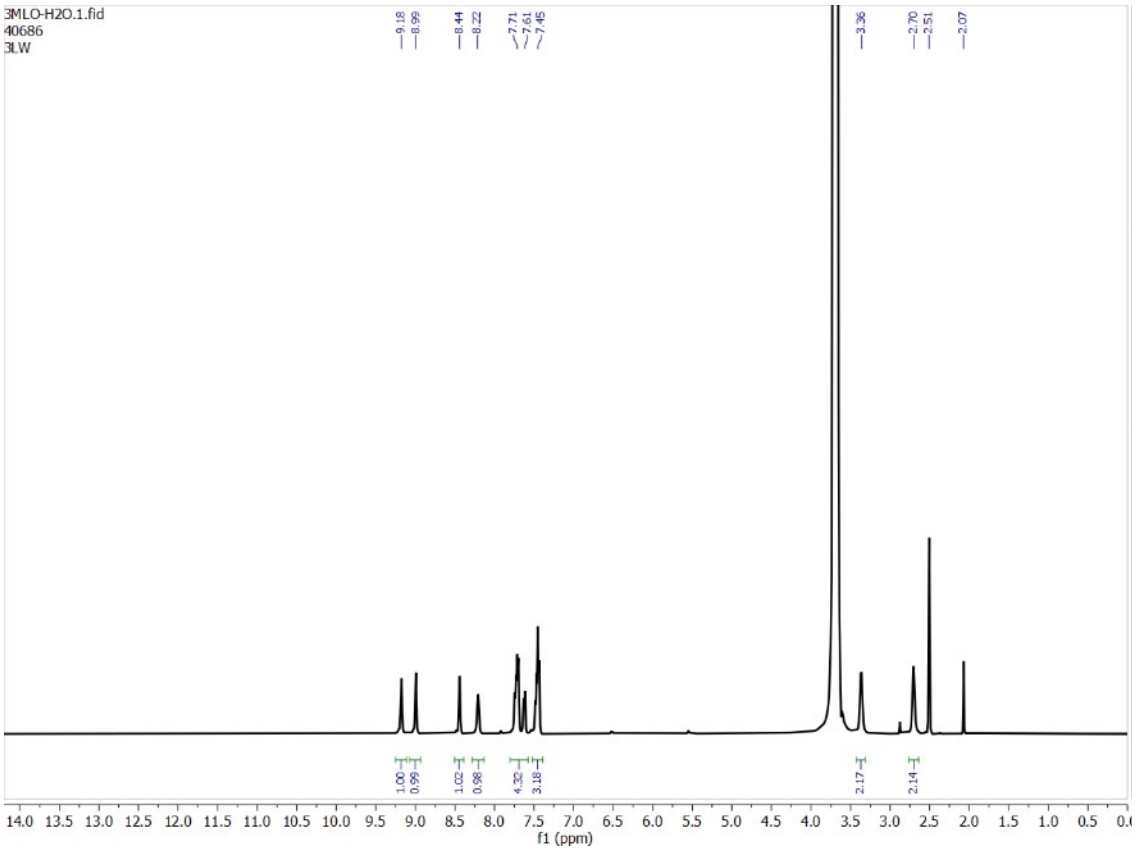

Fig. S51. ^{1}H-NMR spectrum of **L** in DMSO-d_6/H_2O (9:1, v/v).

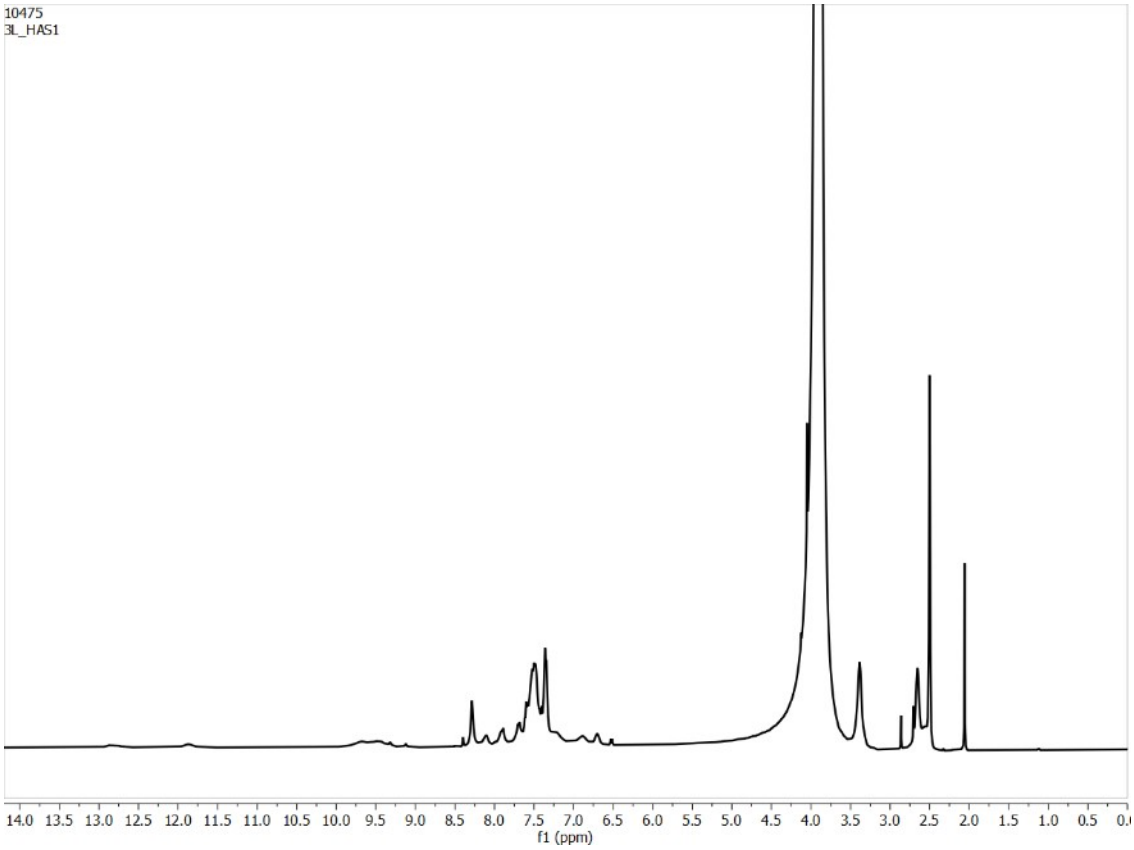

Fig. S52. ^{1}H-NMR spectrum of **L** in DMSO-d_6/H_2O (9:1, v/v) upon addition of 0.25 equiv. of Na_2HAsO_4.

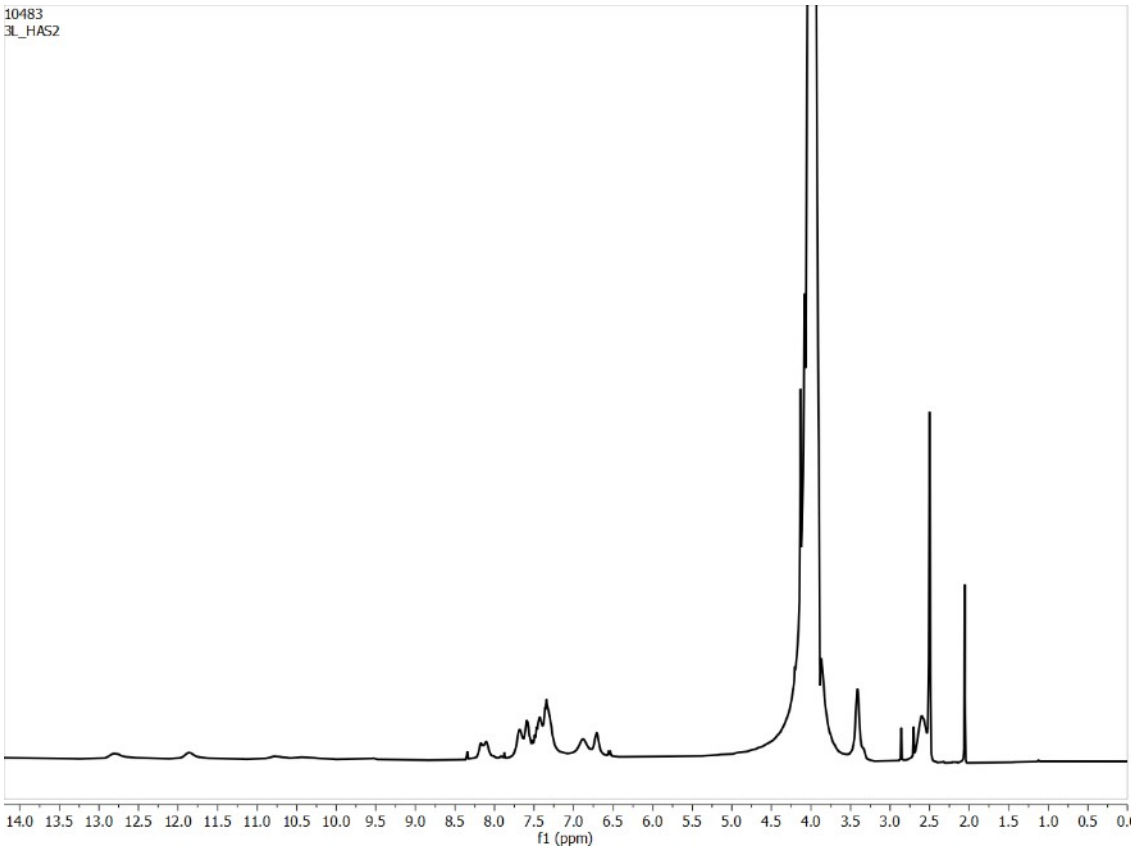

Fig. S53. ^{1}H-NMR spectrum of **L** in DMSO-d_6/H_2O (9:1, v/v) upon addition of 0.50 equiv. of Na_2HAsO_4.

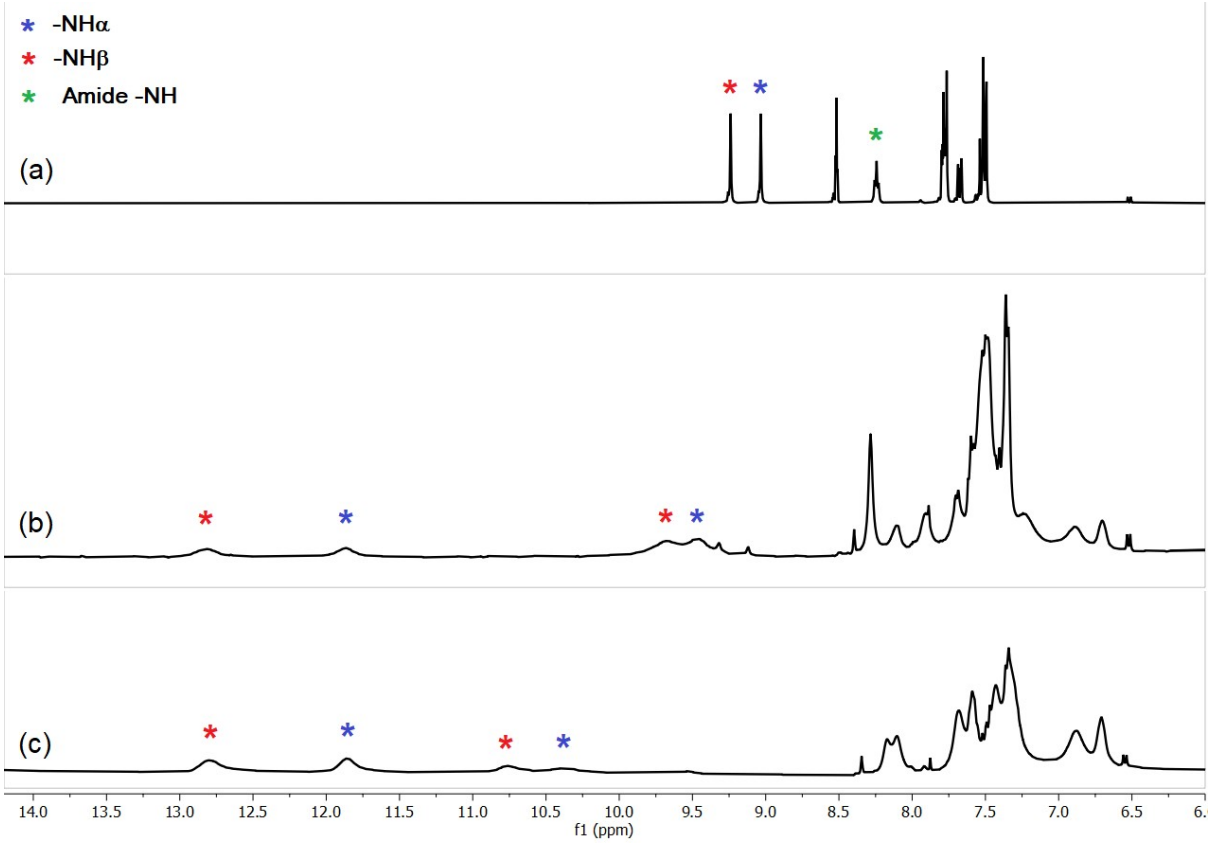

Fig. S54. Aromatic region of the ^{1}H-NMR spectrum of (a) **L** (b) **L** upon addition of 0.25 equiv. of Na_2HAsO_4, (c) **L** upon addition of 0.50 equiv. of Na_2HAsO_4 in DMSO-d_6/H_2O (9:1, v/v).

7. DFT calculation results and energy optimized structures of receptor-oxoanion complexes

Table S1: Binding Energy (B.E.) of 2:1 receptor-oxoanion complexes obtained from DFT calculations at the B97D/6-31G** level of theory, B.E. = ($E_{receptor}$ + E_{anion}) – $E_{complex}$

	$E_{complex}$	$E_{receptor}$	E_{anion}	**B.E.** (Hartree)	**B.E.** (kJ/mol)
$[(Bu_4N)_3\cdot(2\mathbf{L}\cdot AsO_4)]$	-11489.628909	-8954.4745209	-2533.789334	-1.36505339	**-3583.9**
$[(Bu_4N)_3\cdot(2\mathbf{L}\cdot PO_4)]$	-9597.3338541	-8954.4745209	-641.5205039	-1.33882936	**-3515.1**
$[(Bu_4N)_2\cdot(2\mathbf{L}\cdot SO_4)]$	-8968.1216190	-8269.0236106	-698.5572158	-0.54079263	**-1419.9**
$[(Bu_4N)_2\cdot(2\mathbf{L}\cdot CO_3)]$	-8533.0941511	-8269.0236106	-263.4374540	-0.63308653	**-1662.2**
$[(Bu_4N)\cdot(2\mathbf{L}\cdot NO_3)]$	-7902.9938370	-7622.5532129	-280.1429494	-0.29767465	**-781.50**

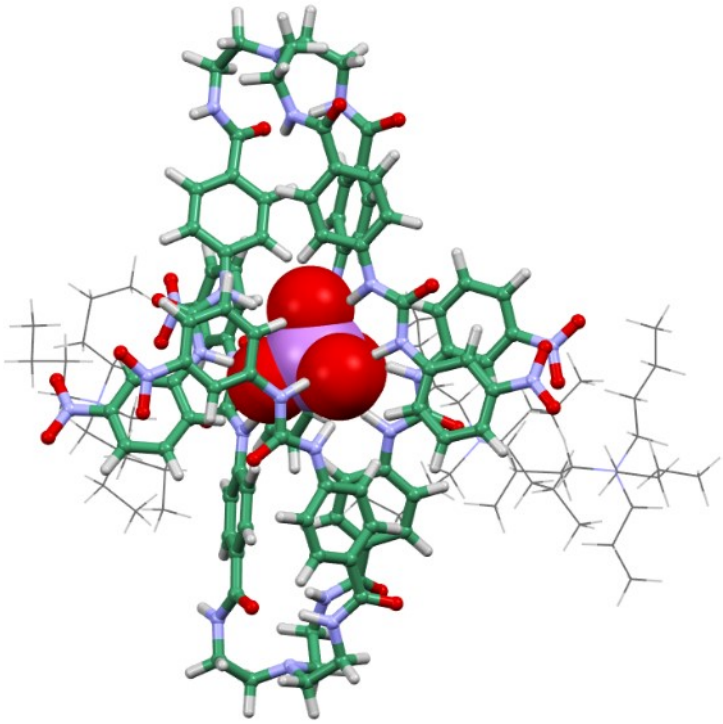

Fig S55. Energy optimized structure of the arsenate complex $[(n\text{-}Bu_4N)_3\cdot(2\mathbf{L}\cdot AsO_4)]$ obtained from DFT calculations.

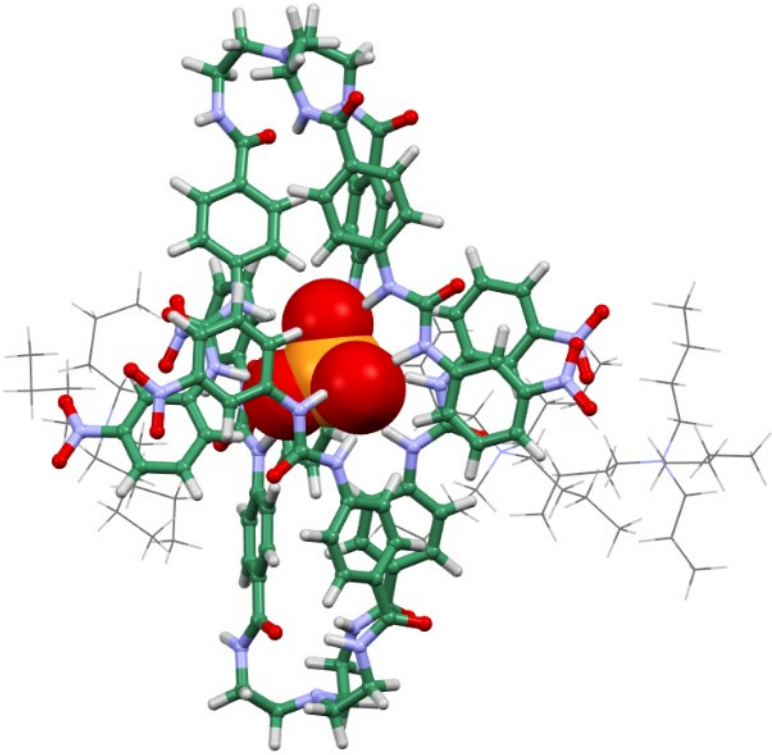

Fig S56. Energy optimized structure of the phosphate complex $[(n\text{-}Bu_4N)_3\cdot(2\mathbf{L}\cdot PO_4)]$ obtained from DFT calculations.

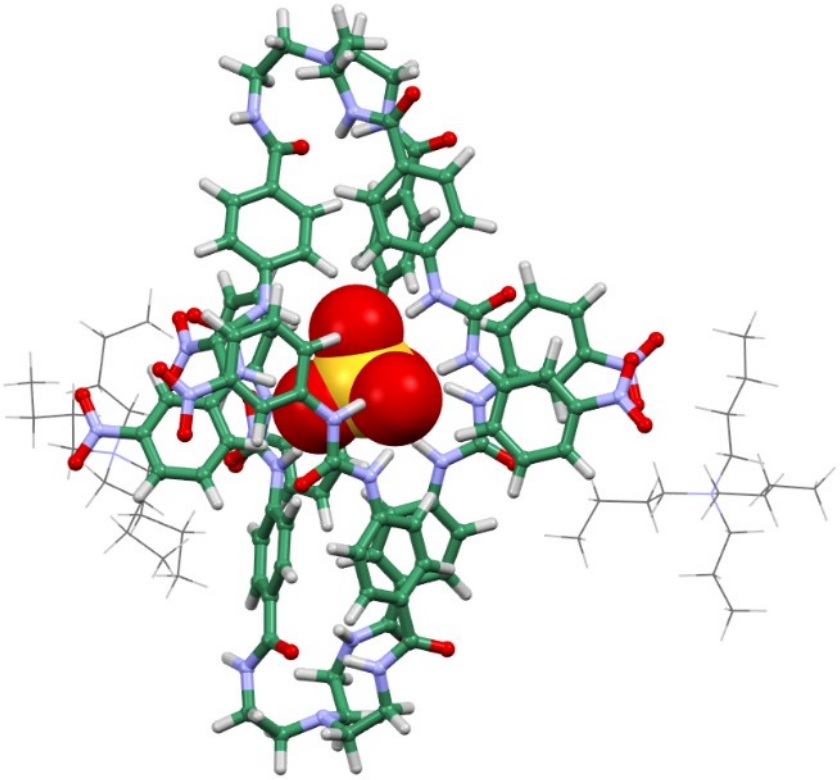

Fig S57. Energy optimized structure of the sulfate complex [(n-$Bu_4N)_2$·(2**L**·SO_4)] obtained from DFT calculations.

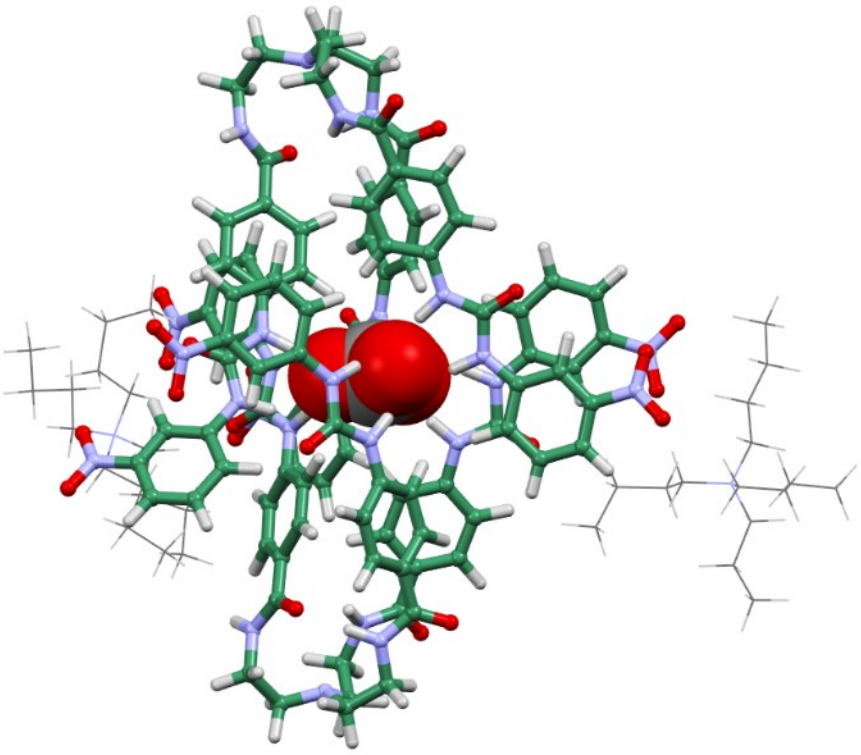

Fig S58. Energy optimized structure of the carbonate complex [(n-$Bu_4N)_2$·(2**L**·CO_3)] obtained from DFT calculations.

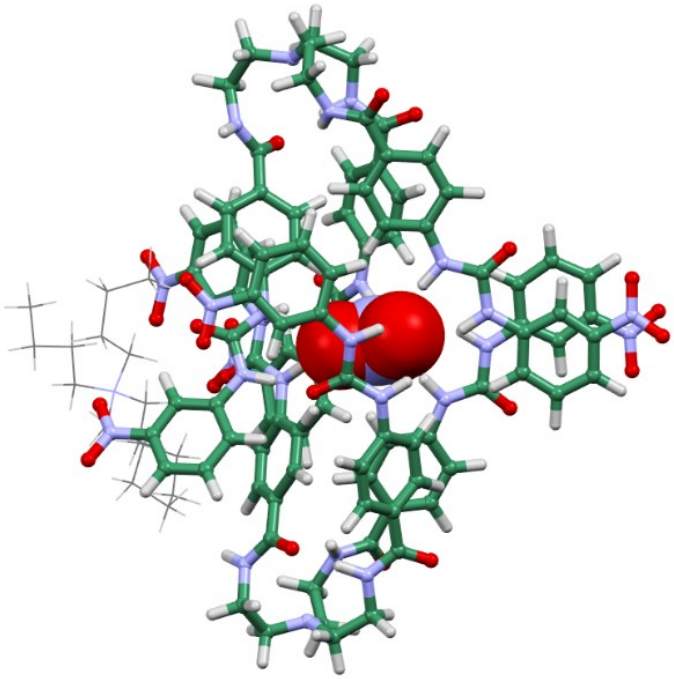

Fig S59. Energy optimized structure of the nitrate complex [(n-Bu_4N)·(2**L**·NO_3)] obtained from DFT calculations.

8. NMR spectra of arsenate complexes obtained at different pH from extraction experiments.

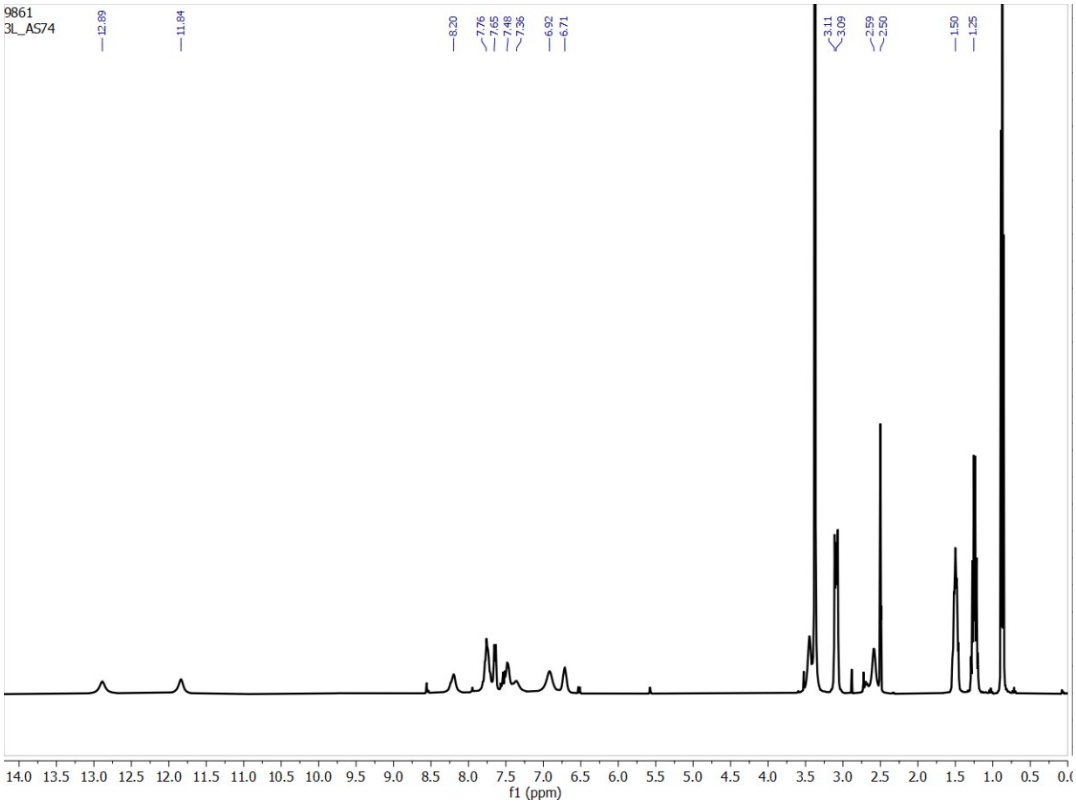

Fig. S60. ^{1}H-NMR spectrum of the arsenate complex [(n-$Bu_4N)_3$·(2**L**·AsO_4)] (DMSO-d_6) extracted from an aqueous solution of Na_2HAsO_4 of pH 7.4 by **L** in DCM.

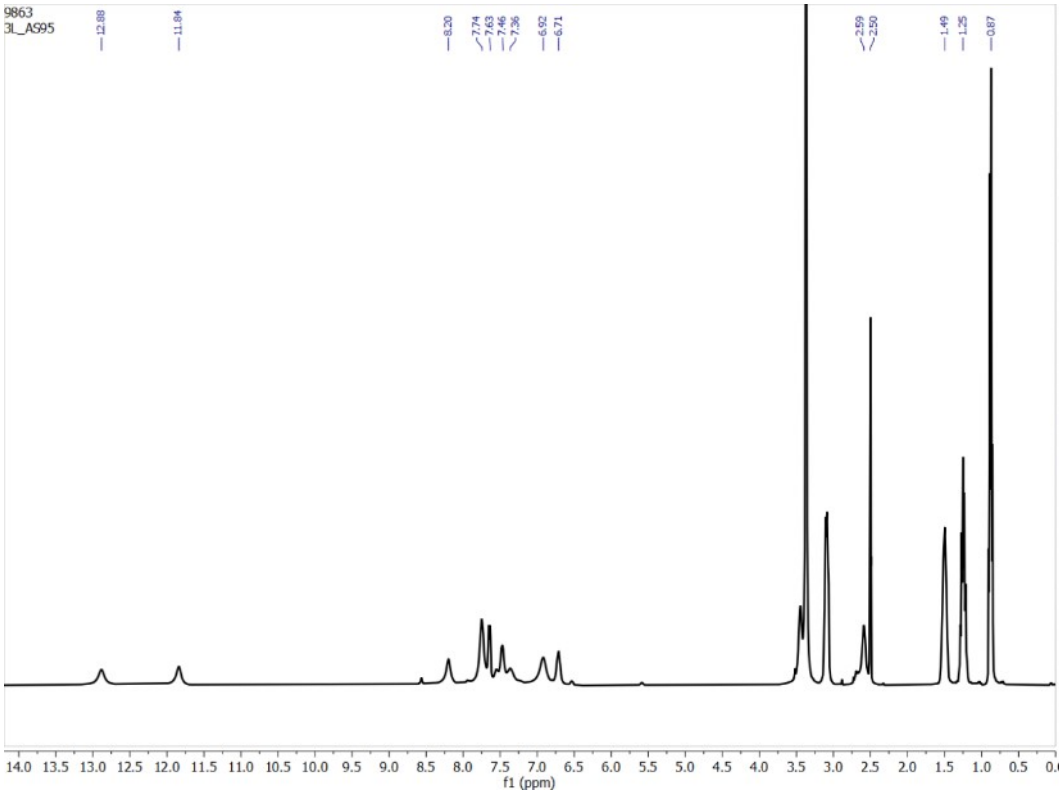

Fig. S61. ^{1}H-NMR spectrum of the arsenate complex [(n-Bu_4N)$_3$·(2**L**·AsO_4)] (DMSO-d_6) extracted from an aqueous solution of Na_2HAsO_4 of pH 9.5 by **L** in DCM.

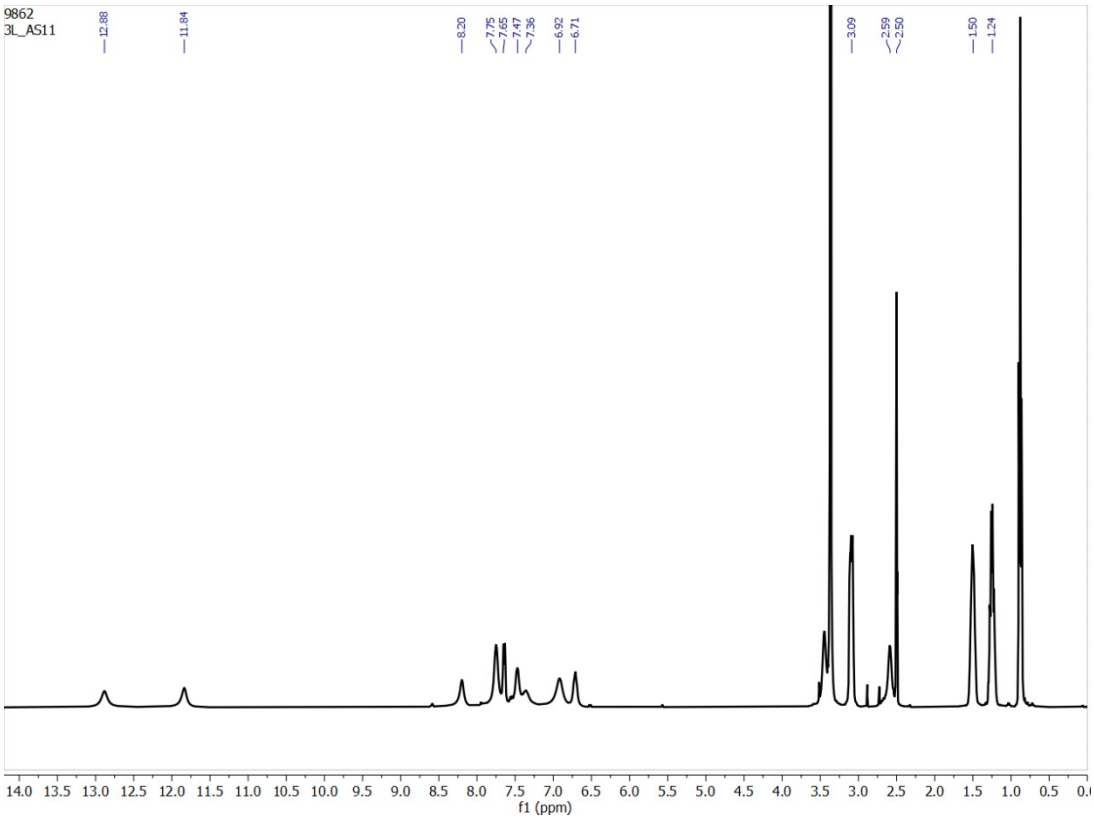

Fig. S62. ^{1}H-NMR spectrum of the arsenate complex [(n-Bu_4N)$_3$·(2**L**·AsO_4)] (DMSO-d_6) extracted from an aqueous solution of Na_2HAsO_4 of pH 11 by **L** in DCM.

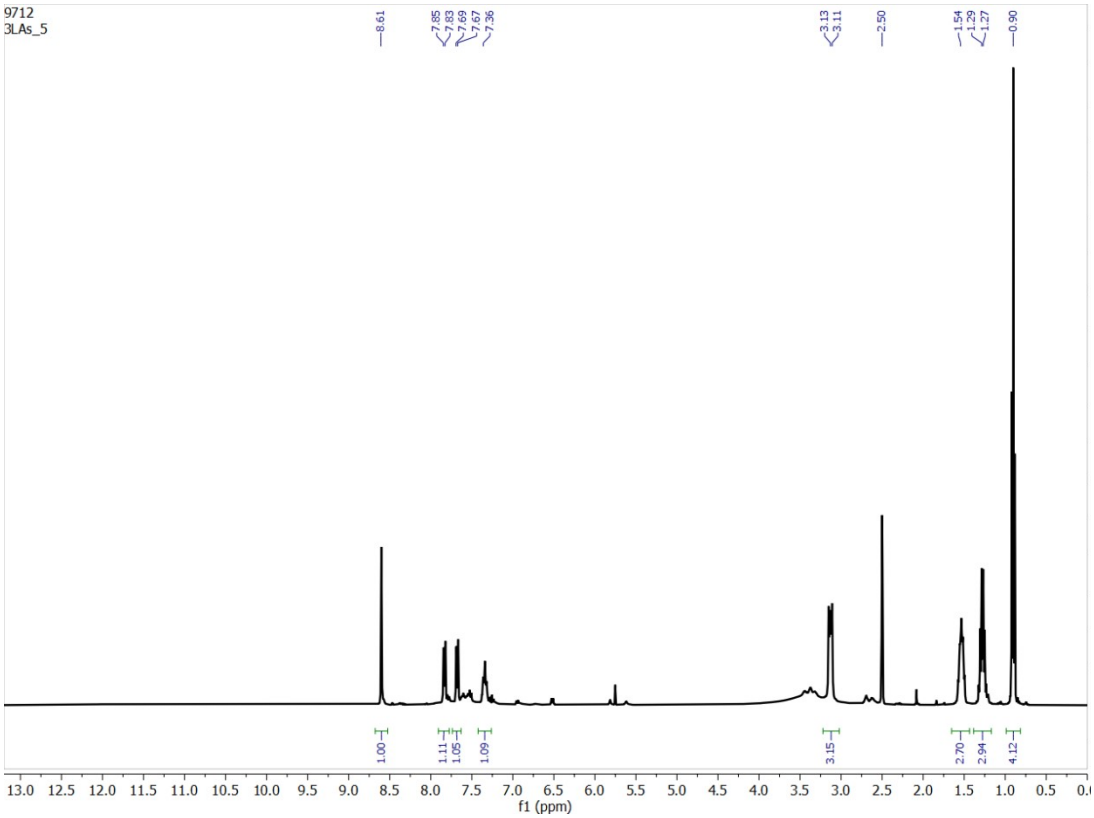

Fig. S63. ^{1}H-NMR spectrum of the isolated compound (DMSO-d_6) extracted from an aqueous solution of Na_2HAsO_4 of pH 5.5 by **L** in DCM.

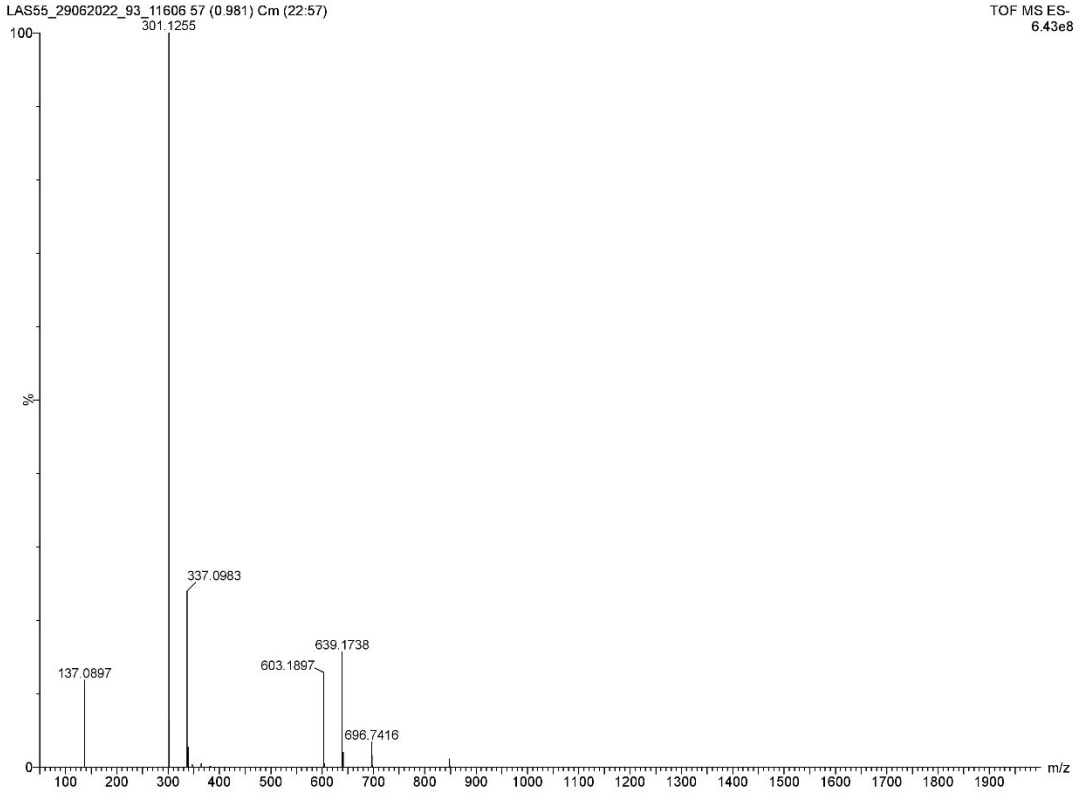

Fig. S64. HR-MS of the isolated compound (acetonitrile) extracted from an aqueous solution of Na_2HAsO_4 of pH 5.5 by **L** in DCM.

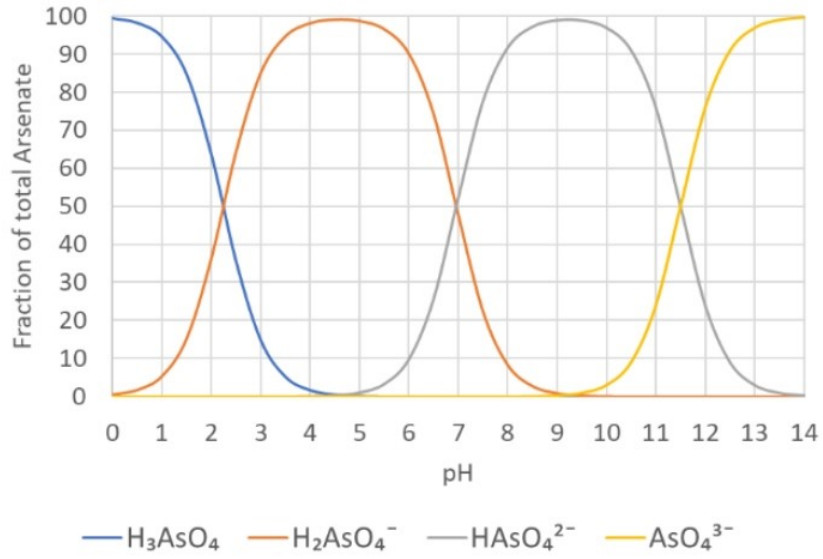

Fig. S65. Distribution of arsenate, As(V) as function of the pH. It is evident that at pH 7, almost equal concentrations of $H_2AsO_4^-$ and $HAsO_4^{2-}$ will be present. The net molecular charge of arsenate is negative (−1 or −2) at pH levels between 5 and 7.

9. Control experiments

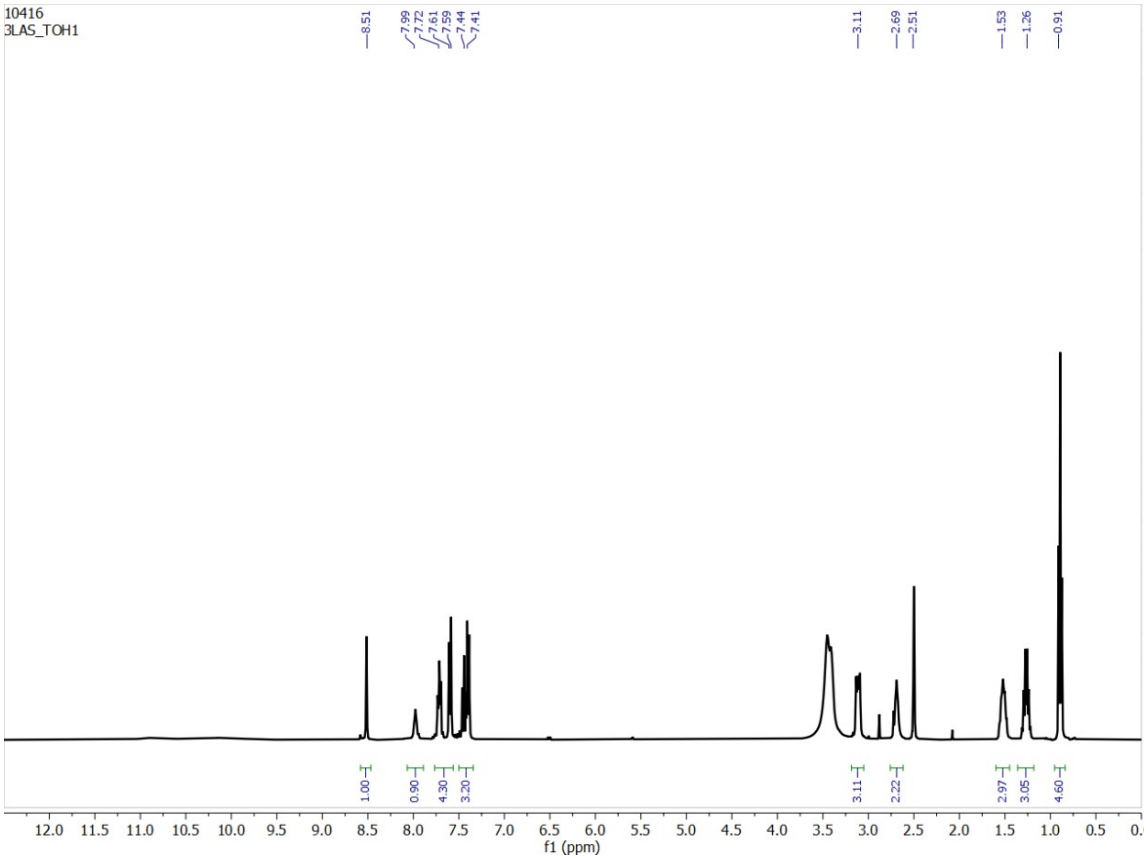

Fig. S66. ^{1}H-NMR spectrum of **L** in the presence of 1 equiv. of (n-Bu_4N)OH in DMSO-d_6.

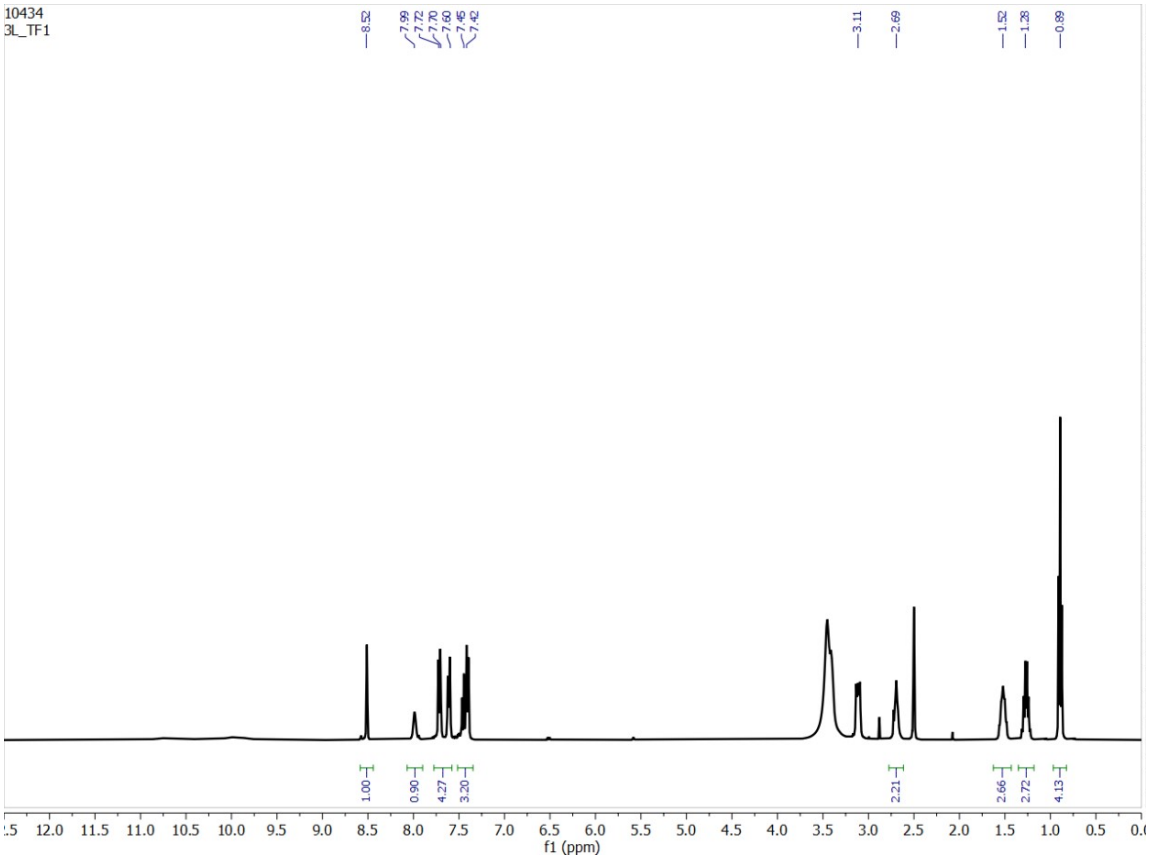

Fig. S67. ^{1}H-NMR spectrum of **L** in the presence of 1 equiv. of (n-Bu_4N)F in DMSO-d_6.

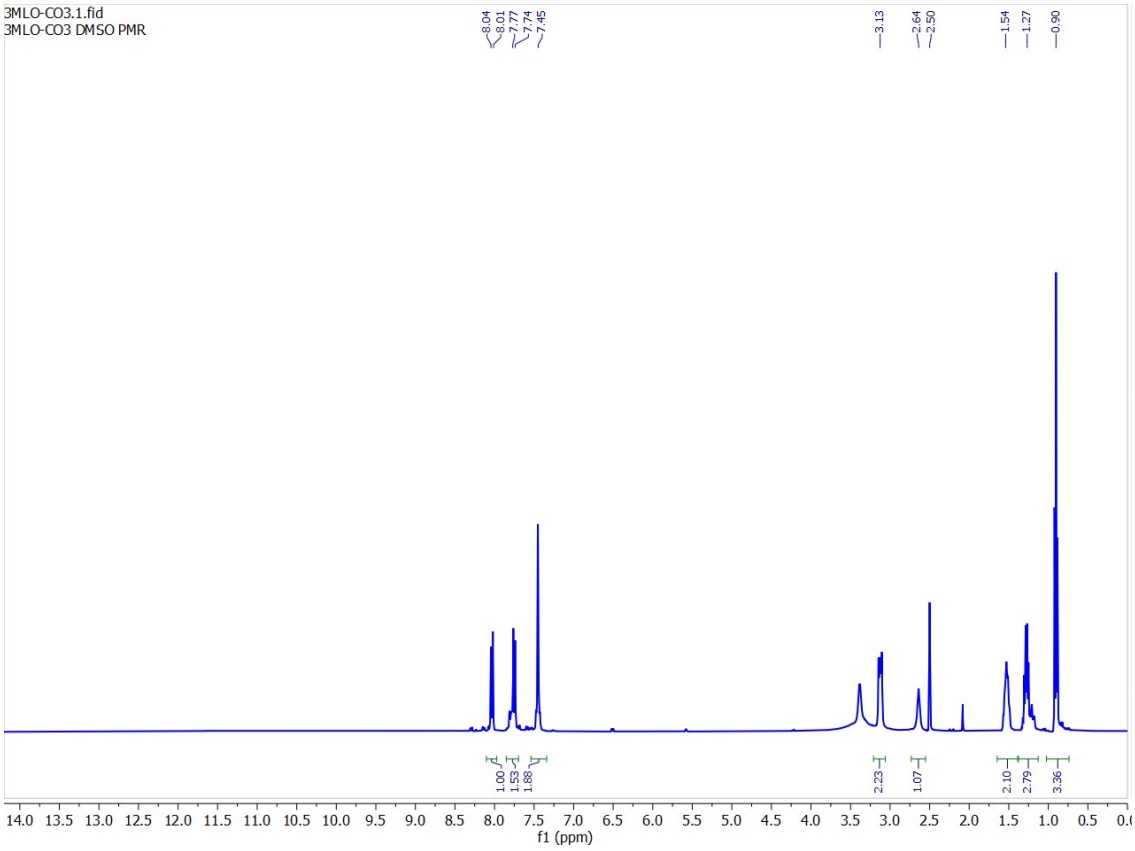

Fig. S68. ^{1}H-NMR spectrum of **L** in the presence of 1 equiv. of (n-Bu_4N)HCO_3 in DMSO-d_6.

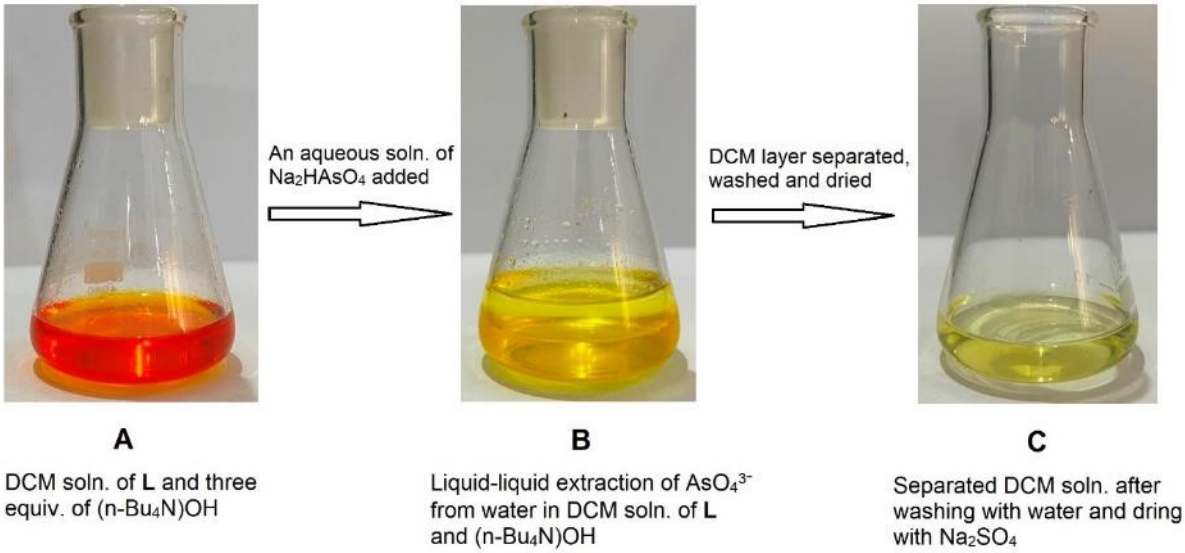

Fig. S69. Photographs of an arsenate extraction experiment showing the changes in colour observed for the (A) dichloromethane (DCM) layer [**L**+3 equiv. $(n\text{-}Bu_4N)OH$] (B) after the DCM layer stirred for half an hour with an equivalent amount of aqueous Na_2HAsO_4 solution, and (C) after washing the dichloromethane layer with water followed by treatment with anhydrous Na_2SO_4.

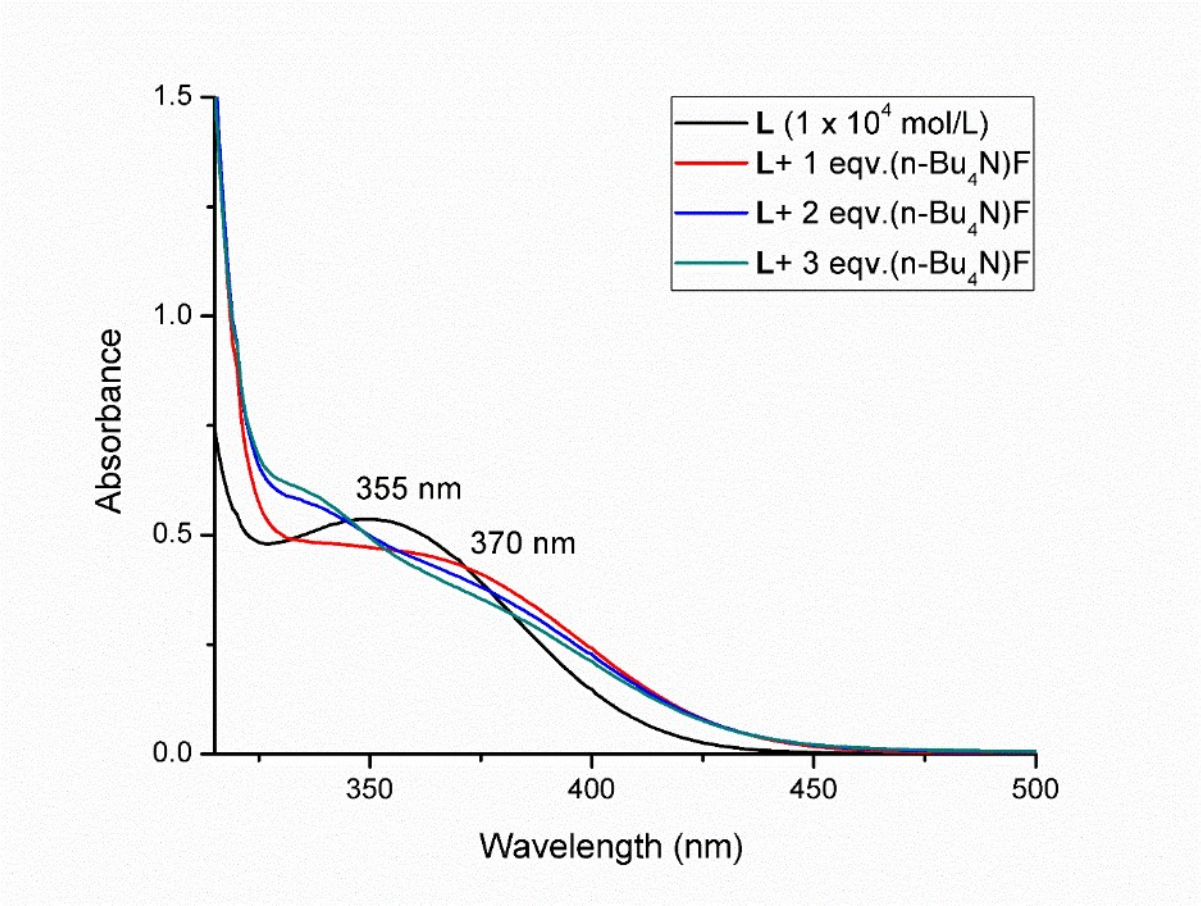

Fig. S70. UV-vis spectra of **L** ($1x10^5$ mol/L) upon addition of three equivalents of $(n\text{-}Bu_4N)F$.

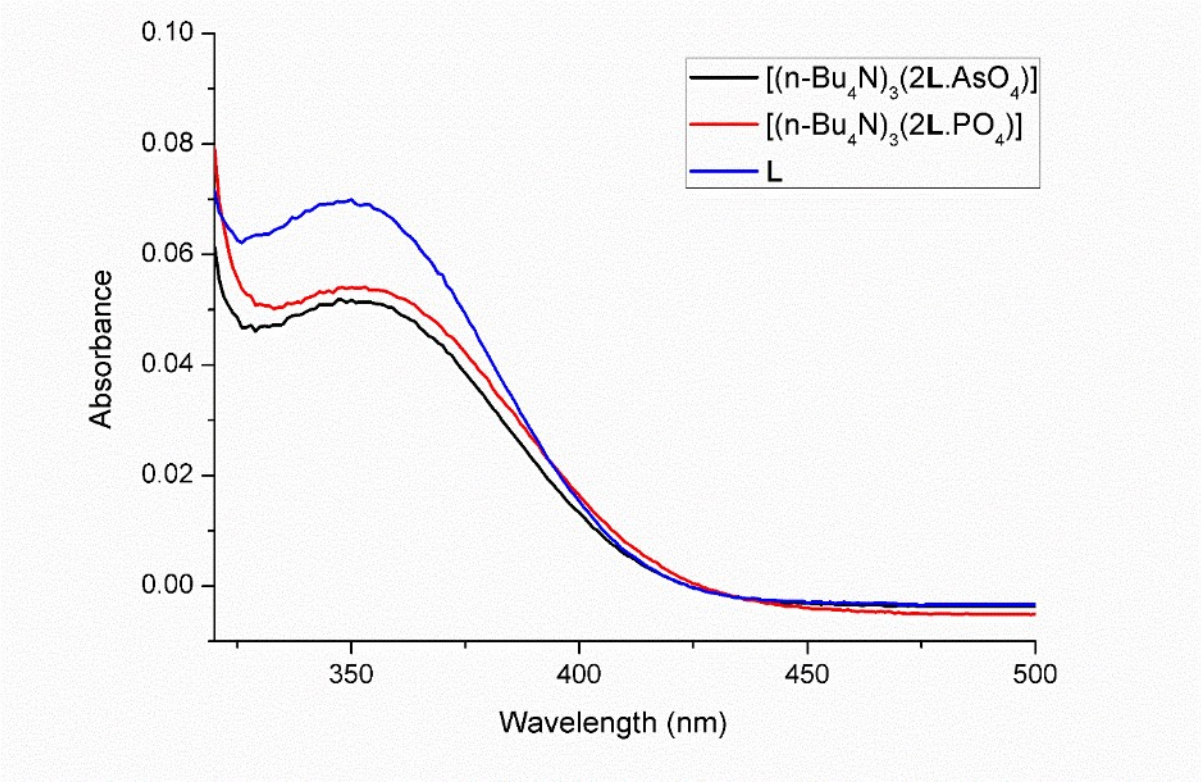

Fig. S71. Comparison of the UV-vis spectra of arsenate and phosphate complexes with **L** in DMSO.

10. Single-crystal X-ray Crystallography

Single crystals of $[(n\text{-}Bu_4N)_3{\cdot}(2\mathbf{L}{\cdot}AsO_4)]$ suitable for X-ray diffraction analysis were obtained under ambient conditions (RT) from a DMSO solution of $[(n\text{-}Bu_4N)_3{\cdot}(2\mathbf{L}{\cdot}AsO_4)]$ which was synthesized by liquid-liquid (dichloromethane-water) extraction of arsenate by receptor **L** in the presence of three equivalents of $[(n\text{-}Bu_4N)OH$. Single crystals of $[(n\text{-}Bu_4N)_3{\cdot}(2\mathbf{L}{\cdot}AsO_4)]$ can reproducibly be obtained under ambient conditions by dissolving 50 mg of the compound in 1 mL of DMSO, which was allowed to crystallize in a 3 mL capacity glass vial.

In each case, a crystal of suitable size was selected from the mother liquor and immersed in paratone oil, and mounted on to a fibre loop holder. Single-crystal XRD data were collected at 120 K with a Bruker SMART APEX-III CCD diffractometer equipped with a fine focus 1.75 kW sealed tube Mo–Kα radiation (λ = 0.71073 Å). The SMART software was used for the data acquisition. Data integration and reduction were undertaken with SAINT and XPREP software.[2] Multi-scan empirical absorption corrections were applied to the data using the SADABS program.[3] The structures were solved by direct methods using SHELXS-97,[4] and refined with full-matrix least-squares on F^2 using SHELXL-97.[5] All non-hydrogen atoms were refined anisotropically, hydrogen atoms attached to all carbon atoms were geometrically fixed (with C–H = 0.95 Å for aromatic CH, C–H = 0.99 Å for CH_2 and C–H = 0.98 Å for CH_3) and the positional and temperature factors were refined isotropically using riding models (AFIX 43, 23 and 137 with $U_{iso(H)}$ = 1.2 $U_{eq(C)}$ (CH,CH_2) and 1.5 $U_{eq(C)}$ (CH_3)). Hydrogen atoms attached to the amide and urea nitrogen atoms were preferred to be positioned geometrically (with N–H = 0.88 Å) and refined isotropically using a riding model (AFIX 43) with $U_{iso(H)}$ = 1.2 $U_{eq(N)}$.

Single crystal X-ray crystallography data of $[(n\text{-}Bu_4N)_3(2\mathbf{L}{\cdot}AsO_4)]$ CCDC No. 2172773, F = $C_{144}H_{198}AsN_{29}O_{28}$, M = 2858.23, T = 120 K, Space group = P−1, a = 17.5033(13) Å, b = 17.7141(13) Å, c = 29.548(2) Å, α = 87.526(4)°, β = 84.116(4)°, γ = 82.468(4)°, V = 9030.5(11) $Å^3$, Z = 2, μ = 0.254 mm^{-1}, D = 1.051 g cm^{-3}, F(000) = 3044, θ (max) = 25.403, total reflections = 122362, unique reflections = 32853, observed reflections ($I > 2s(I)$) = 25931, parameters = 1842, $R_1(F)$ = 0.0964, w$R_2(F^2)$ = 0.2752, S = 1.068.

Table S2. Hydrogen bond distances (Å) and angles (°) of encapsulated arsenate anion (AsO_4^{3-}) with the urea -NH groups of two receptor molecules (**L**) in [(n-$Bu_4N)_3$·(2**L**·AsO_4)] crystal (D = hydrogen bond donor and A = hydrogen bond acceptor).

D−H···A	**N···O (Å)**	**N−H···O (Å)**	**N−H···O (°)**
N2B−H···O1	2.873 (5)	2.057	153.7
N2C−H···O1	2.876 (5)	2.070	151.7
N3C−H···O2	2.734 (5)	1.862	171.1
N2F−H···O2	2.743 (5)	1.905	158.7
N3F−H···O2	2.800 (5)	1.971	156.6
N2E−H···O3	2.786 (5)	1.951	157.8
N3E−H···O3	2.857 (5)	2.028	156.4
N3A−H···O3	2.706 (5)	1.831	172.7
N3B−H···O4	2.752 (5)	1.876	173.4
N2D−H···O4	2.698 (5)	1.863	157.7
N3D−H···O4	2.715 (5)	1.904	152.6

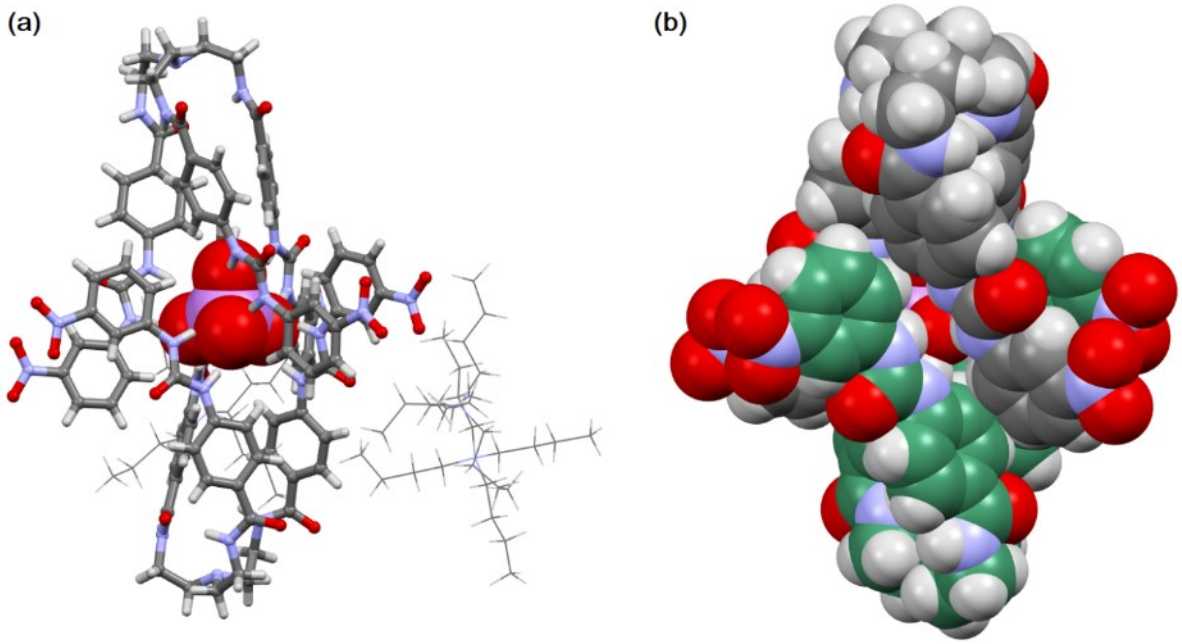

Fig S72. (a) Asymmetric unit of the X-ray structure of the arsenate complex [(n-$Bu_4N)_3$·(2**L**·AsO_4)] (b) Space-filling representation of (2**L**·$AsO_4)^{3-}$ in the X-ray structure of [(n-$Bu_4N)_3$·(2**L**·AsO_4)] (cations are not shown).

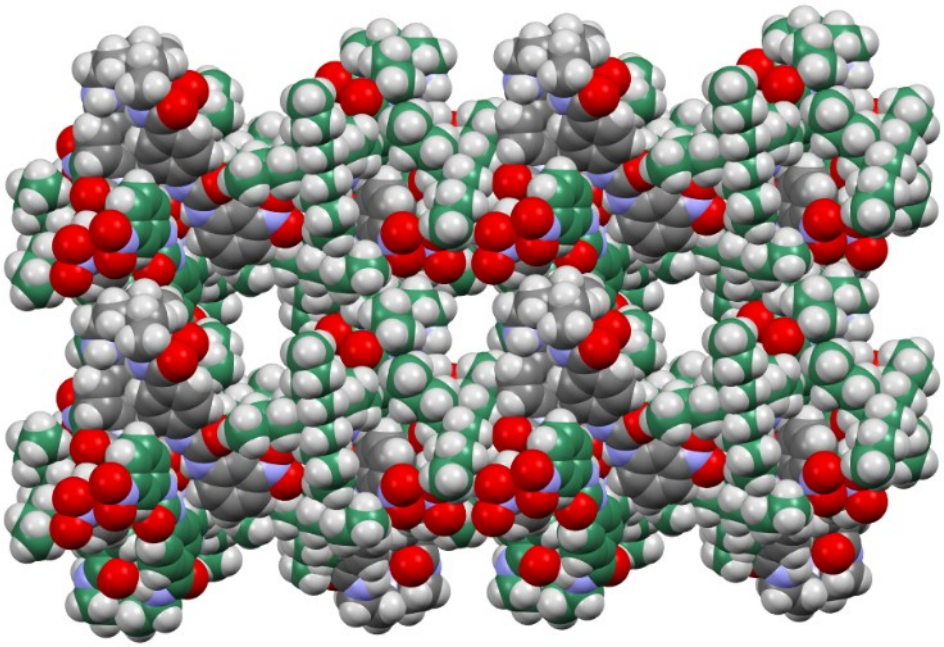

Fig. S73. Packing diagram of the X-ray structure of the arsenate complex [(n-$Bu_4N)_3$·(2**L**·AsO_4)] in space-filling presentation as viewed along crystallographic *a*-axis.

References

1. S. K. Dey and C. Janiak, RSC Adv., 2020, 10, 14689–14693.

2. SMART, SAINT and XPREP, Siemens Analytical X-ray Instruments Inc., Madison, WI, 1995.

3. G. M. Sheldrick, SADABS: Software for Empirical Absorption Correction; University of Gottingen, Institute for Anorganische Chemie de Universitat, Gottingen, Germany, 1999–2003.

4. G. M. Sheldrick, SHELXS-97, University of Gottingen, Germany, 1997.

5. G. M. Sheldrick, SHELXL-97: Program for Crystal Structure Refinement, University of Gottingen, Gottingen, Germany, 1997.